PEOPLE'S DEMOCRATIC REPUBLIC OF ALGERIA

MINISTRY OF HIGHER EDUCATION AND SCIENTIFIC RESEARCH

UNIVERSITY SAAD DAHLEB BLIDA 1

INSTITUTE OF AERONAUTICS AND SPACE STUDIES

DOCTORAL THESIS IN AERONAUTICS

Option: Avionics

Presented by

M. BENGHANEM Yahia

Titled

DESIGN AND DEVELOPMENT OF SOLUTIONS TO ENHANCE THE PERFORMANCE OF MULTI-ANTENNA DEVICES FOR ADVANCED WIRELESS COMMUNICATIONS

Defended before the jury on 15/10/2024

President :	**M. LAGHA Mohand**	Professeur	University of Blida 1
Director :	**M. MANSOUL Ali**	Directeur de recherche	CDTA- Baba Hassen, Alger
Co-Director :	**Mme. MOUFFOK Lila**	MCA	University of Blida 1
Examiner :	**M. HEBIB Sami**	Professeur	University of Blida 1
Examiner :	**M. CHALLAL Mouloud**	Professeur	University of Boumerdes
Examiner :	**M. HAMOUDA Zahir**	MCA	ESTA- Dar El Beida, Alger

الملخص

لتلبية المتطلبات عالية السرعة التي يتطلبها الجيل التالي من الاتصالات اللاسلكية والتوسع الكبير في شبكات الإنترنت عبر الهاتف المحمول في جميع أنحاء العالم (شبكات الجيل الخامس وما بعدها)، يتضمن أحد الحلول زيادة عدد الهوائيات لكل من الإرسال والاستقبال في الوصلات اللاسلكية. وتعرف هذه التكنولوجيا بتقنية الهوائيات ذات المداخل المتعددة والمخارج المتعددة (MIMO). بالإضافة إلى ذلك، يمكن استخدام تقنية الهوائيات القابلة لإعادة التشكيل، القادرة على تعديل خصائص تردد التشغيل ديناميكيًا، بالاقتران مع أنظمة الهوائيات المتعددة لزيادة تعزيز سعة الشبكات الاتصالات اللاسلكية وموثوقيتها.

تركز هذه الأطروحة على دراسة وتصميم الهوائيات المتعددة القابلة لإعادة تشكيل الترددات للاتصالات اللاسلكية المتقدمة. بعد التعريف بتكنولوجية الهوائيات ذات المداخل المتعددة والمخارج المتعددة، يتم تقديم أحدث ما توصلت إليه الأبحاث في مجال الهوائيات المتعددة القابلة لإعادة تشكيل الترددات والأنواع المختلفة لإعادة التشكيل. تم تطوير واختبار العديد من النماذج الأولية ذات أوضاع تشغيل مختلفة. النموذج الأول عبارة عن هوائي ثنائي العناصر قابل لإعادة التشكيل مع أربعة أوضاع تشغيل مختلفة لتطبيقات الجيل الخامس دون 6 جيجاهرتز والتطبيقات اللاسلكية الإدراكية. النموذج الثاني عبارة عن هوائي ثنائي التردد ثنائي العناصر يوفر المرونة اللازمة للتبديل من وضع النطاق المزدوج إلى وضع النطاق الأحادي والعكس. النموذج الثالث عبارة عن هوائي ثلاثي الترددات ثنائي العناصر قادر على العمل في أي مجموعة من النطاقات التي تشمل المعايير اللاسلكية الثلاثة الأكثر استخدامًا (WiFi وWiMAX وWLAN). النموذج الرابع عبارة عن هوائي ثنائي العناصر يعمل في نطاق فائق الاتساع (SWB) بين 3.2 و50 جيجاهرتز للترددات المليمترية للجيل الخامس. النموذج المقترح الأخير يتضمن آليتي ترشيح مدمجتين في كل عنصر من عناصر الهوائي ذو النطاق الترددي العريض للغاية (UWB)الأولى لرفض الترددات بين 5.15 و 5.8 جيجاهرتز و الثانية لإلغاء النطاق بين 6.3 و 7.3 جيجاهرتز على التوالي. تمت محاكاة الأجهزة باستخدام برنامج CST (برنامج استوديو الميكروويف)، وتم تصنيعها وقياسها. تتوافق النتائج التجريبية مع تلك التي تم الحصول عليها عن طريق المحاكاة، وهذا ما يثبت صحة ومصداقية التصاميم المختلفة المقترحة في هذه الأطروحة، سواء مع وضع تشغيل متكامل قابل لإعادة التشكيل (الراديو المعرفي) أو وضع تشغيل بسيط بدون آلية إعادة التشكيل (G5 وG5 دون GHz6).

الكلمات المفتاحية :الهوائيات ذات المداخل المتعددة والمخارج المتعددة، الهوائيات قابلة لإعادة التكوين، الصمام الثنائي، الجيل الخامس، الراديو الإدراكي، UWB، SWB، CST.

Résumé

Pour répondre aux demandes de haut débit requises par les communications sans fil de prochaine génération et l'expansion extensive de l'internet mobile à travers le monde (réseaux 5G et au-delà), une solution consiste à augmenter le nombre d'antennes tant pour la transmission que pour la réception dans les liaisons sans fil. Cette technologie est connue sous le nom de MIMO (Multiple Input Multiple Output). De plus, la technologie des antennes reconfigurables, capable d'ajuster dynamiquement les fréquences de fonctionnement, peut être utilisée en conjonction avec les systèmes MIMO pour améliorer encore la capacité et la fiabilité des réseaux de communication sans fil.

Cette thèse se concentre sur l'étude et la conception d'antennes multiples reconfigurables en fréquence pour les communications sans fil avancées. Après avoir introduit la technologie MIMO (Multiple Input Multiple Output), un état de l'art sur les antennes multiples reconfigurables en fréquence et les différents types de reconfiguration est fourni. Plusieurs prototypes avec un fonctionnement différent ont été développés et testés. Le premier prototype est une antenne MIMO reconfigurable, compacte à deux éléments, offrant quatre modes de fonctionnement différents pour les applications 5G sub-6GHz, et de la radio cognitive. Le deuxième prototype est une antenne MIMO 2×2 bi-bande offrant la flexibilité nécessaire pour passer d'un mode bi-bande à un mode mono-bande et vice-versa. Le troisième prototype est une antenne à deux éléments triple bande capables de fonctionner dans n'importe quelle combinaison de bandes impliquant les trois normes sans fil les plus couramment utilisées (WiFi, WiMAX et WLAN). Le quatrième prototype est une antenne MIMO SWB à deux éléments fonctionnant entre 3,2 et 50 GHz pour les ondes millimétriques (MMW) 5G. Le dernier prototype comprend deux mécanismes de filtrage intégrés dans chaque élément rayonnant de l'antenne MIMO UWB initiale pour rejeter la bande WLAN (5,15 - 5,8 GHz) et la bande C INSAT (6,3 - 7,3 GHz), respectivement. Les structures ont été conçues et simulées à l'aide de CST Microwave studio, fabriqués et mesurés expérimentalement. Les résultats expérimentaux concordent avec ceux obtenus par simulation et valident les différentes approches de conception proposées dans cette thèse, que ce soit avec un mode de fonctionnement reconfigurable intégré (radio cognitive) ou un mode de fonctionnement simple sans mécanisme de reconfiguration (5G et 5G sub-6GHz).

Mots-clés: MIMO, antenne reconfigurable, 5G, radio cognitive, UWB, SWB, CST.

Abstract

To meet the high-speed demands required by next-generation wireless communications and the extensive expansion of mobile internet worldwide (5G networks and beyond), one solution involves increasing the number of antennas for both transmission and reception in wireless links. This technology is known as Multiple Input Multiple Output (MIMO) technique. Additionally, reconfigurable antenna technology, capable of dynamically adjusting the operating frequency characteristics, can be employed in conjunction with MIMO systems to further enhance the capacity and reliability of wireless communication networks.

This thesis focuses on the study and design of frequency reconfigurable multi-antenna for advanced wireless communications. After introducing Multiple Input, Multiple Output (MIMO) technology, a comprehensive state-of-the-art on frequency reconfigurable multi-antenna and various reconfiguration types is provided. Several prototypes with distinct operational mechanisms were developed and tested. The first prototype is a compact, two-element reconfigurable MIMO antenna with four different operating modes for 5G sub-6GHz and cognitive radio applications. The second prototype is a dual-band 2×2 MIMO antenna offering the necessary flexibility to switch from dual-band to single-band mode and vice-versa. The third prototype is a triple-band two-element antenna capable of operating in any combination of bands involving the three most commonly used wireless standards (WiFi, WiMAX, and WLAN). The fourth prototype is a 2-element SWB MIMO antenna operating between 3.2 - 50 GHz for millimeter-wave (MMW) 5G. The final prototype includes two filtering mechanisms integrated into each radiating element of the initial UWB MIMO antenna to reject the WLAN band (5.15 - 5.8 GHz) and the C INSAT band (6.3 - 7.3 GHz), respectively. The structures were designed and simulated using CST Microwave Studio, fabricated, and measured experimentally. The experimental results concur with those obtained by simulation and validate the different design approaches proposed in this thesis, whether with an integrated reconfigurable operating mode (cognitive radio) or a simple operating mode without a reconfiguration mechanism (5G and 5G sub-6GHz).

Keywords: MIMO, Reconfigurable antenna, 5G, cognitive radio, UWB, SWB, CST.

DEDICATION

To my dear parents for their support
To my sisters and brother, Abdelkrim
To all my family, young and old
To all my friends

ACKNOWLEDGMENTS

I would like to express my thanks to almighty **ALLAH** for granting me health, energy, and the will necessary to undertake this work.

My sincere thanks go to those who have not only been guides but also sources of self-confidence for me. To my thesis directors, **Dr.MANSOUL Ali** and **Dr. Mouffok Lila**. Their expertise and mentorship have been instrumental in shaping both the direction and the quality of this thesis.

I extend my heartfelt appreciation to [Laboratory of Aeronautical Sciences, IAES/University of Blida1], [Radio Frequencies and Antennas Laboratory / Centre for Advanced Technologies Development (CDTA), Baba Hassen, Algiers], [Conception and Integration Systems Laboratory (LCIS) / Grenoble Alpes University, Valence, France], [Telecom Laboratory / University of Houari Boumediene, Bab Ezzouar, Algiers], [Radio frequencies Laboratory / Ecole Supérieure de la Défense Aérienne du Territoire -Chahid Ali CHABATI], for providing the necessary resources and facilities essential for conducting this research.

I would like to express my deepest gratitude to **Pr.TEDJINI Smail** and **Dr.ALLANE Dahmane**, who played an essential role in the success of my doctoral thesis. Their warm welcome to France created an environment conducive to research and experimentation, and I was fortunate to benefit from their expertise, generosity, and support throughout this academic sojourn.

My special thanks go to the people dearest to me, those who have supported, encouraged, and never ceased to pray for our success, my dear parents.

To all the members of the jury, I extend my warmest and most distinguished thanks: **Mr.LAGHA Mohand**, Professor at University of Blida 1, for agreeing to chair the jury; **Mr. HEBIB Sami**, Professor at University of Blida 1; **Mr. CHALLAL Mouloud**, Professor at University of Boumerdes; and **Mr. HAMOUDA Zahir**, Associate Professor at the higher school of aeronautical techniques, for agreeing to evaluate this work as examiners.

To all those who have contributed directly or indirectly during my studies, I extend my sincerest thanks.

TABLE OF CONTENTS

LIST OF FIGURES

LIST OF TABLES

LIST OF ABBREVIATIONS

3GPP Third Generation Partnership Project

4G Fourth Generation

5G Fifth Generation

BPSK Binary Phase Shift Keying

CAD Computer-Aided Design

CCL Channel Capacity Loss

CR Cognitive Radio

CSRR Complementary Split-Ring Resonator

CST Computer Simulation Technology

dB Decibel

dBi Decibel Isotropic

DG Diversity Gain

DGS Defected Ground Structure

EBG Electromagnetic Band Gap

ECC Envelope Correlation Coefficient

ETSI European Telecommunications Standards Institute

FDTD Finite Different Time-Domain

FEM Finite Element Method

FETs Field-Effect Transistors

FIT Finite Integration Technique

FR4 Flame Resistant 4

GHz Gigahertz

GPRS General Packet Radio Service

GSM Global System for Mobile communication

HiperLAN High-Performance Radio LAN

HiSWAN High-Speed Wireless Access Network

IBW Impedance Bandwidth

IEEE Institute of Electrical and Electronics Engineers

ISM Industrial, Scientific, and Medical

LNA Low Noise Amplifier

LoS Line of Sight

LPF Low-Pass Filter

LTE Long Term Evolution

MEG Mean Effective Gain

MEMS Micro-Electro-Mechanical Systems

MHz Megahertz

MIMO Multiple-input-multiple-output

MLFMM Multilevel Fast Multipole Method

MoM Method of Moments

MTM MeTaMaterial

MWS Microwave Studio

NL Neutralization Line

NR New Radio

OFDM Orthogonal Frequency Division Multiple Acces

PA Power Amplifier

PCB Printed Circuit Board

PEC Perfect Electric Conductor

PIFA Planar Inverted-F Antennas

PIN P-type Intrinsic N-type

QAM Quadrature Amplitude Modulation

QoS Quality of Service

QPSK Quadrature Phase Shift Keying

RF Radio Frequency

RSRR Rectangular Split Ring Resonator

SBR Shooting and Bouncing Rays

SISO Single-Input-Single-Output

SMA SubMiniature version A

SNR Signal-to-Noise Ratio

SRR Split-Ring Resonator

SWB Super Wide-Band

TARC Total Active Reflection Coefficient

TE Transverse Electric

TM Transverse Magnetic

UMTS Universal Mobile Telecommunication System

UWB Ultra Wide-Band

VARACTOR Variable Reactor

WiMAX Worldwide Interoperability for Microwave Access

WIFI Wireless Fidelity

WLAN Wireless Local Area Network

WMAN Wireless Metropolitan Area Networks

WWAN Wireless Wide Area Networks

WPAN Wireless Personal Area Networks

XPR Cross-Polarization Ratio

GENERAL INTRODUCTION

WITH the rapid evolution of wireless communication systems, particularly with the emergence of 5G networks, research is increasingly focused on enhancing wireless network performance. However, next-generation network design faces challenges such as limited capacity due to narrow bandwidth and restricted transmission power.

In the other hand, the growing demand for higher data rates and richer multimedia experiences has strained available bandwidth and power. Single-Input-Single-Output (SISO) systems are constrained by bandwidth and power limitations imposed by regulatory bodies. Multiple-input-multiple-output (MIMO) technology, introduced in the 1990s [1][2], overcomes these limitations by using multiple antennas to increase data rates linearly. Moreover, the majority of current wireless systems lack flexibility, prompting researchers to integrate various communication services onto a single adaptable network. Reconfigurable antennas, employing switching devices like PIN diodes and microelectromechanical systems (MEMS), offer flexibility to adapt to changing conditions and system requirements, enhancing communication capacity and reliability [3].

The combination of multi-antenna systems and reconfiguration technology offers significant benefits, including reduced interference, improved signal quality, and seamless integration of multiple services across various frequency bands [4][5]. However, the realization of these devices presents significant challenges, both in the simulation and design phases and in the implementation phase. Hence, it is essential to consider RF switches (such as PIN diodes) during the simulation phase, unlike conventional passive antennas. Additionally, these components require continuous voltage supply, necessitating the de-

velopment of biasing circuits, thereby adding complexity to antenna structures [6].

The research endeavors to achieve a dual objective. Firstly, it aims to introduce innovative approaches and concepts for highly efficient multi-antenna systems. These approaches focus on enhancing isolation between antenna elements, optimizing diversity metrics (ECC, DG, MEG, CCL, TARC), and expanding bandwidth capabilities (multiband, UWB, SWB), all while maintaining a compact size. Additionally, the objective is to develop MIMO structures integrated with frequency reconfiguration mechanisms, known as reconfigurable antennas. These antennas aim to merge the benefits of traditional MIMO systems with those of cognitive radio (CR) systems. The reconfiguration mechanisms will accommodate various filtering functions and frequency ranges, enabling adaptation between wideband and narrowband modes, frequency switching (switch between several bands), filter functions (rejection of one or more frequency bands), and bandwidth adjustment. It is important to note that the emphasis is on proposing novel approaches for multi-antenna systems and implementing simple reconfiguration mechanisms, focusing on design-level contributions rather than technological intricacies such as switch types or substrate materials. Furthermore, these proposed concepts are envisioned to be adaptable across different parts of the spectrum, with the flexibility to adjust antenna dimensions as needed.

This thesis is organized into four chapters, each delving into the evolving landscape of wireless communication systems with a focus on the integration of multiple antennas and the utilization of Multiple Input Multiple Output (MIMO) technology. Chapter 1 sets the stage by elucidating the importance of MIMO technology across various applications and standards, laying the groundwork for understanding the communication chain and propagation channel. It also explores the integration of reconfigurable antenna technology into MIMO systems, offering enhanced adaptability to modern wireless applications. A state-of-the-art review of different approaches used in the literature for frequency reconfiguration of multi-antenna systems concludes this chapter.

The subsequent three chapters present the MIMO antennas proposed within the scope of this thesis. Each chapter introduces a different approach to operating frequency bands and methods for achieving reconfiguration. Chapter 2 provides a detailed analysis of a novel reconfigurable MIMO antenna designed for the new radio applications of 5G,

highlighting its versatility in operating different frequency modes and its improved performance through the integration of key functions. In Chapter 3, the focus shifts to frequency-reconfigurable multi-band antennas, offering the flexibility to operate within various wireless standards. This chapter provides an overview of the development process, from initial simulations to prototype fabrication, emphasizing the adaptability and versatility of the proposed antennas. Finally, Chapter 4 explores critical aspects of MIMO antenna design for advanced wireless communication systems, unveiling super-wideband (SWB) and ultra-wideband (UWB) MIMO antennas designed for specific applications. The chapter meticulously characterizes the performance metrics of these antennas and introduces a reconfiguration mechanism for enhanced frequency agility. Through these chapters, the thesis contributes to the advancement of antenna design, reconfigurability, and performance optimization in modern wireless communication systems.

A general conclusion summarizes the results obtained and discusses prospects for continuing the work. Lastly, an appendix is included at the end of this manuscript to present the main parameters of the antennas.

CHAPTER 1

MULTI-ANTENNA SYSTEMS: FROM WIRELESS NETWORKS TO RECONFIGURABLE MIMO ANTENNA

1.1 Introduction

WITH the rapid evolution of wireless communications, the integration of multiple antennas for both transmission and reception has become a crucial factor in these systems. Multiple Input Multiple Output (MIMO) technology has gained prominence across various applications and recent standards, such as Wireless Local Area Network (WLAN) (IEEE 802.11n for WiFi), Wireless Metropolitan Area Networks (WMAN) (IEEE 802.16e for WiMAX), and Wireless Wide Area Networks (WWAN) (Fifth Generation (5G) cellular systems).

Following a general presentation of wireless local networks, we delve into the communication chain, specifically focusing on the propagation channel. This approach enables us to comprehend the phenomena upon which various multi-antenna techniques are grounded. Moreover, we explore the integration of reconfigurable antenna technology with MIMO systems, offering increased flexibility to adapt to the changing needs of wireless applications. Finally, the chapter concludes with a state-of-the-art overview of reconfigurable MIMO antennas.

1.2 Wireless networks

The constant evolution of wireless technologies significantly alters the way humans live, work, and entertain themselves. The success achieved at the consumer level can be attributed, in comparison with wired communication, to the mobility it offers and the availability of convenient connectivity. Additionally, wireless networks are generally easy to deploy and can connect users in hard-to-reach areas. This section provides an overview of wireless communication systems. Wireless communication networks are often classified based on their size, service type, and data transmission rate. According to these criteria, a wireless communication network falls into one of the following categories: Wireless Personal Area Networks (WPANs), Wireless Local Area Networks (WLANs), Wireless Metropolitan Area Networks (WMANs), and Wireless Wide Area Networks (WWANs).

• Wireless personal area networks (WPANs)

WPAN networks cover a small area extending a few tens of meters around the user [7], facilitating the interconnection of personal devices. The technologies within these networks adhere to standards specified by the IEEE 802.15 (Institute of Electrical and Electronics Engineers) and Home RF (Home Radio Frequency) [7]. Compared to a wired connection, they offer great flexibility in usage. Figure (1.1) illustrates the main technologies used in this network category, which operate in the unlicensed ISM (Industrial, Scientific, and Medical) band at 2.4 GHz and 868 – 928 MHz for ZigBee.

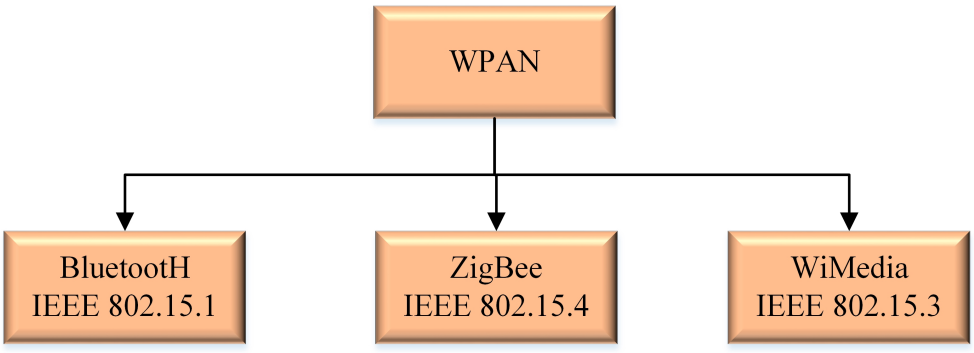

Figure 1.1: The main technologies used in WPAN [7]

• Wireless local area networks (WLANs)

Wireless local area networks (WLANs) cover an area ranging from a few meters to a few hundred meters. They are designed to complement wired local networks. The most well-known wireless networks are specified in the IEEE 802.11 standard. Other wireless local networks include the European standard HiperLAN (High-Performance Radio LAN) and the Japanese standard HiSWAN (High-Speed Wireless Access Network). A WLAN standard is defined by its central frequency, bandwidth, maximum theoretical data rate, and modulation type [8]. In the IEEE 802.11 standard, several protocols have been implemented, as shown in table (1.1). In addition to the protocols listed in the table, the IEEE 802.11e standard was developed to provide Quality of Service (QoS) improvements, and the IEEE 802.11i standard was developed to enhance security [7].

Table 1.1: Specifications of protocols implemented for the IEEE 802.11 standard [7]

Protocol	**Frequency (GHz)**	**IBW (MHz)**	**Data rate (Mbps)**	**Modulation**	**Coverage (m)**
IEEE802.11b	2.4	22	11	BPSK, QPSK	100
IEEE802.11a	5	20	54	OFDM	50
IEEE802.11g	2.4	20	54	BPSK, QPSK 16QAM,64QAM	50
IEEE802.11n	2.4 / 5	20 / 40	300	smart coding	100

For The HiperLAN standard which is an ETSI (European Telecommunications Standards Institute) operating at 5 GHz, it directly competes with the IEEE 802.11a standard. Specifically designed for office networks, it offers a throughput of 54 Mbit/s over distances of 50 to 100 meters [8].

• Wireless metropolitan area networks (WMANs)

Wireless Metropolitan Area Networks (WMANs) are network types primarily aimed at providing high-speed wireless access over a larger geographical area than WLANs, potentially spanning up to the scale of a city. Their main advantage lies in their quick deployment and relatively low cost. They serve as an alternative to cables for connecting

users in areas where cable deployment is challenging [9].

These network types are outlined in the IEEE 802.16 standards, also recognized as WiMAX (Worldwide Interoperability for Microwave Access). The various IEEE 802.16 standards developed to operate without Line of Sight (LoS) propagation, and use multi-carrier modulation such as OFDM (Orthogonal Frequency Division Multiple Acces) [10].

• Wireless Wide Area Networks (WWANs)

Wireless Wide Area Networks (WWANs) are networks that incorporate cellular mobile technologies. These networks include GSM (Global System for Mobile communication), UMTS (Universal Mobile Telecommunication System), GPRS (General Packet Radio Service), and LTE (Long Term Evolution) networks. They have undergone rapid evolution over the past three decades, with advancements categorized into “generations”. Figure (1.2) shows the specific characteristics of the different generations of mobile communication systems [11].

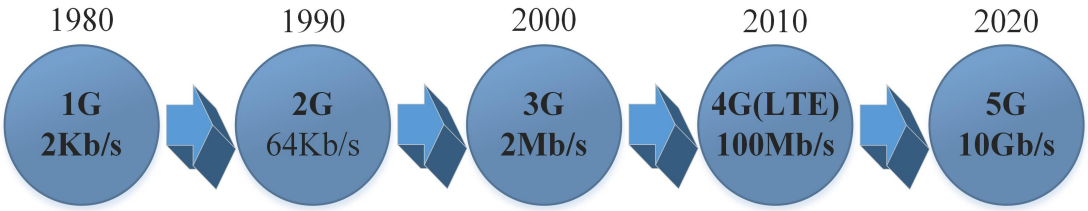

Figure 1.2: Various generations of mobile communication systems [11]

The fifth generation (5G) of wireless communication technology offers higher data rates, lower latency, increased network capacity, and a high reliability compared to fourth generation (4G) systems. One of the most discussed technologies these days is 5G new radio (NR). Due to the limited bandwidth available in the microwave sector, along with high latency and restricted data rates, there is a rapidly increasing demand for more efficient use of this technology. Third generation partnership project (3GPP) after taking rigorous studies has enlisted the spectral bands suitable for the deployment of 5G NR technology. The band lies from 400 MHz to 6.0 GHz specified as FR1 (frequency range 1) or sub-6-GHz band, and from 24 to 100 GHz referred as FR2 (frequency range 2) or mm-wave band [11]. FR1 combined of "medium" and "low" frequencies as shown in figure (1.3).

The medium band (1 −6 GHz) are suitable to deliver the best compromise between wide-area coverage and good capacity. However, spectrum below 1 GHz providing wide-area coverage. Higher frequencies (mm-wave band) will be essential to provide additional capacity and ensure the very high data rates required for certain 5G applications [12]. Table (1.2) defines the new bands and the agreed sharing combinations of LTE-NR for 5G NR in FR1 and FR2 according to 3GPP.

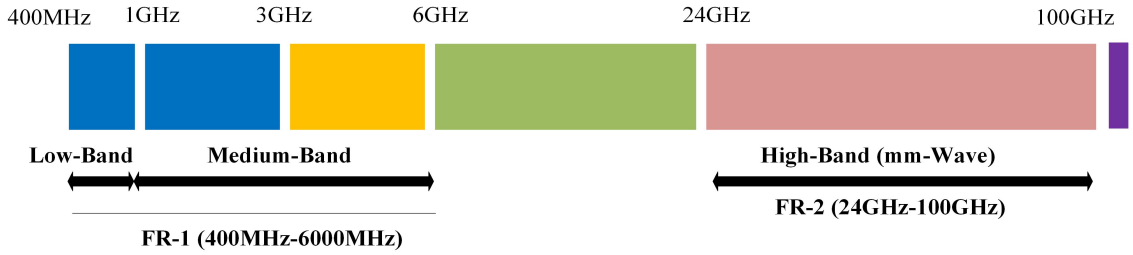

Figure 1.3: Spectral Bands for 5G NR Technology [11]

Table 1.2: 5G NR bands specified in 3GPP [13]

bands	NR operating band	Operating band (MHz)
FR I for 5G-NR	n77	3300 - 4200
	n78	3300 - 3800
	n79	4400 - 5000
FR I for LTE/5G-NR	n1	1920-1980
	n2	1850-1910
	n3	1710-1785
	n5	824-849
	n7	2500-2570
	n8	880-915
	n12	699-716
	n20	832-862
	n25	1850-1915
	n28	703-748
	n34	2010-2025

	n38	2570-2620
	n39	1880-1920
	n40	2300-2400
	n41	2496-2690
	n50	1432-1517
	n51	1427-1432
	n66	2496-2690
	n70	1695-1710
	n71	663-698
	n74	1427-1470
FR II for 5G-NR	n257	26500 - 29500
	n258	24250 - 27500
	n260	37000 - 40000
	n261	27500 - 28350

1.2.1 The communications chain

• General Architecture

Transmitting information between two geographically separated points generally requires a transmitter to adapt the data for transmission through the medium and a receiver for the recipient to intelligibly receive the data. Wireless communication utilizes electromagnetic waves as its medium, thus heavily relying on the communication environment. An example communication chain is illustrated in figure (1.4). It is considered bidirectional (full duplex) [14].

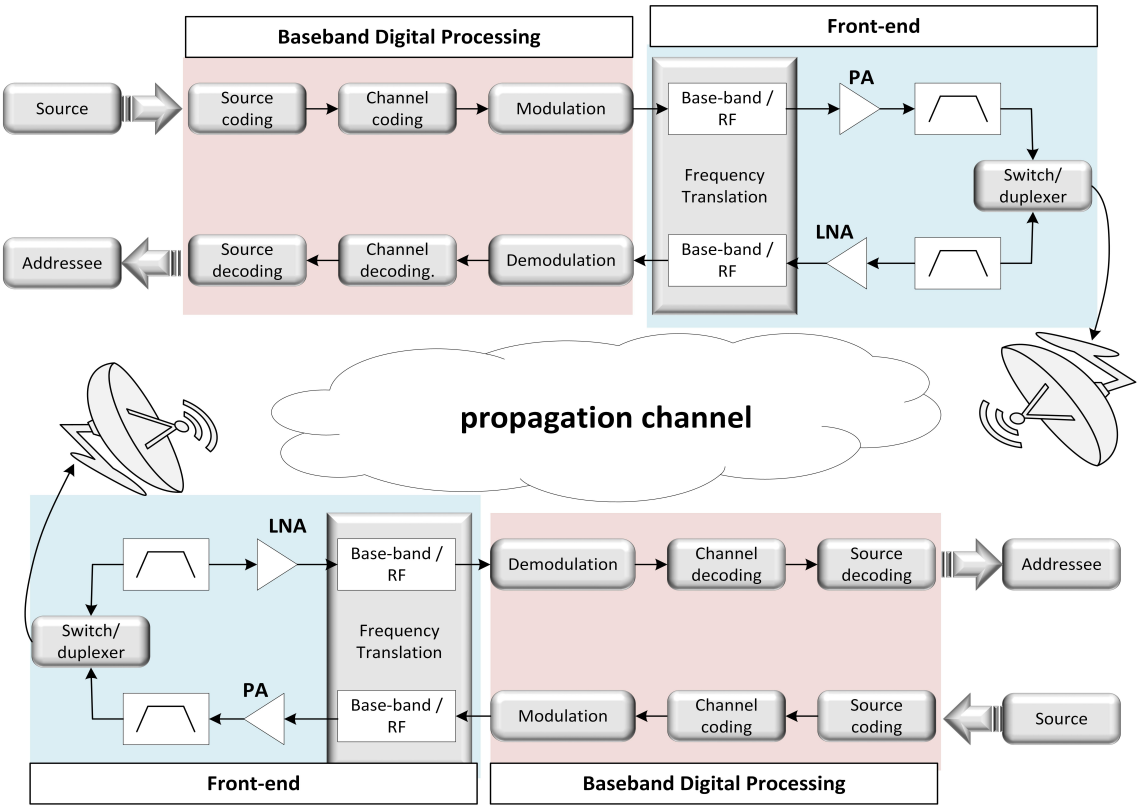

Figure 1.4: Functional Architecture of a Communication Chain

The communication chain comprises the transmitter, transmission channel, and receiver. Through processing, the transmitter adapts the information for transmission, regardless of its nature, to the transmission channel. The receiver, in turn, performs the reverse operation and provides the message to the recipient. The transmission channel commonly consists of the propagation channel, antennas, front-ends, as well as modulation/demodulation and frequency translation stages. The propagation channel (or radio-electric channel) represents the environment in which the transmitted signal evolves. Consequently, it heavily influences communication performance. This is why the following section provides a detailed description of it.

• The propagation channel

The propagation environment plays a crucial role in shaping the characteristics of the emitted electromagnetic wave. Unlike scenarios involving multiple paths, in free space where obstacles are absent, the wave travels directly from the transmitter to the

receiver, presenting an ideal scenario. The Friis transmission equation expresses the received power (P_r) in relation to the transmitted power (P_e), the gains of the transmitter (G_e) and receiver (G_r), their propagation distance, and the wavelength [14].

$$P_r = P_e G_e G_r (\frac{\lambda}{4\pi d})^2 \tag{1.1}$$

This formula is valid when the receiving antenna is considered to be in the far-field of the transmitting antenna, meaning that the distance 'd' between the antennas is greater than the Fraunhofer distance d_F, which is linked to the largest dimension 'D' of the transmitting antenna by:

$$d_F > \frac{(2D^2)}{\lambda} \tag{1.2}$$

However, in reality, the propagation channel is a space composed of multiple paths due to the obstacles surrounding the transmitter and the receiver as shown in figure (1.5). In this case, several replicas of the transmitted signal reach the receiver through multiple paths, each with different states of attenuation, phase shifts, and delays due to the length of the path. Depending on the nature of the objects encountered during the course of multiple paths, various electromagnetic phenomena are observed, such as reflection, diffraction, and scattering on obstacles [15], [16].

Figure 1.5: Multipath propagation in free space

The RF signal power transmitted between two antennas, which is attenuated through space due to multipath effects, can impact reception performance. The attenuation of power between the transmitter and the receiver is attributed to several phenomena, including [15]:

- **Slow fading:** or path loss caused by obstacles encountered along the path (buildings, mountains, etc.). It represents the attenuation experienced by a wave as it travels the distance between the transmitter and the receiver.

- **Fast fading :** is an attenuation that irregularly varies between maximum and minimum values. The user moves through areas with obstacles of various sizes that can completely attenuate the signal, such as buildings, tunnels, and more.

- **Rayleigh fading:** leads to irregular and unpredictable variations in the signal, making it challenging to account for. It is particularly prevalent in urban areas. Different versions of the same signal, with varying phases and amplitudes, may reach the receiver with a cumulative or subtractive effect after following various paths.

We have seen previously that for a propagation channel, the transmitted signals suffer several phenomena during their transmission, causing fading at both small and large scales. To effectively exploit multipath effects, another commonly used solution is the diversity technique. This consists of repeating the transmission of the same message via several different paths with independent fading statistics.

1.3 Multi antenna system

The majority of wireless communication devices operate in demanding environments, often characterized by considerable distances between the base station and the mobile unit. The various types of transmission are therefore strongly affected by multipath environments. To solve the signal fading problems inherent in these multipath scenarios and to improve the performance of wireless communications in these demanding environments, the use of diversity techniques and MIMO (multiple-input, multiple-output) technology is crucial.

1.3.1 MIMO System

Wireless communication systems are demanding higher transmission capacity to enhance data transmission. In conventional communication systems, a single antenna is employed, resulting in communication occurring between one transmitting antenna and

another receiving antenna (SISO), as depicted in figure (1.6). Consequently, to address the growing demands and requirements for enhanced capacity in traditional SISO systems, both bandwidths and power levels have been significantly increased [17].

Figure 1.6: General Model of traditional SISO systems [17]

Then, more advanced studies have demonstrated that employing multiple antennas for both transmission and reception can increase data transmission rates without enlarging either the antenna bandwidth in SISO systems or the signal power during transmission. This transmission technique is called MIMO (Multiple Input, Multiple Output), a general model of the MIMO system is depicted in figure (1.7) where Tx represents multiple transmitting antennas, Rx represents multiple receiving antennas. The various propagation channels created through reflection and/or diffraction of waves in a multipath environment can be exploited by a MIMO system to enhance transmission capacity. Obtaining independent signals across antennas becomes advantageous in this context [18].

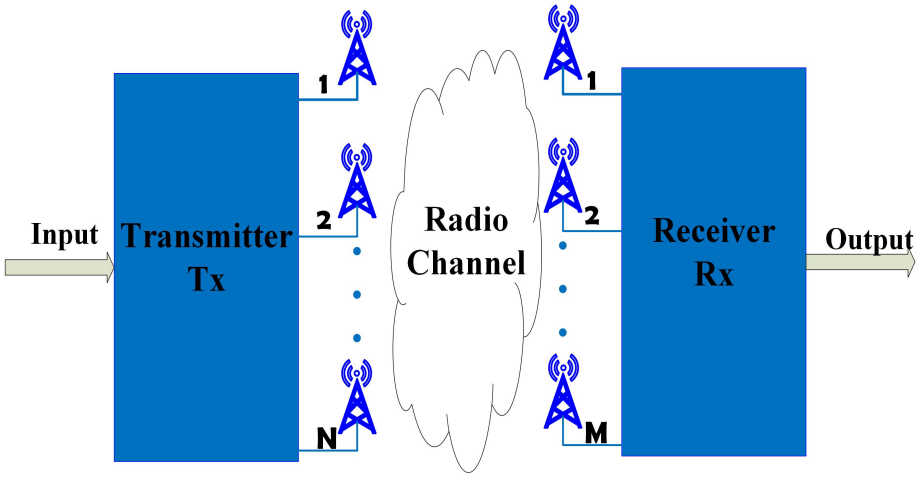

Figure 1.7: General Model of the MIMO systems with N transmit antennas and M receive antennas [18]

The initial studies were conducted in Bell Laboratories [1], [2], and since then, MIMO

systems have attracted particular interest in the scientific community. Indeed, they provide a means to combat signal fading and achieve significant spectral efficiencies. By employing spatial multiplexing, the spectral efficiency of MIMO systems can increase while using the same modulation for transmitted symbols and the same frequency band. Consequently, the bandwidth remains unchanged, and spectral efficiency is enhanced. MIMO technology provides a diverse range of benefits and advantages that enhance and optimize wireless performance [17], [18], [19]:

- **Improved Data Rates:** MIMO antennas enable faster data transfer rates by transmitting and receiving multiple data streams simultaneously over the same frequency band;
- **Increased system Capacity :** Utilizing numerous antennas enables multiple users to transmit and receive data concurrently, thereby enhancing the capacity of the wireless network;
- **Better Range and Coverage:** MIMO technology uses intelligent signal processing techniques to improve signal range and making it more resistant to interference, this leads to expanded network coverage and enhanced performance across the wireless network;
- **Enhanced Reliability:** With its ability to mitigate the efects of interference and signal fading, resulting in communication that is more reliable;
- **Improved Power Efficiency :** MIMO technology can allows for a high energy efficiency by using beamforming techniques to focus the transmitted power, which can reduce the interference and optimizes power consumption of the system;
- **Security of the system:** The intentional user is protected through the use of beam steering in the transmitted signal. Consequently, the risk of signal loss is minimized in a MIMO system compared to SISO systems.

1.3.2 Diversity

Diversity is a technique for combining the multipath signals present in a mobile communication channel to attenuate fading and improve the overall quality of the radio link.

The basic principle is that the receiver combines more than one copy of the transmitted signal, with each copy being received by a different branch. This means that the receiver will have several copies of the signal received on independent channels.

Figure (1.8) shows two fading signals received by a receiver and their combined signal. Since the signals are independent, they are less likely to fade at the same time, so the combined signal obtained by selecting the best SNR is of better quality (higher average output SNR of a single branch) [20] , [21].

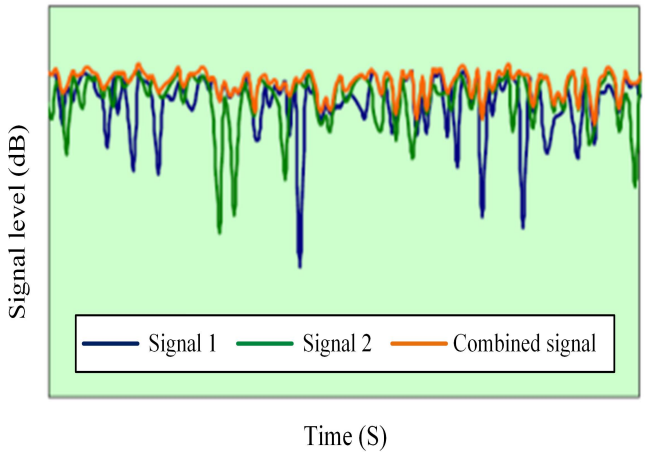

Figure 1.8: Illustration of two signals received individually and the combined signal [20]

Presently available mobile devices require the MIMO antennas for high capacity and high data rate applications. However, the close proximity of radiators in a MIMO leads to the degradation in antenna performance parameters. Consequently, far-field gain, efficiency, correlation, and current distribution require the high attention for the desired quality of user services. These effects are controlled using antenna diversity. It allows guard against fading paths, resulting in an increase in the overall signal-to-noise ratio (SNR) of the communication. Furthermore, a judicious recombination of signals from each antenna allows for an increase in instantaneous SNR: the useful information received by the antennas is a priori identical, while the noise on each antenna is theoretically independent. In this context, it is possible to define several forms of diversity: spatial, polarization and pattern diversity.

• Spatial Diversity

This represents the most essential method for attaining diversity [22]. It employs multiple antenna systems that need to be adequately spaced apart to ensure significant differences in the relative phases of multipath contributions across the various antennas figure (1.9). By placing two identical antennas sufficiently apart, the received signals exhibit a phase difference that renders them independent. Consequently, the probability of simultaneous fading for both signals is minimized. While this technique is effective, it presents a challenge in terms of overall dimensions. In theory, the antennas need to be spaced at least half a wavelength apart for the received signals to be considered independent. This can be problematic in situations with limited space, prompting the exploration of alternative diversity techniques.

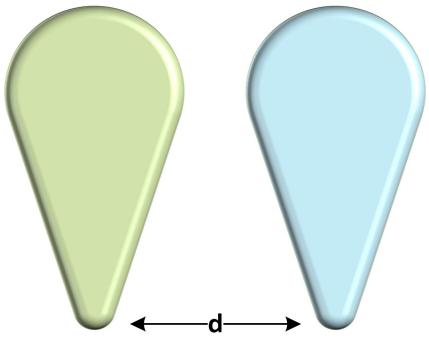

Figure 1.9: Antenna with spatial diversity

• Pattern Diversity

Spatial diversity often demands significant physical space, which may not always be readily available. In cases where adequate space is limited, the MIMO system can employ pattern diversity as an alternative [23]. Also referred to as angle diversity, pattern diversity achieves the necessary diversity gain through the utilization of distinct beams figure (1.10). Various studies describe pattern diversity as a natural extension of traditional orthogonal polarization diversity, as the orthogonal nature between patterns helps in signal decorrelation [24].

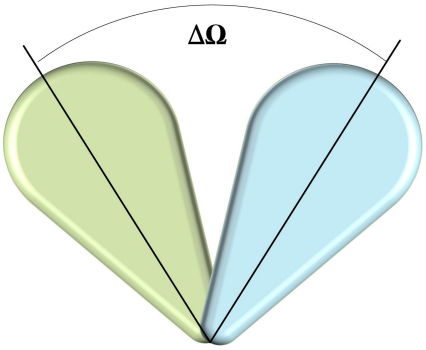

Figure 1.10: Antenna with pattern diversity

• Polarization diversity

Polarization diversity involves using radiating elements with two orthogonal polarizations [25]-[26], as shown in figure (1.11). Antennas with orthogonal polarizations exhibit low correlation levels with minimal spacing [27]. Therefore, the space constraint encountered in the previous type of diversity is no longer an issue, as the received signals are naturally uncorrelated. This significantly reduces the size of the antenna system, many studies on polarization diversity have been carried out at base stations and have been widely applied in practice to new base stations, resulting in space and cost savings [28], [23]. In [29], it has been reported that combining polarization diversity with the spatial diversity discussed earlier results in even better diversity performance.

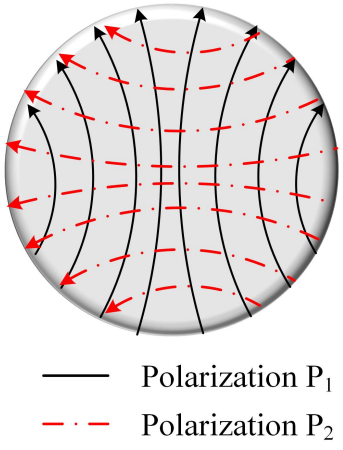

Figure 1.11: Antenna with polarization diversity

1.3.3 Mutual Coupling Reduction Techniques

For an effective MIMO antenna system, it is crucial to maintain low mutual coupling between the antennas (the terms coupling and isolation are often interchanged in literature, as low coupling yields high isolation). Poor isolation results in some of the energy fed or received by one port coupling to the other, degrading antenna and system efficiency, as the coupled power is effectively lost from the receiving path [30], [31]. Therefore, port isolation is vital in MIMO antenna systems. The system and antenna designer should always check for port isolation, and values exceeding 15 dB are considered to provide acceptable isolation. Various simple and cost-effective techniques have been documented in the literature that target MIMO antenna isolation improvement [32], [33]. These techniques include the use of defected ground structure (DGS), parasitic elements, neutralization lines, Antenna placement and orientation, metamaterial (MTM), electromagnetic band gap (EBG) structures.

In this section, we review each technique, present its characteristics, and give some implementation examples from the literature that show how each antenna is utilized and its effect on MIMO antenna performance.

• Antenna placement and orientation

Arranging radiating components in various locations or directions is one of the fundamental techniques to reduce mutual coupling. In the literature review of mutual coupling reduction techniques, the arrangement of antenna elements is predominantly orthogonal figure (1.12). For example in reference [34], to enhance the isolation of the designed two-port rectangular monopole antenna with arrow-shaped slot etching on each radiating element, angular variation techniques, and distinct ground planes were employed to achieve increased isolation. In other examples, a high isolation is achieved for the designed two-element MIMO antenna in [35] by tuning the distance between them without additional decoupling structure. Furthermore, for better isolation and polarization diversity, the four coplanar waveguide fed radiating elements were placed orthogonally to each other in [36], [37].

(a) [34]

(b) [35]

(c) [36]

(d) [37]

Figure 1.12: different locations or directions for antenna elements : (a) [34], (b) [35], (c) [36], and (d) [37]

• Parasitic Elements (stubs / slots)

This technique involves the use of stubs/slots to achieve improved isolation between radiating elements. One or more stubs/slots are inserted to create opposing coupling paths, and enhancing isolation figure (1.13). The method is simple, compact, and readily applicable in PCB (Printed Circuit Board) technology. Various types of decoupling stubs are used for isolation, such as F-shaped [38], and T-shaped [39] stubs, which are incorporated within the common ground plane of the proposed antennas to achieve significant isolation between the MIMO antenna elements. However, in [40], the parasitic decoupling structure consists of three open-ended slots (a wide slot and a pair of narrow slots). These slots essentially perturb the surface current distribution at the ground plane in such a manner that the electromagnetic energy coupling between ports is reduced and good isolation is achieved. In addition, parasitic components including a T-shaped ground stub with a vertical slot inserted between the two square monopole antennas are used to reduce mutual coupling to below -15 dB [41].

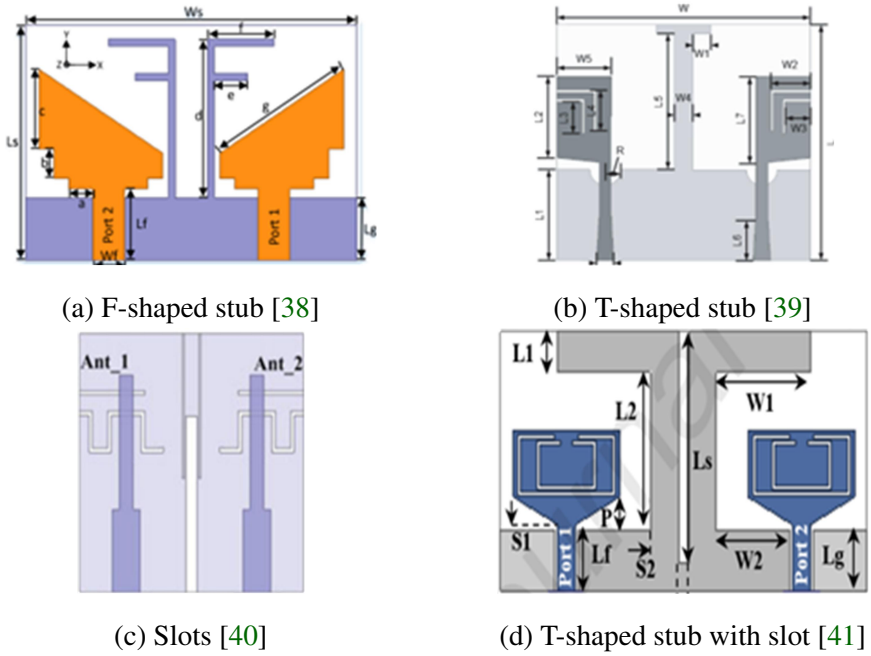

(a) F-shaped stub [38]

(b) T-shaped stub [39]

(c) Slots [40]

(d) T-shaped stub with slot [41]

Figure 1.13: Decoupling using Parasitic Elements: (a) [38], (b) [39], (c) [40], (d) [41]

• Defected Ground Structures (DGS)

The Defected Ground Structure (DGS) plays a crucial role in increasing isolation between elements. The current generated on the ground plane can lead to high coupling with adjacent elements, intensifying isolation challenges in MIMO antenna systems. This coupling can be mitigated by modifying the ground plane, effectively employing DGS as a band-stop filter figure (1.14). By reducing the current on the ground substrate, DGS inhibits coupled fields between adjacent antenna elements. In [42], two antenna elements are arranged in an orthogonal configuration. Additionally, the antenna incorporates two ground slots positioned orthogonally to achieve substantial isolation. To further enhance isolation between antenna elements, a narrow rectangular slot with a length equal to $\lambda_g/4$ is cut into the ground surface. In [43], a Vivaldi MIMO antenna design with a modified ground surface and dual microstrip line feedings is presented. The introduction of a T-slot in the ground plays a pivotal role in significantly augmenting port isolation. In [44], a DGS are created by etching symmetrical square slots and half-rings in the bottom layer of the proposed four elliptical monopoles placed orthogonally, this technique lessen the return loss of the MIMO antenna to 22 dB for the whole operating band $(2-16\,\text{GHz})$.

In [45], T-shaped and narrow slots are added to the ground plane to implement the DGS feature. The T-shaped slot suppresses surface current and diverts its direction, while the narrow slot provides better isolation at the lower resonant frequency of 3 to 4 GHz.

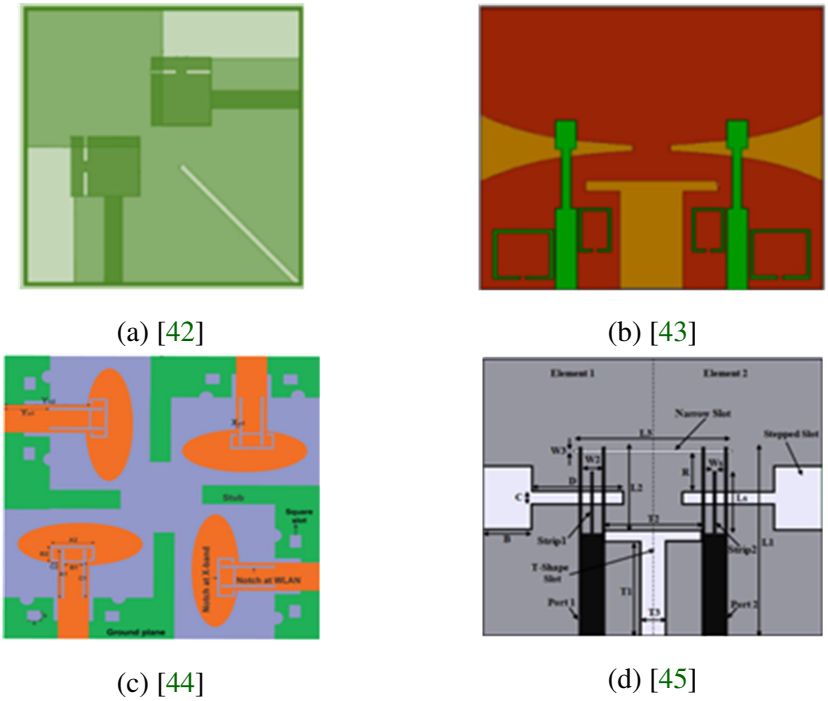

(a) [42] (b) [43]

(c) [44] (d) [45]

Figure 1.14: Decoupling using defected ground structures: (a) [42], (b) [43], (c) [44], and (d) [45]

• Neutralization Line (NL)

A neutralization line is a small-width metal structure that resolves matching issues and enhances isolation between antenna elements by creating an additional current path in dual antenna elements of MIMO systems. The shape, size, and orientation of the neutralization line depend on the specific antenna elements. This structure is simple and easy to implement,as depicted in figure (1.15). However, determining an appropriate path for neutralization can be challenging. In the study referenced as [46], to enhance isolation a Neutralization Line (NL) was introduced between the two antenna elements, comprising two conducting strips and a circular disc. The circular disc facilitated multiple decoupling current paths of varying lengths, effectively canceling the coupling current on the ground plane. Consequently, the implementation of this configuration led to the attainment of

wideband isolation. In addition [47], the design of a four-element MIMO antenna involved the integration of a semi-circular patch along with a modified rectangular patch. A pair of antennas were combined with neutralization lines to improve the isolation between the two ports. Moreover, the multi-NL structure can also be applied to multi-band MIMO. The two U-shaped lines corresponding to different frequency decoupling were proposed in [48]. The U-shaped neutralization line (NL) connects with two microstrip lines enhancing isolation in the high-frequency band, and the inverted U-shaped NL, in contact with two radiation patches, achieves decoupling in the middle-frequency band.

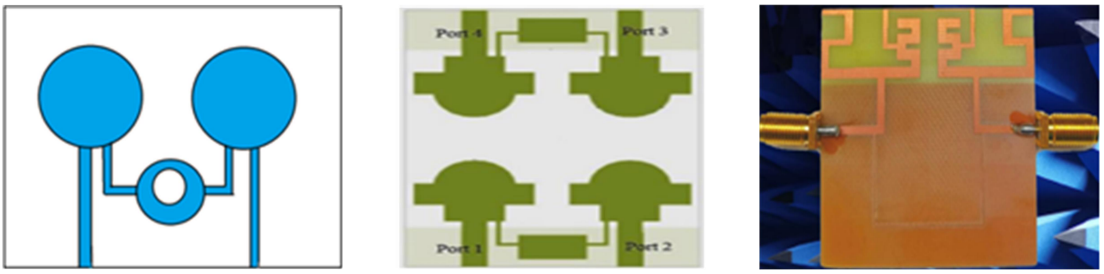

(a) [46] (b) [47] (c) [48]

Figure 1.15: Neutralization Line: (a) [46], (b) [47], and (c) [48]

• Metamaterials

Metamaterials represent an artificial structural approach to effectively reduce mutual coupling by influencing the transmission of electromagnetic (EM) waves. The design of metamaterial structures involves creating negative permeability or permittivity or both, depending on specific requirements. The split-ring resonator (SRR) and complementary split-ring resonator (CSRR) are widely used metamaterials for isolation enhancement, and they come in various shapes, as shown in figure (1.16). For instance, in [49], a slotted complementary split-ring resonator (CSRR) is integrated into the ground plane to improve the isolation of 33 dB for the suggested 2-elements MIMO antennas. In [50], a metamaterial based on SRR was placed in the top layer of the proposed multiband 4-ports MIMO antenna, achieving an isolation better than 15 dB for the third operating band at 5.1 GHz. Additionally, in [51], a metamaterial structure was placed on both sides of the feed line for mutual coupling reduction and bandwidth improvement.

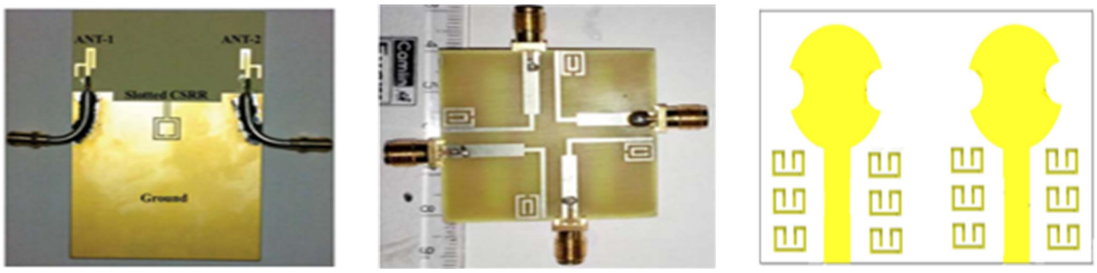

(a) [49] (b) [50] (c) [51]

Figure 1.16: Decoupling using metamaterials: (a) [49], (b) [50], and (c) [51]

• Electromagnetic band gap (EBG)

The Electromagnetic Band Gap (EBG) structures are metallic or dielectric elements arranged periodically, exhibiting one or more frequency band gaps. EBG structures are employed to reduce mutual coupling; however, they are complicated and require a large structure figure (1.17). In [52], the Mushroom EBG structure acts as a parasitic element and it is integrated between two antenna elements that support either Transverse Electric (TE) or Transverse Magnetic (TM) waves and function as a band-notch filter. A mushroom EBG structure can be viewed as equivalent to a parallel LC resonant circuit, with capacitance introduced from the gap and inductance from the current along neighboring cells. This configuration prevents surface waves from propagating, thereby reducing coupling between antenna elements. In [53], a configuration involving a four-element Electromagnetic Band Gap (EBG) array was introduced between two antenna elements. The EBG array manifested multiple stop bands effectively suppressing undesired surface waves with an isolation improvement of 18 dB. In [54], an EBG configuration resembling a mushroom, featuring distinct square plates positioned at both the top and bottom layer of the designed two-port rectangular patch antenna. This EBG structure resulting in excellent isolation of -55 dB and -25 dB in both operating bands 2.4 and 5.2 GHz bands, respectively. In [55], to achieve the best radiation performance for the designed microstrip MIMO antenna, with minimal inter-element spacing and mutual coupling, eight EBG cell elements arranged in two columns between the two ports are used to provide the lowest mutual coupling of 25 dB.

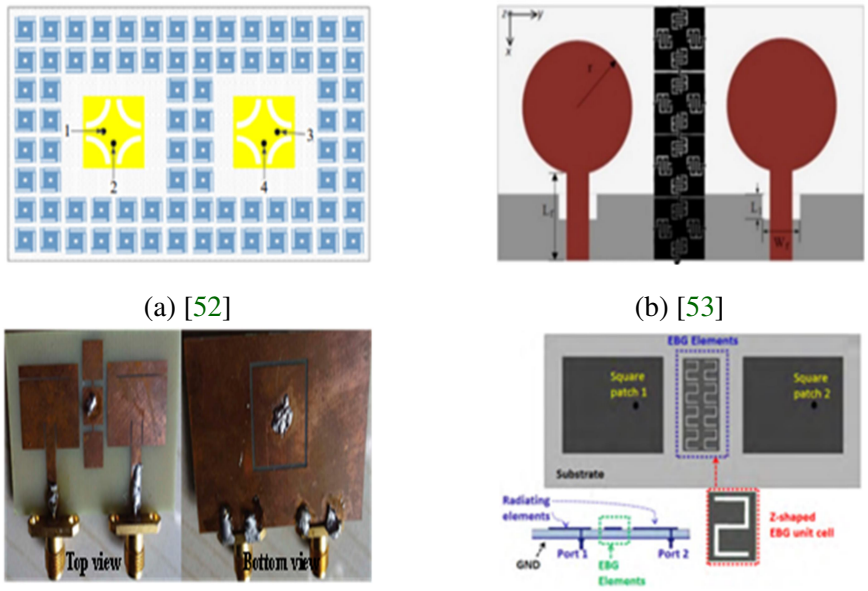

(a) [52] (b) [53]

(c) [54] (d) [55]

Figure 1.17: Decoupling using electromagnetic band gap (EBG): (a) [52], (b) [53], (c) [54], and (d) [55]

Table (1.3) summarize the advantages and drawbacks of the presented techniques.

Table 1.3: Different methods for mutual coupling reduction [33]

Technique	Role	Advantages	Drawbacks
Neutralization line	The current from the adjacent radiating element is cancelled by taking the current at a precise position on the radiating element and inverting its phase	Strong impedance matching, good diversity gain, and simple construction	The selection of connection locations is challenging, and the bandwidth is limited
Antenna placement and orientation	Arranging the radiating components in various locations or directions	Simple, good isolation	Requires larger space and results in poor polarization

Parasitic elements (stubs / slots)	Lowers the initial coupling field by generating an opposite coupling field	Reduced ohmic loss due to simple construction and strong diversity gain	Reduced antenna efficiency may result from the change in operating frequency
Defected ground structure (DGS)	Between the radiating elements, the flaw in the ground structure acts as a band-stop filter	Reduced size, multiband or wideband benefits, and improved BW	Reduces back-lobe radiation and antenna gain
Metamaterial	Reduces coupling at that band by creating a stop band at a specific frequency	Increasing gain, channel capacity, and improved BW	Narrow bandwidth and poor antenna efficiency are caused by the need to describe the unit cell attributes
Electromagnetic band gap (EBG)	Acts as a band-stop filter	better channel independence, increased system capacity	Complicated structure and increases antenna size

1.3.4 Diversity performance

In order to ensure the quality of a MIMO antenna, in addition to S-parameters and radiation characteristics, certain diversity parameters are used. The MIMO antennas must satisfy the predefined values of the diversity parameters for practical applications. Therefore, some basic diversity parameters for MIMO antennas are mentioned in this section [33], [56].

• Envelope Correlation Coefficient (ECC)

The correlation coefficient (ρ) is a measure that describes how much the communication channels are isolated or correlated with each other. This measure takes into account the radiation pattern of the antenna system and the influence of the patterns on each other when operating simultaneously (as is the case in a MIMO antenna system). The square of the correlation coefficient is called the envelope correlation coefficient. The envelope correlation coefficient (ρ_e) can be calculated using equation (1.3) [57],[58].

$$ECC = \rho_{\mathrm{e}} = |\rho|^2 = \frac{|\iint_{4\pi}[\overrightarrow{\mathrm{F_1}}(\theta,\varphi) * \overrightarrow{\mathrm{F_2}}(\theta,\varphi)\Big]\, \mathrm{d}\Omega|^2}{\iint_{4\pi}\left|\overrightarrow{\mathrm{F_1}}(\theta,\varphi)\right|^2 \mathrm{d}\Omega \iint_{4\pi}\left|\overrightarrow{\mathrm{F_2}}(\theta,\varphi)\right|^2 \mathrm{d}\Omega} \tag{1.3}$$

Where $\left(\overrightarrow{\mathrm{F_1}}(\theta,\varphi)\right)$ is the antenna's three-dimensional radiation pattern when the i^{th} port is excited, Ω is the solid angle, and $(*)$ is the Hermitian product operator. This is a complicated expression that requires measurements of the three-dimensional radiation pattern and numerical integration (requires very precise estimation of the radiation patterns and thus leads to heavy calculations). Another simplified solution is to calculate the correlation envelope using the S parameters [39], [40] (suitable for lossless antennas that have radiation efficiency near 100%). In the case of an N-antenna system, equation (1.4) can be used as follows [58]:

$$ECC = \left|\rho_{\mathrm{ij}}\right|^2 = \rho_{\mathrm{eij}} = \frac{\left|S_{ii}^* S_{ij} + S_{ji}^* S_{jj}\right|^2}{\left(1 - \left|S_{ii}\right|^2 - \left|S_{ji}\right|^2\right)\left(1 - \left|S_{jj}\right|^2 - \left|S_{ij}\right|^2\right)} \tag{1.4}$$

Here, ρ_{ij} represents the correlation coefficient between elements i and j, ρ_{eij} is the envelope correlation coefficient, and S_{ij} denotes the S parameter indicating coupling between the ith and jth elements. This formula requires only the knowledge of S-parameters which are relatively straightforward to assess compared to the three-dimensional radiation patterns needed for equation (1.3). To improve MIMO performance, the ECC value should be below 0.5 [38].

It is important to note that isolation and correlation coefficients are different things. Equation (1.4) tells us that having less coupling (or higher isolation) between antenna input ports reduces correlation, but this only considers the antenna's structure, not the

radiated fields. Equation (1.3), on the other hand, does account for radiated field coupling. Therefore, just having low coupling (high isolation) does not necessarily mean you will have a low correlation coefficient, and vice versa. For a MIMO antenna system to work well and provide good diversity performance, you need both high isolation and low correlation coefficients.

• Diversity Gain (DG)

Diversity is usually achieved when the receiver takes multiple versions of the input signal via different propagation channels since multiple antennas are present. If the signals are not correlated to each other, the combined signals at the receiver will offer a better Signal-to-Noise Ratio (SNR) level, and thus better signal reception is obtained. Diversity gain is a measure of the effect of diversity on the communication system. It is defined as the ratio of the SNR of multiport MIMO antenna system to the SNR of single-port antenna system. The value of diversity gain can also be obtained from the ECC value [33]:

$$DG = 10\sqrt{1-(ECC)^2} \tag{1.5}$$

As a result, diversity gain and ECC are inextricably linked. A higher diversity gain value can be achieved by decreasing the ECC values. In practical applications, a diversity gain value of around 10 is acceptable for improving MIMO performance.

• Channel Capacity Loss (CCL)

Is the maximum level transmission rate for which the signal can be transmitted over the MIMO antenna system, it can be defined using the s-parameters in particularly, the value of CCL should be less than 0.4bit/s/Hz [59]. The CCL can be calculated using the following equation (1.6).

$$CCL = -\log_2 \det\left(\alpha^R\right) \tag{1.6}$$

Where

$$\alpha^R = \begin{bmatrix} \alpha_{11} & \alpha_{12} \\ \alpha_{21} & \alpha_{22} \end{bmatrix} \tag{1.7}$$

And

$$\alpha_{ii} = 1 - \left(|S_{ii}|^2 + |S_{ij}|^2\right) \tag{1.8}$$

$$\alpha_{ij} = \left(S_{ii}^{*} S_{ij} + S_{ji}^{*} S_{ij}\right) \tag{1.9}$$

• Mean Effective Gain (MEG)

The Mean Effective Gain (MEG) represents the average power received by antennas to the average incident power of the antenna system. It takes into account antenna radiation patterns, efficiency, and propagation effects, thus establishing a crucial link between the correlation envelope and the multipath environment. The mathematical expressions for the mean effective gain calculation are shown in equations (I.10) [33]:

$$MEG = \int_0^{2\pi} \int_0^{\pi} \left[\frac{XPD}{1+XPD} G_\theta(\theta,\varphi) P_\theta(\theta,\varphi) + \frac{1}{1+XPD} G_\varphi(\theta,\varphi) P_\varphi(\theta,\varphi) \right] \mathrm{d}\Omega \tag{I.10}$$

$$XPD = \frac{P_V}{P_H} \tag{I.11}$$

Where XPD is the cross-polarization power ratio, which represents the distribution of the ratio between the vertical mean incident power to the horizontal mean incident power, $\mathrm{G}_\theta(\theta,\varphi)$ and $\mathrm{G}_\varphi(\theta,\varphi)$ are antenna gain components, and $\mathrm{P}_\theta(\theta,\varphi)$ and $\mathrm{P}_\varphi(\theta,\varphi)$ represent the statistical distribution of the incoming waves in the environment. This numerical method is very timeconsuming and costly, other simple equations used to calculate the MEG have been proposed in [58]. In that case, MEG can be simplified and it would be 50% of the total antenna efficiency as depicted in equation (I.12).

$$MEG_i = 0.5\mu_{irad} = 0.5\left(1 - \sum_{j=1}^{N} \left|s_{ij}\right|^2\right) \tag{I.12}$$

Here N is the number of antennas, i is the active antenna, and μ_{irad} radiation efficiency of i^{th} antenna. The MEG values for two MIMO antenna elements are found using the below equation (I.13) and (I.14):

$$MEG_1 = \left(1 - |s_{11}|^2 - |s_{12}|^2\right) \tag{I.13}$$

$$MEG_2 = \left(1 - |s_{12}|^2 - |s_{22}|^2\right) \tag{I.14}$$

The value of MEG should be less than -3dB and must be greater than -12dB ($-12\text{dB} \leq \text{MEG} \leq -3\text{dB}$) for achieved a good diversity performance [58].

• Total Active Reflection Coefficient (TARC)

For MIMO antenna systems, adjacent antenna elements influence each other and when operating simultaneously affect the overall operating bandwidth and efficiency. Consequently, basing predictions only on the S-parameters may not reflect the complete behavior of the system. A new measure, called Total Active Reflection Coefficient (TARC) was introduced to take account of this effect in [60]. TARC is defined as "the ratio of the square root of the total reflected power divided by the square root of the total incident power in a multi-port antenna system". TARC can be computed using the S-parameters of the MIMO antenna system. For an N-element antenna, it is given by equation (I.15):

$$\mathrm{r} = \frac{\sqrt{\sum_{i=1}^{N} |b_i|^2}}{\sqrt{\sum_{i=1}^{N} |a_i|^2}} \tag{I.15}$$

Where a_i and b_i are the incident signals and reflected signals, respectively, which are related by their scattering matrix as explain in equation (I.16):

$$[b] = [s][a] \tag{I.16}$$

TARC takes values between 0 and 1 , zero meaning that all power has been radiated, while 1 means that all incident power has been reflected and nothing has been radiated. The available power is the sum of powers available on all the ports of the antenna system. It also includes the effect of feed phase differences between the antenna ports. Consequently, a single TARC curve can be used to determine the resonant frequency and impedance bandwidth of the entire antenna system for a specified phase excitation between its ports [60]. For a 2-port MIMO antenna system, the TARC (r) can be evaluated using equation (I.17) [61].

$$\mathrm{r} = \frac{\sqrt{\left(\left|s_{ii} + s_{ij}e^{j\theta}\right|^2\right) + \left(\left|s_{ji} + s_{jj}e^{j\theta}\right|^2\right)}}{\sqrt{2}} \tag{I.17}$$

In the equation, θ represents the input feeding phase, S_{ii} is the reflection coefficient of the port, and S_{ij} is the coupling between the two ports associated with the antenna structure. Once the sparameters of a 2-port network are determined, a random phase is varied between 0 and 180 degrees to examine how the phase variation between the two ports affects the resonance behavior of the antenna. This process generates the corresponding TARC curves for an effective bandwidth assessment.

1.3.5 Comparative analysis of some proposed MIMO antennas in literature

The various MIMO antenna using various reduction coupling techniques are compared, in terms of antenna size, MIMO elements, operating frequency, isolation, and ECC, as shown in Table (1.4).

Table 1.4: Comparison of different MIMO antennas

Ref.	Size (mm^3)	Ports	Operating frequency (GHz)	Operating	Notched band (GHz)	Isolation technique	Max. Gain (dBi)	Isolation (dB)	ECC
[34]	34×80×0.764	2	2.7–11	UWB	No	Orthogonal arrangement	3.38	17.4	0.001
[35]	21×90×1.6	2	2.22-2.54 3.14-3.9 5.3-5.7	Tri-band	No	Spatial arrangement	3.22	37.37	0.001
[36]	52×52×1.6	4	1.25–40	SWB	3.5/5.5	Orthogonal arrangement	4.5	18	0.09
[37]	81×42×1.6	4	3.03–10.74	UWB	4.8/7.7	Orthogonal arrangement	4	18	0.2
[38]	50×30×1.6	2	2.5–14.5	UWB	No	F-shaped stub	4.3	20	0.04
[39]	26×28×0.8	2	2.90–10.80	UWB	No	T-shaped stub	4	15	0.08
[40]	24×25×1.6	2	2.40–2.67 5.46–5.73	Dual-band	No	Ground slots	3.88	20	0.004
[41]	18×35×1.6	2	2.3-12	UWB	No	T-shaped stub and rectangular slot	4	20	0.035
[42]	32×32×0.8	2	2.9–12	UWB	No	DGS and Orthogonal arrangement	4.2	15	0.04
[43]	26×26×1.6	2	2.9–11.6	UWB	5.5/8.2	DGS	4.8	16	0.02
[44]	45×45×1.6	4	2–16	UWB	5.5/7.5	DGS and Orthogonal arrangement	4	22	0.01
[45]	22×26×0.8	2	3.1–11.8	UWB	5.7/8.2	DGS	6	20	0.03

[46]	35×33×0.8	2	3.1-5	WB	No	NL	3.5	22	0.1
[47]	48×34×1.6	4	3.52–10.08	UWB	No	NL	2.91	23	0.039
[48]	48×49×1.6	2	2.24-2.45 3.3-4 5.6- 5.75	Tri-band	No	multi-NL structure	No	15	0.02
[49]	70×90×0.7874	2	2.39-2.5 5.15-5.5	Dual-band	No	Slotted CSRR in ground plane	4.025	20	0.016
[51]	30×30×1.6	2	2.6-12	UWB	No	Metamaterial	5.5	20	0.01
[52]	44.5×77.5×1.6	2	5.70– 5.93	Narrow-band	No	Mushroom EBG	5.4	20	No
[53]	27.2×46×1.6	2	3.6-17.6	UWB	No	Four EBG element	4	18	0.018
[54]	51×29.6×1.6	2	2.38-2.45 5.17-5.32	Dual-band	No	Mushroom EBG	3.8	25	0.07
[55]	45×90×1.6	2	5.48-5.78	Narrow-band	No	Eight EBG element	2.42	25	No

1.4 Reconfigurable MIMO antenna

A reconfigurable MIMO antenna is defined as a device capable of dynamically modifying its operational characteristics (operating frequency, bandwidth, polarization, and radiation pattern) after manufacture. These adaptations enable the multi-antenna system to adjust its performance and provide a higher degree of flexibility compared to conventional single operating band MIMO antennas, where parameters and characteristics remain fixed and unchangeable. MIMO antenna reconfigurability is achieved by modifying one of its electrical, optical, or physical parameters (mechanical modification) or by integrating controllable materials (ferrites, liquid crystals) as shown in figure (1.18), the antenna's characteristics can be altered, even during real-time operation. Firstly, the electrical reconfiguration are based on the use of switches to connect or disconnect antenna parts and redistribute currents by modifying the radiated fields of the effective antenna aperture [62]-[63]. Electronic switching components such as (RF-MEMS), PIN diodes, varactor diodes or field-effect transistors (FETs) are integrated into the antenna to redirect their source currents. In the Optical reconfiguration techniques, optical switching

elements such as photoconductors must be used [64]. Similarly, reconfigurability can be achieved by mechanical modification of the antenna structure, known as physical reconfigurability [65]. Finally, reconfigurable MIMO antennas can be implemented using smart materials such as metamaterials, ferrites, and liquid crystals, dielectric fluids etc [66]. Table (1.5) provides a comprehensive summary of the advantages and disadvantages of various reconfiguration techniques.

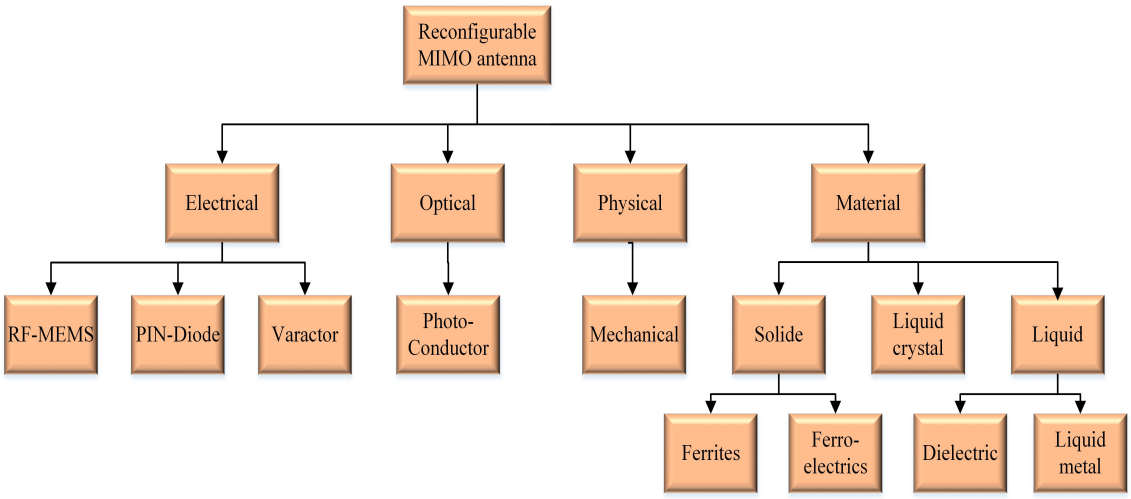

Figure 1.18: Reconfigurable MIMO antenna techniques [68]

Table 1.5: Advantages and drawbacks of different reconfiguration techniques [67],[68]

Reconfiguration Technique	**Advantages**	**Drawbacks**
Electrical Reconfiguration	• Ease of implementation • Low-cost	• Complex structure • Requires biasing systems
Optical Reconfiguration	• No need the use of bias lines • No intermodulation distortion	• Lossy behavior •Complex activation mechanism

Mechanical Reconfiguration	• No need of active elements • No need of biasing systems	• Slow response • Requires power source
Smart-Materials-Based Reconfiguration	• Low-profile • Lighter weight	• Low efficiency • Limited application

The most commonly employed method for adjusting MIMO antenna characteristics involves electrical reconfiguration through active switches (PIN diodes, varactors, RF-MEMS). When size and efficiency are critical considerations, electrically reconfigurable MIMO antennas prove to be the optimal solution. MEMS switches provide several benefits compared to PIN diodes or varactors. These advantages include high isolation and linearity, a broad impedance bandwidth, and minimal power losses [3]. However, they require a high-control voltage, exhibit slower switching speeds, and have a limited life cycle. A comparison of different electronic switching components are introduced in table (1.6). In our study, we focus specifically on electrical MIMO reconfigurability antenna using PIN diodes; figure (1.19) shows a simple equivalent circuit of a PIN switch that can be activated or deactivated. In the ON state, the switch can be represented as a resistor and an inductor. A capacitor in parallel with a resistor, all in series with an inductor, is in the OFF state.

Table 1.6: A comparison of the various electronic switch components [3]

Reconfiguration Technique	Advantages	Drawbacks
PIN-Diodes	• Very reliable • Extremely low-cost • Common choice for reconfiguration	• High tuning speed • High DC bias in ON-state • High power handling capacity
Varactors	• Small current flow • Continuous tuning • Ease of integration	• Nonlinear • Low dynamic range • Complex bias circuitry

RF MEMS	• High isolation and linearity • Wide impedance bandwidth • Low power losses and low noise figure	• High-control voltage • Slow switching speed • Limited life cycle

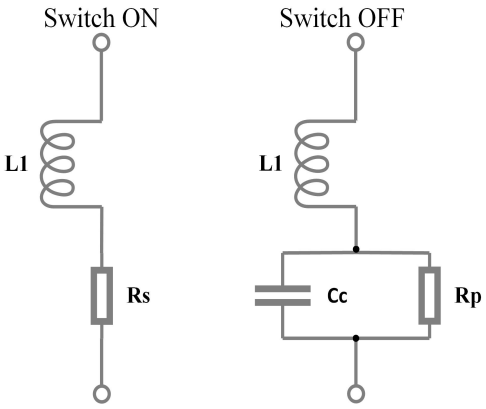

Figure 1.19: Equivalent circuit model of PIN diodes [3]

There are several criteria for classifying reconfigurable antenna systems based on dynamically adjusted operational properties, shown in figure (1.20) [3], such as operating frequency, radiation pattern [69], polarization [70], or a combination of these properties [71], [72].

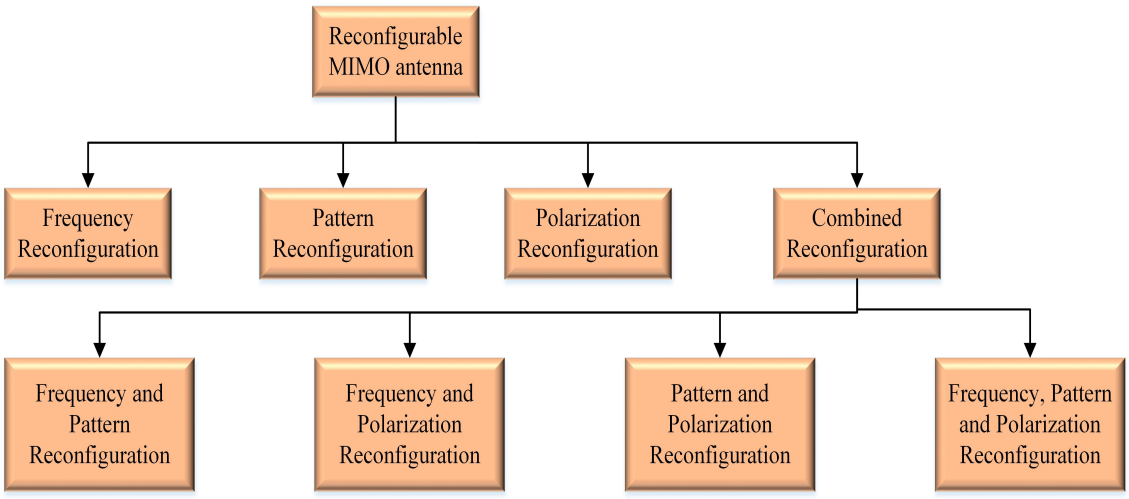

Figure 1.20: Classification of MIMO antenna reconfiguration [3]

Frequency-reconfigurable antennas present a more integrated and generally simpler solution to implement compared to antennas reconfigurable in radiation pattern or polarization, which are often designed for specific applications and may require complex reconfiguration mechanisms. By simply adjusting the operating frequency, frequency-reconfigurable antennas offer customizable performance across diverse conditions, thereby streamlining both design processes and wireless system management. Moreover, they offer enhanced bandwidth and spectral coverage, rendering them ideal for applications demanding frequency flexibility. This dynamic adaptability to varying frequency bands proves pivotal in scenarios with strict spectrum constraints or in integration within multi-standard systems. In the remainder of our study, we will focus solely on frequency-reconfigurable antennas.

1.5 Overview of Frequency Reconfigurable MIMO Technology

Frequency reconfiguration comprises several functions such as frequency switching (switch between several bands), frequency tunability (possibility of continuously varying one or more resonance frequencies), bandwidth change, and filter functions (rejection of one or more frequency band). Several authors have already presented various techniques for achieving frequency reconfigurability by manipulation of antenna current distribution by using active elements like PIN diodes, varactors and MEMS. For example in [6], a reconfigurable dual-band notched UWB MIMO antenna with a compact design, as depicted in figure (1.21a). This antenna functions within the entire UWB band but can reject interference from WiMAX or WLAN bands as needed (three operating mode). Utilizing two conventional square-shaped monopoles featuring multiple branched T-shaped grounded strips, the antenna achieves a UWB, as shown in figure (1.21b). The selective band is notched out through the implementation of PIN diodes into a resonant grounded parasitic structure.

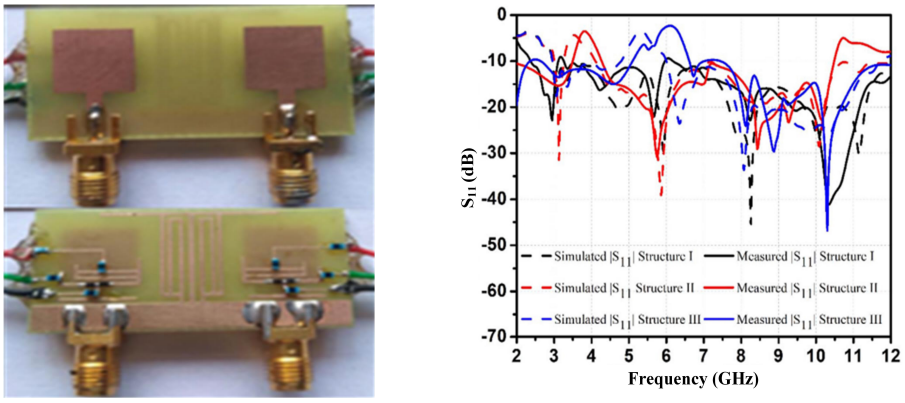

(a) (b)

Figure 1.21: Example of reconfigurable rejected band MIMO antenna using PIN diodes: (a) fabricated antenna and (b) Measured and simulated S_{11} [6]

In [4], authors presented the implementation of a frequency reconfigurable antenna with tunable operating frequency range from 1.3 to 1.8 GHz for the lower band and from 1.8 to 2.6 GHz for the upper band using varactor diodes. The designed antenna consist of four rectangular patch antenna fed by a microstrip line with two slots inserted in each radiating element for dual band characteristic and DGS integrated in the ground plane for isolation enhancement, as shown in figure (1.22a). The operating frequency is obtained by varying the reverse bias voltage of varactor diode from 0 to 5V, as shown in figure (1.22b).

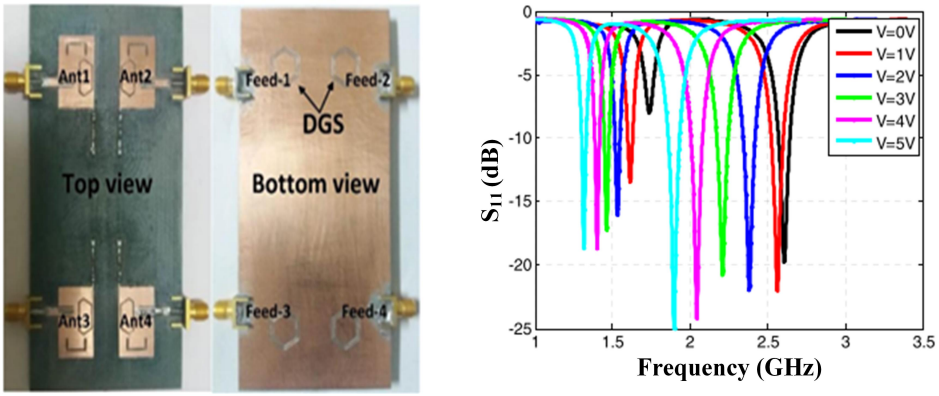

(a) (b)

Figure 1.22: Example of frequency tunable MIMO antenna using varactor diodes : (a) fabricated antenna and (b) measured and simulated S_{11} [4]

In [5], two-element frequency reconfigurable MIMO antenna using RF MEMS which

can be switched between four operating modes that are controlled by control pins, as depicted in figure (1.23b). The RF MEMS has been switched between three capacitors as shown in figure (1.23a). For mode 1 (C1 = 17.5 pF), tri-operating was achieved at $0.6-0.7$, $3.9-4$, and $5.3-6$ GHz. In case of mode 2 (C2 = 9 pF), dual-band operation was observed at $1.7-1.9$ and $5.6-5.9$ GHz. Mode 3 (C3 = 1 pF) provides tri operating band at $2.4-2.7$, $4-4.2$, and $5.1-6$ GHz. For mode 4, which is the case of open circuit state (O.C), dual-band operation at $3.2-4.1$ and $5.1-5.9$ GHz is observed.

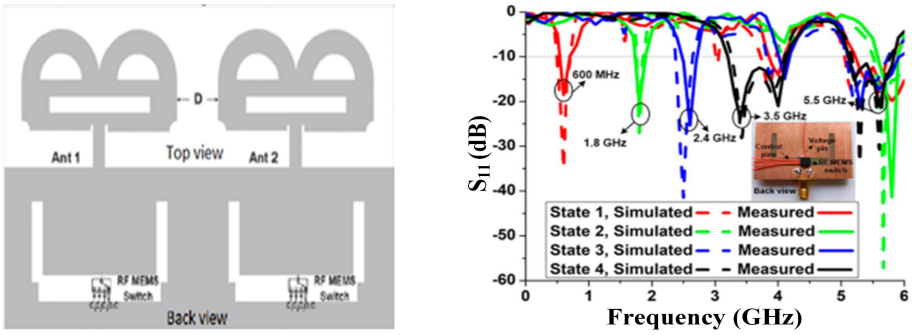

(a) (b)

Figure 1.23: Example of frequency switchable MIMO antenna using RF MEMS: (a) designed antenna and (b) Measured and simulated S_{11} [5]

In addition, a hybrid approach involving a broadband or ultrawideband (UWB) antenna for spectrum sensing and a frequency-reconfigurable MIMO antenna for spectrum utilization have been proposed for cognitive radio (CR) communications due to their ability to detect signals of any frequency over a wide frequency spectrum as in [73], [74], [75],[76], [77], [78]. Finally, the frequency reconfigurable multi antenna system is a promising technology to support the 5G requirements as it enhances the spectral efficiency with better channel capacity. In the recent years, different reconfigurable MIMO antennas have been reported, covering the broad spectrum of frequencies targeted by 5G. Some of them focus on the lower frequency segment (5G sub-6GHz band) while others address the reconfigurable MIMO setup for frequencies surpassing 20 GHz (mm-wave band). For example in [79], frequency reconfigurable two elements MIMO antenna for 5G (sub-6 GHz) applications, the designed antenna has capability to switch between two single operating modes (mode 1 from 2.2 to 2.7 GHz, and mode 2 from 3.3 to 4.02 GHz). In [72], reconfigurable two planar inverted-F antenna (PIFA) elements using PIN diodes and DC biasing circuits,

the designed structure is suitable for sub-6 GHz 5G mobile terminal applications. In [80], a reconfigurable quad-element antenna design covers the n41/n46/n48/n79 5G sub 6 GHz application bands. The antenna switching between triple and dual operating band using pin diodes. Another reconfigurable four-element antenna for 5G applications (the medium band of the 5G) is presented in [81]. The proposed structure offers three selective modes: wideband mode (2.00 − 5.70 GHz), narrowband mode (3.21 − 4.00 GHz), and wideband with notched band (3.37 − 4.00 GHz). However in [82], frequency reconfigurable eight–element MIMO suitable for millimeter-wave (MM-Wave) 5G applications, the designed antenna have the ability to switching between two operating mode (28 GHz or 38 GHz). Table (1.7) reflect a comparative study of recently proposed frequency reconfigurable MIMO antennas in term of antenna specifications and fundamental characteristics such as; reconfiguration type, number of switches used, operation frequency, ECC, gain, peak gain and the overall size.

Table 1.7: Comparative study of some proposed reconfigurable MIMO antennas

Ref.	Size (mm^3)	Ports	Operating band (GHz)	Reconfigurability type	Swithes	Max. Gain (dBi)	Isolation (dB)	ECC	Peak efficiency
[62]	40×20×1.6	2	3–11	Reconfigurable rejected dual band	Four PIN diodes	4.6	15	0.3	80
[63]	32×98×1	2	0.5–0.8 3–3.1 3.7-3.9 5–5.8	Switching between four operating band	Two RF MEMS	5.14	15	0.04	76
[4]	120×60×1.6	4	1.3-1.8 1.8-2.6	Dual band frequency tunability	Four varactor diodes	2.48	12	0.2	78
[72]	120×60×1.575	2	0.8-1.06 2.44-2.66 3.67-5.67	Hybrid (frequency and Pattern)	Four PIN diodes	2.97	12	0.26	74.5
[74]	65×120×1.56	2	0.72-3.44 0.57-0.68 0.83-1.12 2.4-2.5	Frequency reconfigurable	Two PIN and Two varactor diodes	4.48	11.5	0.078	44.67

[76]	100×50×1.5	2	1.42-2.27	Frequency tunability	Two varactor diodes	2.2	12	0.2	78
[77]	120×60×1.5	2	1-4.5	Frequency tunability (0.9-2.6)	Six PIN and Two varactor diodes	3.98	12.5	0.19	88
[78]	160×60×1.6	8	2-12 2.17–4.74 4.57–8.62 8.62–12	Frequency reconfigurable	Without using any switches	2.5	12	0.42	90
[79]	120×60×1.52	2	2.2-2.7 3.3-4.02	Switching between two operating band	Two PIN diodes	4.2	12	0.005	64
[80]	70×70×1.6	4	2.5, 3.3, 3.5, 4.7, 5.2	Multiband frequency reconfigurable	Four PIN diodes	1.74	28	0.3	85
[81]	51.8×51.8×1.6	4	2-5.7 3.21- 4 3.37-4	Switching between three operating mode	Three PIN diodes	1.5	15	0.5	87
[82]	39.8×3.25×0.5	8	27.2-29.8 37.4-40.2	Switching between two operating band (28 and 38GHz)	Sixteen PIN diodes	9.8	12	No	No

1.6 Conclusion

GAINING insights into the physical phenomena that degrade the transmission channel paves the way for conceiving solutions to enhance both the throughput and robustness of transmission. In our context of 5G wireless networks, multiples antennas techniques appear to be the most appropriate method. The significant number of publications in the literature demonstrates that the study of antenna devices dedicated to MIMO systems generates considerable interest. The presented research provides solutions for reducing device size and optimizing the performance of MIMO systems. In this state-of-the-art review that reconfigurable antennas constitute a significant research avenue for MIMO communications, given their dual interest: in some scenarios, they have the potential to replace several distinct antennas with a single reconfigurable one to save space. Furthermore, by providing an additional degree of freedom in the context of adaptive MIMO links, they optimize the efficiency of the overall system, eliminating the need for a

large number of antennas to achieve desired performance. The frequency-reconfigurable MIMO antenna stands out as the most important type of reconfiguration due to its simplicity of implementation, ability to provide a more integrated and versatile solution, and facilitating wireless system management. In the remainder of our study, our focus lies specifically on frequency-reconfigurable MIMO antennas. We will propose MIMO structures integrating a frequency reconfiguration mechanism to combine the dual advantages of a conventional MIMO system and a cognitive radio (CR) system.

CHAPTER 2

FREQUENCY RECONFIGURABLE WIDEBAND MIMO ANTENNA

2.1 Introduction

FIRST, this chapter introduces the employed methodology for designing a frequency-reconfigurable MIMO antenna. Then, an in-depth analysis and discussion of a novel reconfigurable MIMO antenna designed for 5G new radio applications operating in the sub-6 GHz frequency range is presented. The proposed antenna offers significant versatility through its ability to operate in 4 distinct frequency modes thanks to the two independent filtering mechanisms. These modes include a wideband operating mode, a wideband mode with notching WiMAX band, a low-pass filter mode notching WLAN band, and a dual-band mode notching WLAN and WiMAX bands simultaneously. Finally, integrating an isolation mechanism between the two antenna elements is presented to ensure robust MIMO diversity performances.

2.2 Antenna design methodology

This section introduces the methodology employed for designing a frequency-reconfigurable MIMO antenna, as follows:

- Design of single antenna element: To design a single antenna effectively, it is crucial to understand the specific requirements and specifications of the application (select the desired resonant frequency), including size and placement limitations. Once understood, one should select a suitable antenna type such as PIFA (Planar Inverted-F Antennas), printed monopole antenna or Vivaldi. In cases where the proposed antenna is reconfigurable, we should introduce reconfiguration mechanism by typically adding resonant elements that would alter its frequency behavior like slots, short-circuits or stubs. These resonant elements are incorporated into the antenna using ideal switches (where their connection involves adding a metallic conductor, and their disconnection involves removing the metal) or by using a real switch (PIN diodes with biasing circuit);

- Utilizing appropriate computer-aided design (CAD) software tools, such as CST (Computer Simulation Technology), to model the antenna behavior accurately, we incorporate the characteristics of PIN diodes through S2P files obtainable directly from their respective websites. Additionally, employ performance enhancement techniques like miniaturization and bandwidth broadening, integrating methods such as introducing slots or shorting walls, and conducting thorough parametric studies via simulations before prototype fabrication. Developing a prototype of the basic antenna structure is essential. This prototype facilitates the comparison between simulated and measured results, and revealing any disparities between the simulated and fabricated design (characterizing the reconfigurable single antenna in terms of its S-parameters for the various operating modes is crucial at this stage);

- Create MIMO antenna from elementary structures to meet design/application requirements. Use simulation models to predict system parameters and identify areas for improvement, including isolation methods. Adapt isolation techniques according to the different operating frequency band and element spacing. Perform parametric simulations to optimize antenna performance;

- Prototype MIMO antenna and characterize its performance. Once the design has been optimized with the simulation tool, the files can be extracted and a prototype realized. The next step is to carefully solder the switches (PIN diodes) and bias circuit components to ensure a good match between simulated and measured parameters. The performances of the multi-antenna systems (S-parameters, radiation patterns, gain and diversity performance) should be measured. Based on the obtained results, the designer might need to fine-tune the design to achieve the required performance values for the application under consideration. Once this stage has been completed, the antenna can be re-realized.

Figure (2.1) shows a flowchart that presents the design procedure for printed frequency reconfigurable MIMO antenna systems for different applications. This chart is intended to give the reader a multi-antenna system design process for any printed MIMO antenna system (with or without frequency reconfiguration).

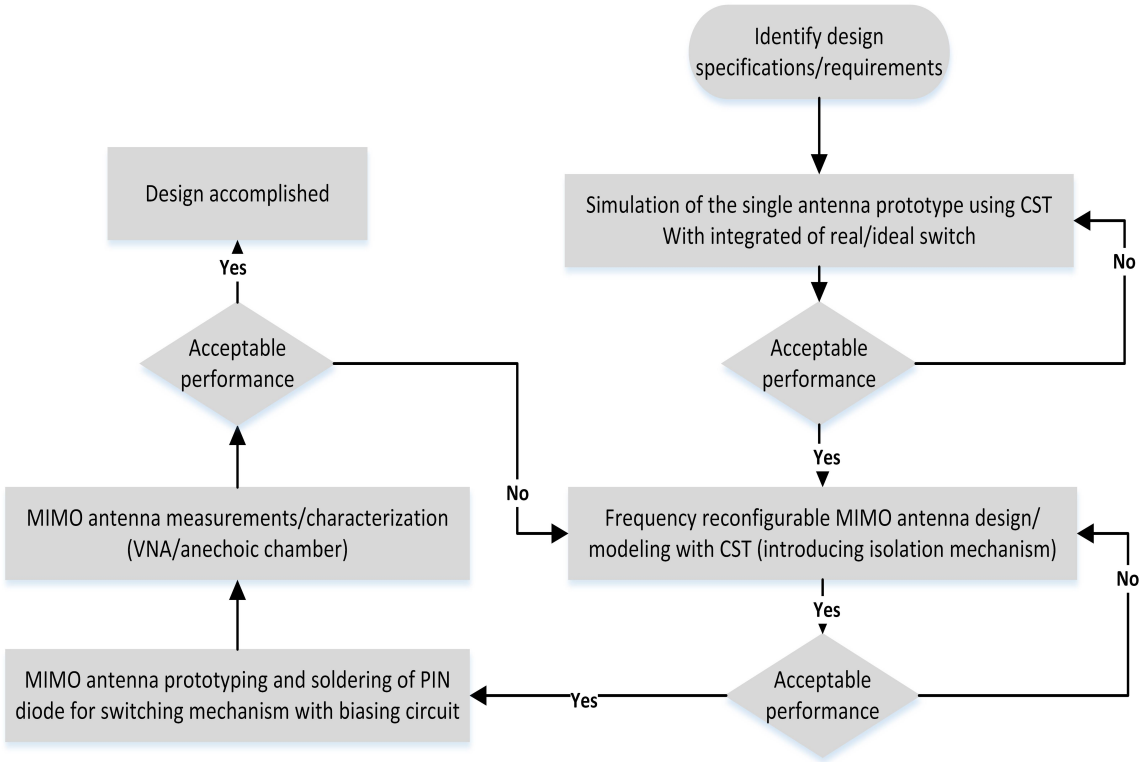

Figure 2.1: Flowchart showing the design procedure for printed MIMO antenna designs with and without reconfigurability mechanism

2.3 Reconfigurable wideband antenna

For the design and the simulation of all proposed structures, we utilized CST Microwave Studio software, developed by CST (Computer Simulation Technology), for electromagnetic analysis and design. CST MWS is an electromagnetic tool for 3-D simulation of high-frequency devices of antennas, filters, couplers, as well as planar and multilayer structures. In addition to its flagship solver module using the finite integration technique (FIT), CST MWS also includes modules based on finite different time-domain (FDTD) and frequency-domain methods including Finite Element Method (FEM), Method of Moments (MoM), Multilevel Fast Multipole method (MLFMM), and shooting and bouncing rays (SBR) with distinct advantages in their own domains. The time-domain solver can find the broadband behavior of the device being modeled in one simulation run given a sufficient fine time step. As a general purpose of electromagnetic simulator with automatic direct meshing and many different types of solver.

The antenna design is realized on a Rogers RT5880 substrate characterized by a dielectric constant (ε_r) of 2.2, a thickness (h) measuring 1.57 mm, and a loss tangent (tanδ) of 0.0009. Figure (2.2) illustrates the single antenna element, constructed with overall dimensions of 30$\times$ 25 $\times$ 1.57 mm^3. This element comprises a 50Ω microstrip feed line etched on the top layer of the substrate, while the bottom layer features the ground plane, depicted in figure (2.2).

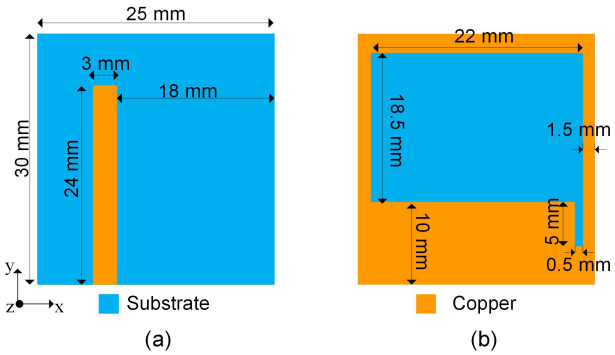

Figure 2.2: Layout of the single antenna element (a) Front view (b) Back view

To achieve wide frequency band operation, several modifications are applied to the ground plane of the initial structure, outlined in figure (2.3). Initially, the ground plane consisted of a partial rectangular configuration measuring 25$\times$ 10 mm^2, denoted as An-

tenna 1. The simulated reflection coefficient in this case of a partial ground plane, presented in figure (2.4), shows that the antenna operates at 4.2 GHz, with an impedance bandwidth of 1.7 GHz, corresponding to a relative bandwidth of 50%. Subsequently, the ground plane is extended (Antenna 2) to broaden the frequency operation range, spanning from 2.6 GHz to 6 GHz, as depicted in figure (2.4). Finally, to further enhance bandwidth, a vertical open slot with dimensions of $5\times$ 0.5 mm^2 is introduced into the ground plane (Antenna 3). This modification enables a broadened operating range from 2.4 GHz to 6 GHz, as evidenced in figure (2.4).

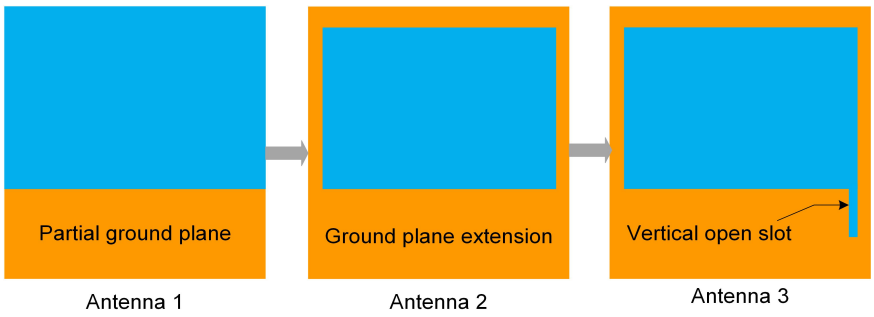

Figure 2.3: Geometric evolution of the single antenna element (ground plane)

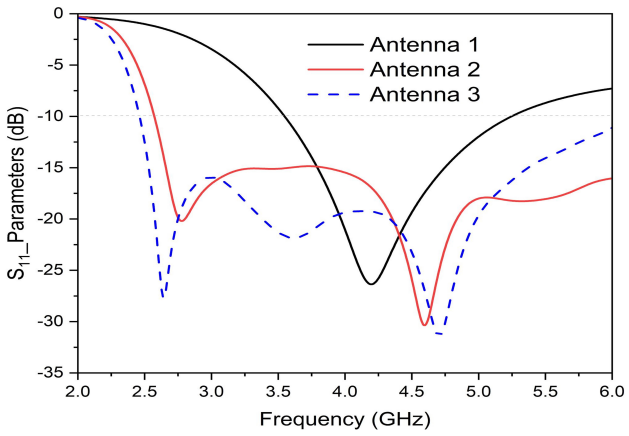

Figure 2.4: The evolution of the simulated reflection coefficient curve according to the modifications

In order to introduce reconfigurability into the antenna element, two distinct filters are incorporated. The first serves to establish a notched band within the WiMAX frequency range $(3.3-3.8\,\text{GHz})$ through the integration of a half-wavelength $(\lambda/2)$ Rectangular

Split Ring Resonator (RSRR) etched into the top layer of the substrate, with dimensions denoted as $L_r \times W_r$, as depicted in figure (2.5a). The second is used to filter the higher frequencies within the band $(5.15 - 5.925\ \text{GHz})$ by incorporating a horizontal straight slot (acting as a low-pass filter) on the backside of the antenna in the ground plane, with a length of 21 mm and a width of 0.5 mm, as illustrated in figure (2.5b). The dimensions of the RSRR and LPF, tailored to achieve filtering at 3.5 GHz and 5.15 GHz respectively, are determined utilizing equations (2.1) and (2.2).

$$f_{\text{notche}} = \frac{c}{2 \times L_{RSRR} \times \sqrt{\varepsilon_{eff}}} \tag{2.1}$$

$$f_{\text{filter}} = \frac{c}{2 \times L_{LPF} \times \sqrt{\varepsilon_{eff}}} \tag{2.2}$$

Where $L_{RSRR} = 2 \times l_r + 2 \times w_r - g_r$ is the length of the RSRR at the desired notch frequency, and $L_{LPF} = w_l + g_l$ is the length of the straight slot (LPF) at the desired filter frequency and ε_{eff} is the effective dielectric constant of the substrate.

Two switches S_1 and S_2 are used for frequency reconfiguration, as shown in figure (2.5). The role of each switch is to enable/disable the filtering caused by the two mechanisms (RSRR and straight slot in the ground plane). The antenna has four different operating modes depending on the state of the two switches.

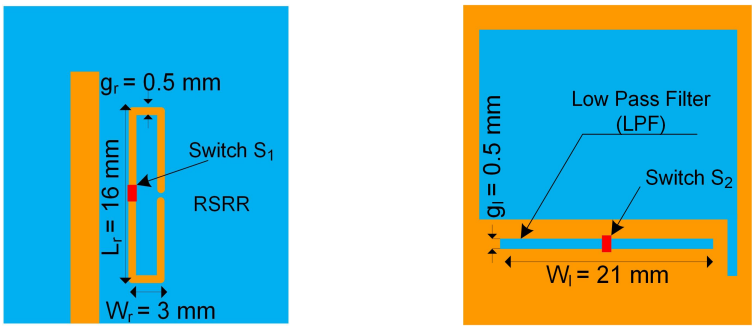

(a) Top view (b) Back view

Figure 2.5: Layout of the reconfigurable single antenna element

The single antenna element was modeled considering only the switch represented by a conductive strip (ideal case). The simulation distinguishes between the ON and OFF states based on the presence/absence of the conductive strip. Activation of the notch filter (RSRR) occurs when switch S_1 is in the ON state, while the low-pass filter (LPF)

is engaged when switch S_2 is in the OFF state. Consequently, the antenna supports four distinct frequency-operating modes, as outlined in table (2.1).

Table 2.1: Switches configuration for each mode of the proposed single antenna

Modes / Switches	**Wideband**	**Notched band**	**LPF**	**Dual band**
S1	OFF	ON	OFF	ON
S2	ON	ON	OFF	OFF

The prototype has been realized as is shown in figure (2.6) and measured. The comparison between the simulated and measured reflection coefficient S_{11} for the various operation modes can be detailed as follows:

1. Wideband mode: the initial wideband operating mode is obtained when S_1 is in the OFF state and S_2 is in the ON state (RSRR and LPF are disabled). As illustrated in figure (2.7a), the reflection coefficient indicates that the operational frequency range extends from 2.4 GHz to 6 GHz (with $|S_{11}| < -10$ dB) in simulation and from 2.55 GHz to 6 GHz in measurement.

2. Notched band mode: the notched band occurs at 3.5 GHz (WiMAX band) and it is obtained when all switches are turned to ON state (RSRR is enabled, and LPF is disabled). From the S-parameters, which are shown in figure (2.7b), we note that the simulated notched band is from 2.92 GHz to 4.06 GHz, whereas the measured band is from 3.1 GHz to 3.86 GHz. The filtering property, with a good insertion loss, can be noticed at 3.49 GHz (greater than -1dB), in simulation as well as in measurement. This notched band can be shifted by changing the electrical length of the RSRR as shown in figure (2.8a).

3. Low-Pass Filter (LPF) mode: It is obtained when the switches (S_1 and S_2) are in the OFF state. The LPF mode gives a simulated reflection coefficient with bandwidth from 2.43 GHz to 4.69 GHz (relative bandwidth of 63.4%), where the measured bandwidth is from 2.68 GHz to 4.82 GHz (relative bandwidth of 58.07%), as shown in figure (2.7c). The bandwidth can be reduced/increased by changing the electrical length of the horizontal slot as shown in figure (2.8b).

4. Dual band mode: It is obtained when S_1 is in the ON state and S_2 is in the OFF state. As shown in figure (2.7d), the antenna has two frequency operating bands, the first from 2.4 GHz to 2.85 GHz with a relative bandwidth of 17.7%, and the second from 3.9 GHz to 4.7 GHz with a relative bandwidth of 17.9%. For measured results, the antenna operates in two bands of operation, $2.58-3.27$ GHz (23.2 %), and $3.86-4.58$ GHz (17.06 %). This mode is used when WLAN and WiMAX bands are filtered simultaneously.

Furthermore, a good agreement between simulation and measurement results is observed. We only notice a small shift in the bands, which is essentially due to the quality of the manufacturing process.

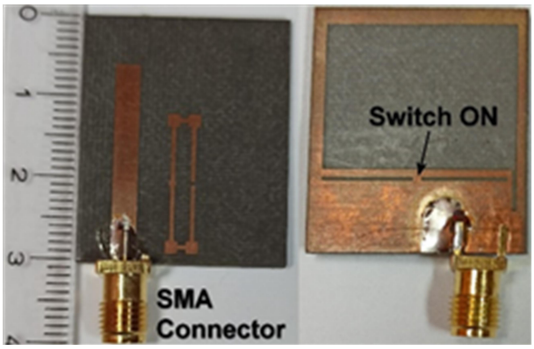

Figure 2.6: Realized antenna element prototype with ideal switches (case of notched band mode)

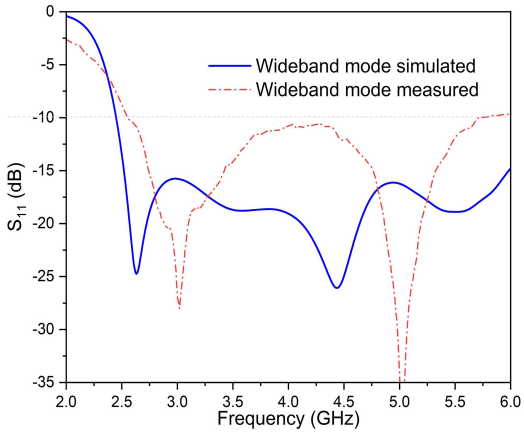

(a) Wideband mode

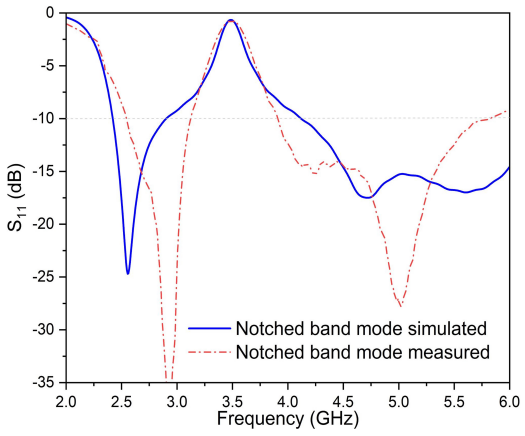

(b) Notched band mode

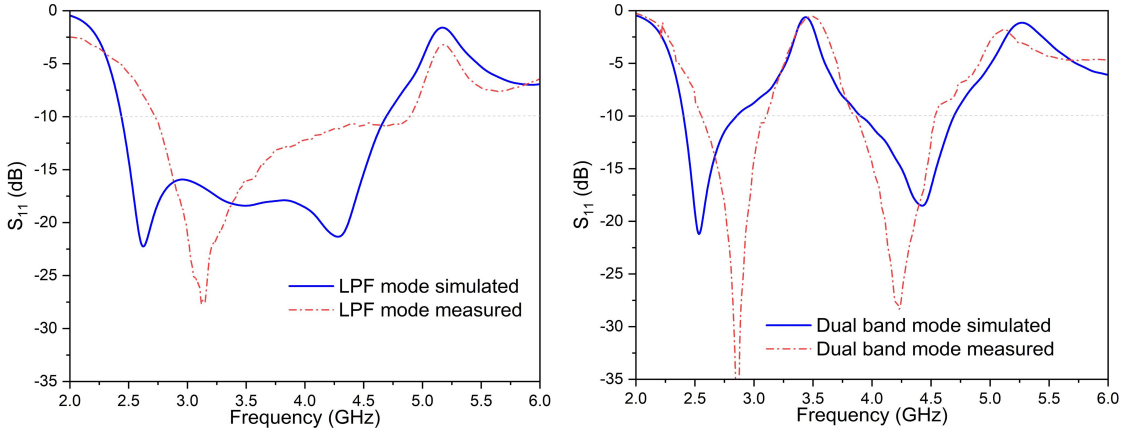

(c) LPF mode (d) Dual band mode

Figure 2.7: Measured and simulated reflection coefficient of the proposed reconfigurable single antenna element

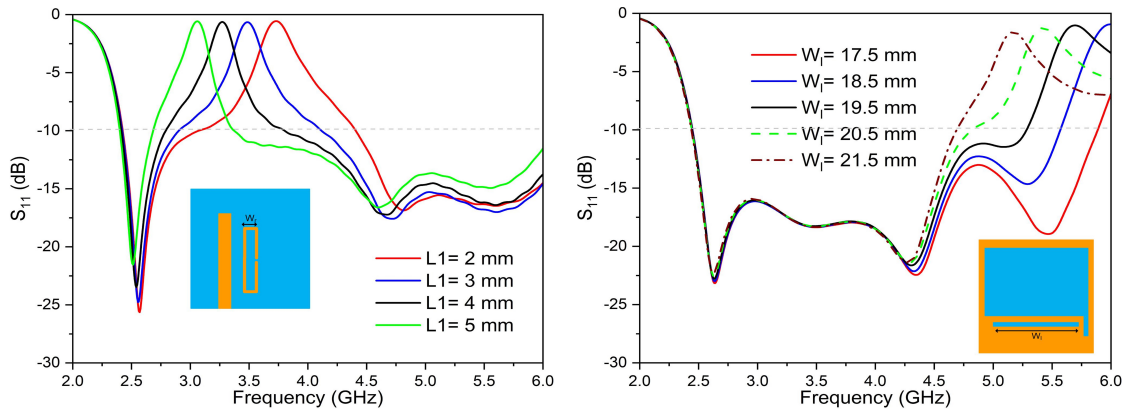

(a) Variation of W_r (b) Variation of W_l

Figure 2.8: Parametric studies on the reflection coefficient $|S_{11}|$

2.4 Reconfigurable wideband two-element MIMO antenna

2.4.1 Implementation with ideal switch

Initially, the reconfigurable MIMO antenna configuration comprises two individual reconfigurable single antenna elements employing ideal switches (the ON/OFF states are modeled by the presence/absence of a PEC) before advancing to the final prototype implementation utilizing PIN diodes. These two antenna elements are symmetrically arranged about the y-axis and share a common ground plane, maintaining a separation distance of

10mm between their edges, as depicted in figure (2.9). The MIMO antenna system is fed through two 50Ω SMA connectors.

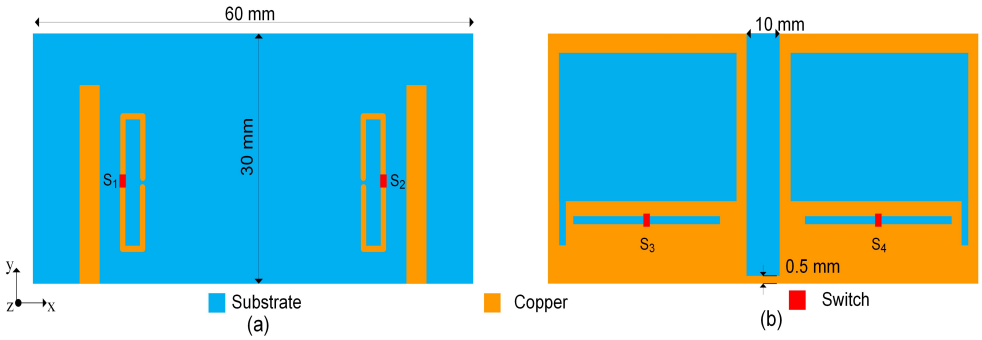

Figure 2.9: Layout of the reconfigurable two-element MIMO antenna (a) Front view, (b) Back view

a) Isolation mechanism

To improve the isolation between the two ports of the reconfigurable MIMO antenna for wideband mode, while keeping a compact structure, some modifications are introduced to the common ground plane as shown in figure (2.10). Due to the structure symmetry, we only represent S_{11} and S_{12}. We can note a clear improvement in the isolation inside the operating band of the antenna thanks to the modifications made to the ground plane. As shown in figure (2.11), the minimum isolation increased from 12 dB (configuration A) to 18 dB in configuration C.

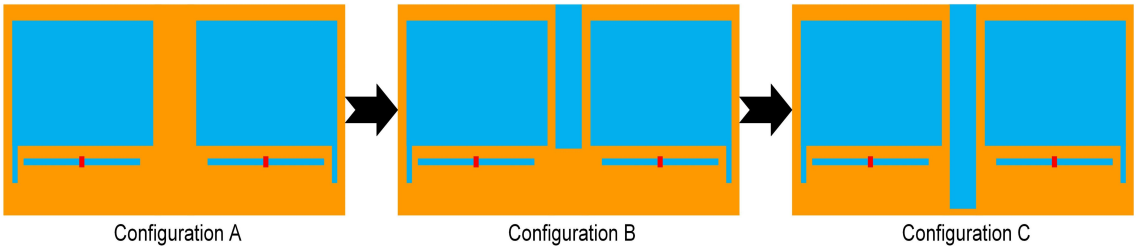

Figure 2.10: Evolution of isolation mechanism

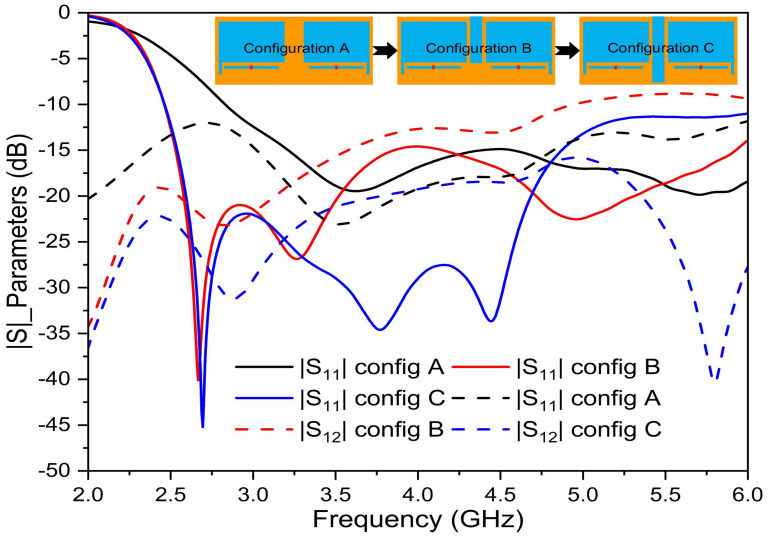

Figure 2.11: S-parameters of the antenna for each configuration (wideband case)

The superposed simulated scattering parameters of the MIMO antenna, with and without isolation (configurations A and C), for the four operating modes, are depicted in figure (2.12). Analysis of the simulation results reveals notable enhancements in minimum isolation within the operating bands following modifications to the common ground plane. Specifically, in both wideband and notched-band modes, the minimum isolation has been augmented by a minimum of 6 dB. Moreover, for the remaining two modes, the minimum isolation has escalated from 11 dB to 19 dB. Additionally, it is observed that the introduction of an isolation mechanism leads to a shift in the lowest operating frequency, transitioning from 2.71 GHz to 2.43 GHz across all operation modes. The switch states corresponding to each operating mode are detailed in table (2.2).

Table 2.2: Switches configuration for each mode of the proposed MIMO antenna

Modes / **Switches**	**Wideband**	**Notched band**	**LPF**	**Dual-band**
(S1 , S2)	OFF	ON	OFF	ON
(S3 , S4)	ON	ON	OFF	OFF

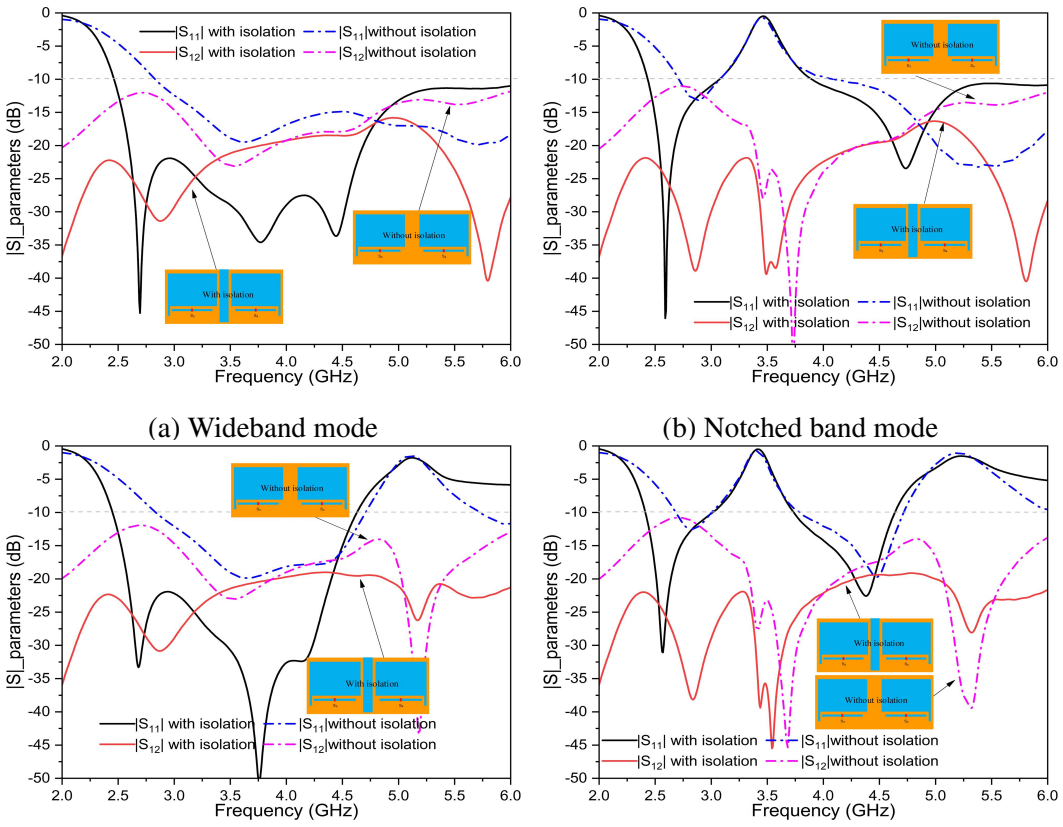

(a) Wideband mode

(b) Notched band mode

(c) LPF mode

(d) Dual band mode

Figure 2.12: Simulated S-parameters for the four operating modes with and without ground plane modifications

b) Surface current distributions

Surface current distributions of the proposed reconfigurable MIMO antenna are observed in the four operating modes (wideband mode, notched band mode, LPF mode, and dual-band mode) at 3.5 GHz (WiMAX) and 5.2 GHz (WLAN), as shown in figure (2.13), to understand the filtering mechanisms of RSRR and LPF. The surface current distributions for the wideband mode (with disabled RSRR and LPF) are shown in figures (2.13a) and (2.13b) at 3.5 GHz and 5.2 GHz, respectively. At both frequencies, a notable concentration of current is observed on the feedline and the ground plane, providing evidence of the antenna's functionality within these frequency ranges. In notched band mode at 3.5 GHz (figure (2.13c)), it can be noticed that a strong current distribution exists on the RSRR, which proves that the filtering mechanism (RSRR) at 3.5 GHz works. We

can also see that the current distribution is normally distributed between the feed line and the ground plane at 5.2 GHz, as shown in figure (2.13d). For the LPF mode, there is a strong current concentration along the right slot in the ground plane at 5.2 GHz, as shown in figure (2.13f). This concentration disappears at 3.5 GHz, as shown in figure (2.13e), which proves that the horizontal slot in the ground plane filters the high frequencies of the working band (the LPF filtering mechanism is activated). Finally, in dual-band mode (RSRR and LPF are enabled), we can see a high current distribution on the RSRR in figure (2.13g), and along the horizontal slot in figure (2.13h), which confirms that the two filters operate simultaneously, respectively at 3.5 GHz and 5.2 GHz. We also notice very good isolation between the two ports for all modes of operation, with very low surface current distribution on the second antenna element as shown in figure (2.13).

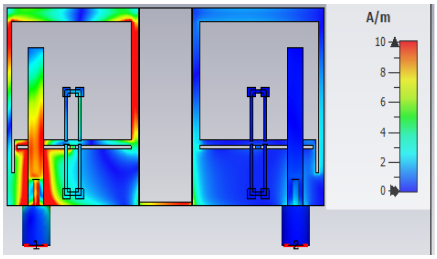

(a) Wideband mode at 3.5 GHz

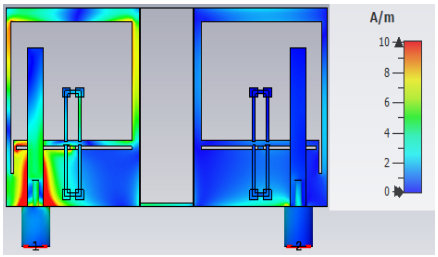

(b) Wideband mode at 5.2 GHz

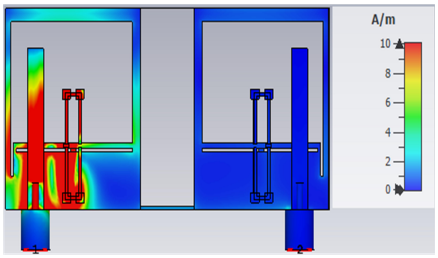

(c) Notched band mode at 3.5 GHz

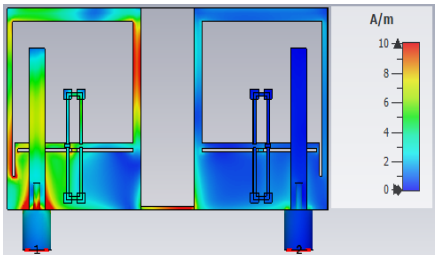

(d) Notched band mode at 5.2 GHz

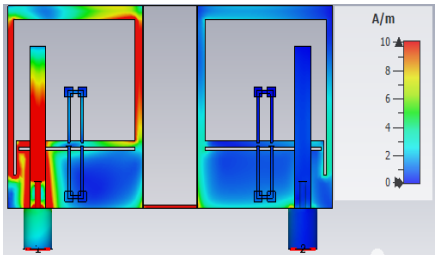

(e) LPF mode at 3.5 GHz

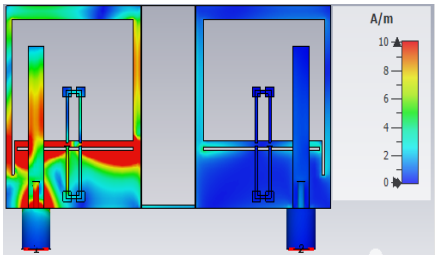

(f) LPF mode at 5.2 GHz

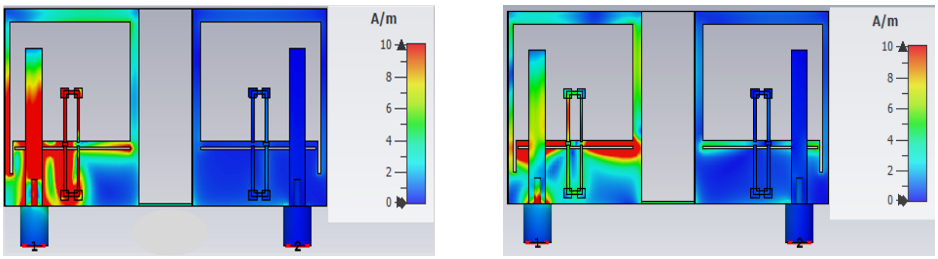

(g) Dual band mode at 3.5 GHz (h) Dual band mode at 5.2 GHz

Figure 2.13: Surface current distribution for the proposed reconfigurable wideband two-element MIMO antenna

c) S-parameters

To validate the proposed MIMO antenna design employing ideal switches, a prototype was fabricated for each antenna mode. Figure (2.14) illustrates the realized prototypes for both dual and wide-band modes.

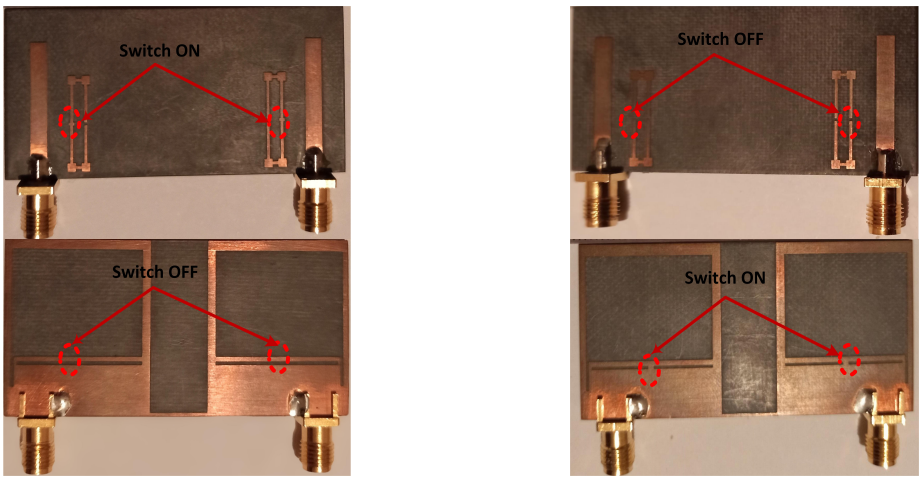

(a) case of Dual band mode (b) case of wide-band mode

Figure 2.14: The fabricated two-element reconfigurable MIMO antenna with ideal switch (top and back view)

The simulated and measured $|S|$ parameters of the proposed reconfigurable MIMO antenna in the ideal case are presented in figure (2.15). In the wideband mode, the simulated impedance bandwidth (IBW) spans from 2.44 to 6 GHz (a relative bandwidth of 84.4%)

with a minimum isolation of 17 dB between the two antenna elements. It is also observed that the measured IBW of the manufactured prototype supports a wideband from 2.71 to 6 GHz (a relative bandwidth of 75.54%) with a minimum isolation of 15 dB over the operating band, as depicted in figure (2.15a). The same performance is achieved in the notched band mode, as shown in figure (2.15b), with a rejected band from 3.08 to 3.88 GHz to eliminate WiMAX interferences. At the measured and simulated rejection band, the antenna exhibits a peak rejection of approximately -0.5 dB at 3.5 GHz, indicating a strong and reliable rejection band.

In LPF mode, as depicted in figure (2.15c), the simulated IBW is 2.44 to 4.7 GHz (a relative bandwidth of 63.3%), while the measured bandwidth is 2.71 to 4.63 GHz (a relative bandwidth of 52.3%). The isolation exceeds 19 dB and 15 dB over the operating frequency band for simulation and measurements, respectively.

In dual-band mode, as shown in figure (2.15d), the simulated results indicate that the antenna operates in two frequency bands: the first one from 2.41 to 3 GHz (a relative bandwidth of 21.85%), and the second one from 3.73 to 4.63 GHz (a bandwidth of 20.7%), with isolation better than 23 dB and 20 dB for the two frequency bands, respectively. For the measured results of the manufactured prototype, the antenna supports two operational bands: 2.54 to 2.99 GHz (a bandwidth of 16.03%) and 3.77 to 4.59 GHz (a bandwidth of 19.61%). The isolation exceeds 18 dB and 16 dB for the two frequency bands, respectively. A good agreement is observed between simulation and measurement results for the different modes, with small shifts in the bands, primarily due to manufacturing errors.

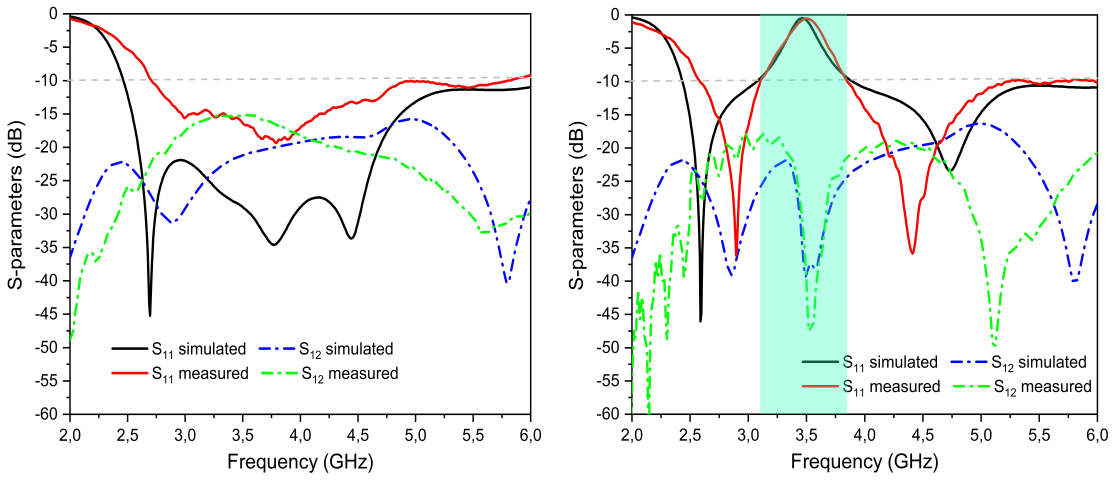

(a) Wideband mode

(b) Notched band mode

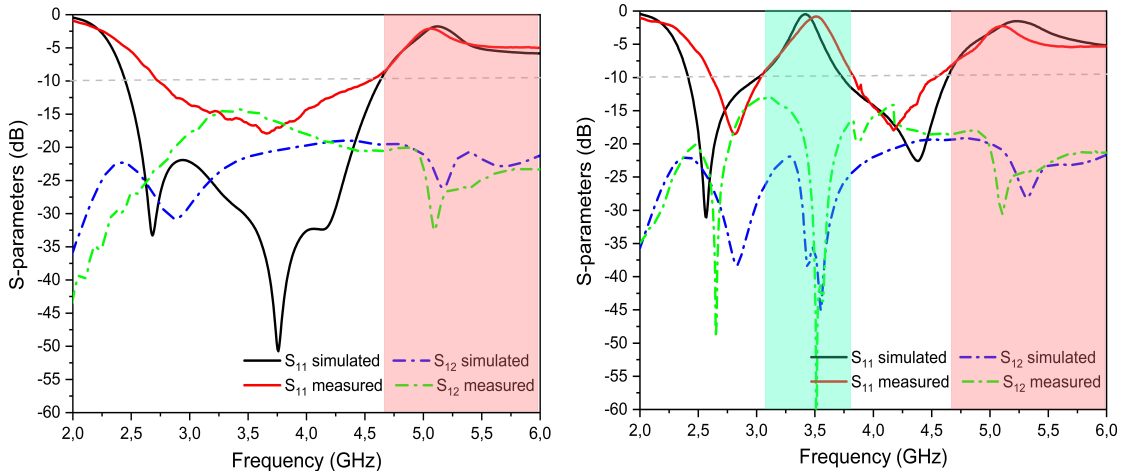

(c) LPF mode

(d) Dual band mode

Figure 2.15: S-parameters for all operating modes of the reconfigurable MIMO antenna using ideal diode

2.4.2 Implementation with PIN diodes

After completing the ideal reconfiguration introduction phase, the next step is to move on to inserting real switches, which are active components (pin diodes). Figure (2.16) shows the layout of the reconfigurable MIMO antenna with the integration of real switches and the bias circuit necessary for the operation of the PIN diodes. The type of diode that is used is BAR50-02V from the manufacturer's Infineon. To take their effect into account in the simulations its S-parameters (s2p file) downloadable from the manufacturer's website have been inserted in the antenna with CST Microwave Studio software as shown in figure (2.17) (Simulating within the "Schematic" section of CST). For the biasing of the diodes, decoupling capacitors of 100 pF and inductors (RF chokes) of 100 nH were used. Capacitors allow high-frequency currents to pass while blocking direct current (DC) signals. Conversely, inductors work oppositely (blocking high-frequency currents while allowing DC to pass through).

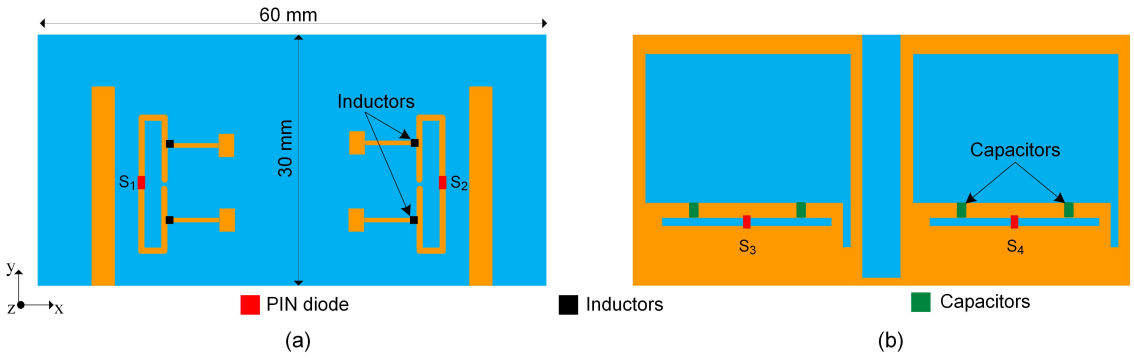

Figure 2.16: Layout of the two-element reconfigurable MIMO antenna with PIN diodes and biasing circuit (a) Front view (b) Back view

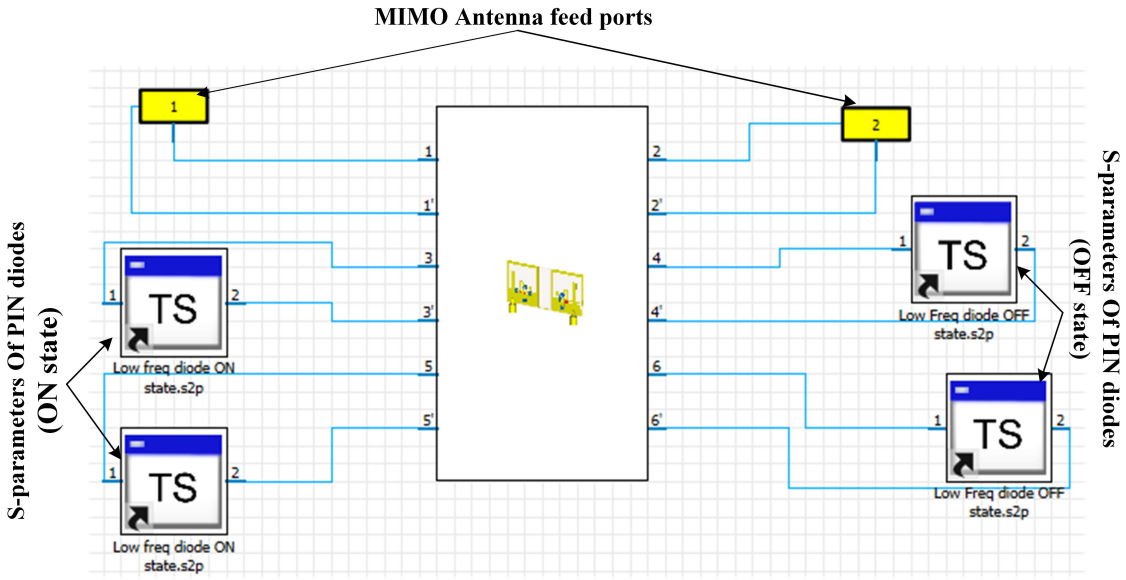

Figure 2.17: Simulating of the designed antenna within the "Schematic" section of CST

The performance of the proposed two-element MIMO antenna with the frequency reconfiguration circuit is evaluated in terms of s-parameters, radiation pattern, realized gain and diversity performances. The prototype have been fabricated on a Rogers RT5880 substrate. Eight (8) electrical wires and a stabilized power supply incorporating an adjustable current limiter were employed to bias the diodes with continuous voltages around 5 V. Figure (2.18) depicts a photo of the final prototype with the biasing circuit and the Pin diodes soldered onto the structure.

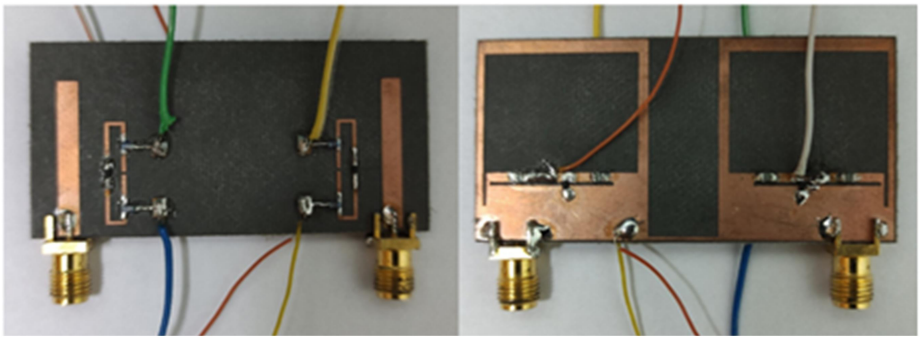

Figure 2.18: Photographs of the realized prototype with PIN diodes and bias circuit (a) Front view (b) Back view

The operating frequency range of the BAR50-2V diode extends from 10 MHz to 6 GHz. It has a low forward bias resistance and a low capacitance at zero volts (off state). The Pin diode features a current-controlled RF resistance, which decreases as the forward bias current increases. Applying a forward bias current of 100 mA (maximum value) to the diodes ensures that diode parasitic resistance is minimal.

a) S-parameters

The simulated and measured S-parameters of the proposed reconfigurable MIMO antenna are shown in figure (2.19). Which were measured using Rohde & Schwarz vector network analyzer. To consider their impact in the simulation, in the simulation, the S-parameters of the components provided by the manufacturer were introduced during the design and simulation phase of the antenna figure (2.20). The configurations of the diodes (conducting or blocking) for each operating mode remain the same as with an ideal switch case. The discussion of the various results obtained for the different operating modes are as follows:

1. Wideband mode: The simulated impedance bandwidth (IBW) is from 2.41 GHz to 6 GHz, with a relative bandwidth of 84.4% and a minimum isolation of 17 dB between the two ports. It is also observed, that the measured IBW of the realized prototype is from 2.51 GHz to 6 GHz with a relative bandwidth of 82.70%, and a minimum isolation of 18 dB over the operating band as shown in figure (2.19a).

2. Rejection band mode: A good result is obtained in this operating mode as shown in figure (2.19b), with a notched band from 3.2 GHz to 3.66 GHz at -10 dB to reject the WiMAX frequency band. The reflection coefficient has a peak of about -2 dB at 3.5 GHz, which signifies a strong and reliable rejection band.

3. LPF mode: As shown in figure (2.19c), the simulated IBW is $2.4-4.7$ GHz (relative bandwidth of 63.3%), and the measured is $2.61-4.53$ GHz (relative bandwidth of 53.7 %). The isolation is greater than 19 dB and 18 dB over the operating frequencies for simulation and measurement results, respectively.

4. Dual-band mode: it is observed in figure (2.19d) from simulated results that the antenna has two frequency operating bands: the first one is from 2.41 GHz to 3.16 GHz (relative bandwidth of 29.18%), and the second one is from 3.64 GHz to 4.7 GHz (relative bandwidth of 24.31%) with isolation greater than 23 dB, and 18 dB for the two frequency bands, respectively. For the measured results of the manufactured prototype, the antenna supports two bands of operation $2.47-3.08$ GHz (23.10%) and $3.59-4.34$ GHz (19.09%). The isolation is greater than 20 dB and 18 dB for the two frequency bands, respectively.

A good agreement is observed between simulation and measurement results for the different modes with small shifts of the bands, which are essentially due to manufacturing errors and electric wires

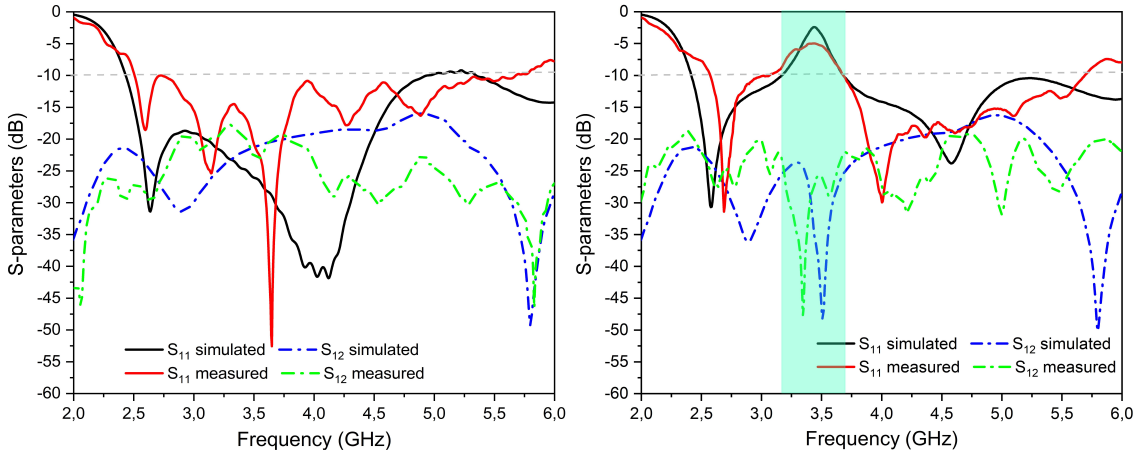

(a) Wideband mode

(b) Notched band mode

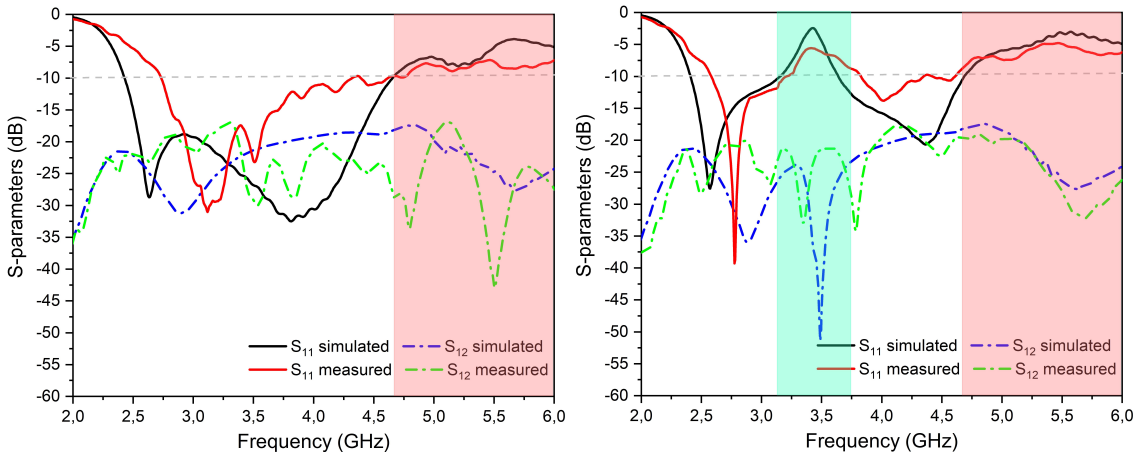

(c) LPF mode (d) Dual band mode

Figure 2.19: S-parameters for all operating modes of the reconfigurable MIMO antenna with PIN diodes

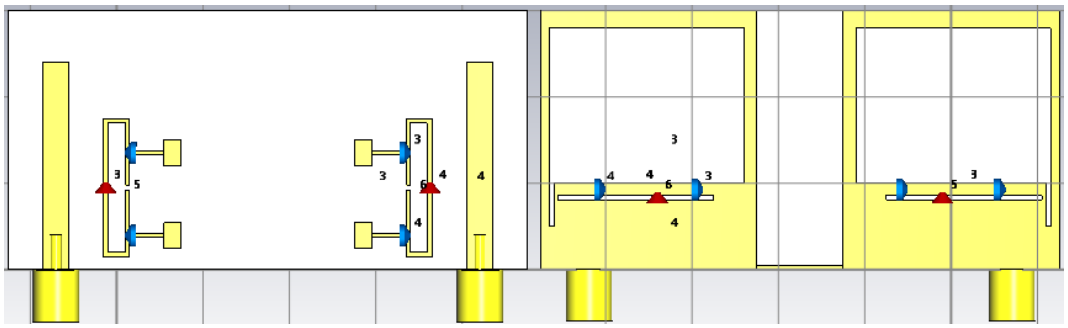

Figure 2.20: Reconfigurable MIMO Antenna simulation with CST Microwave studio

b) Radiation patterns

The radiation pattern of MIMO antenna systems can be measured using an anechoic chamber. An anechoic chamber creates a reference environment with excellent repeatability for direct transmit/receive wireless systems because it eliminates any reflections other than the line-of-sight (LOS) signal within the chamber. Figure (2.21) shows a simplified diagram of an anechoic chamber. The device with an antenna that needs to be tested is placed on a rotating positioner that can cover the whole sphere around the device and record its 3D radiation patterns. The position controller records the angle at which the device is actually tilted and tilts it accordingly while the measurements are being conducted and recorded. A vector network analyzer (VNA) is used to perform the power

measurements. A PC is usually used to map the measured power levels and positions and create the completed radiation pattern measurement, as well as extract and compute other parameters for the device under test.

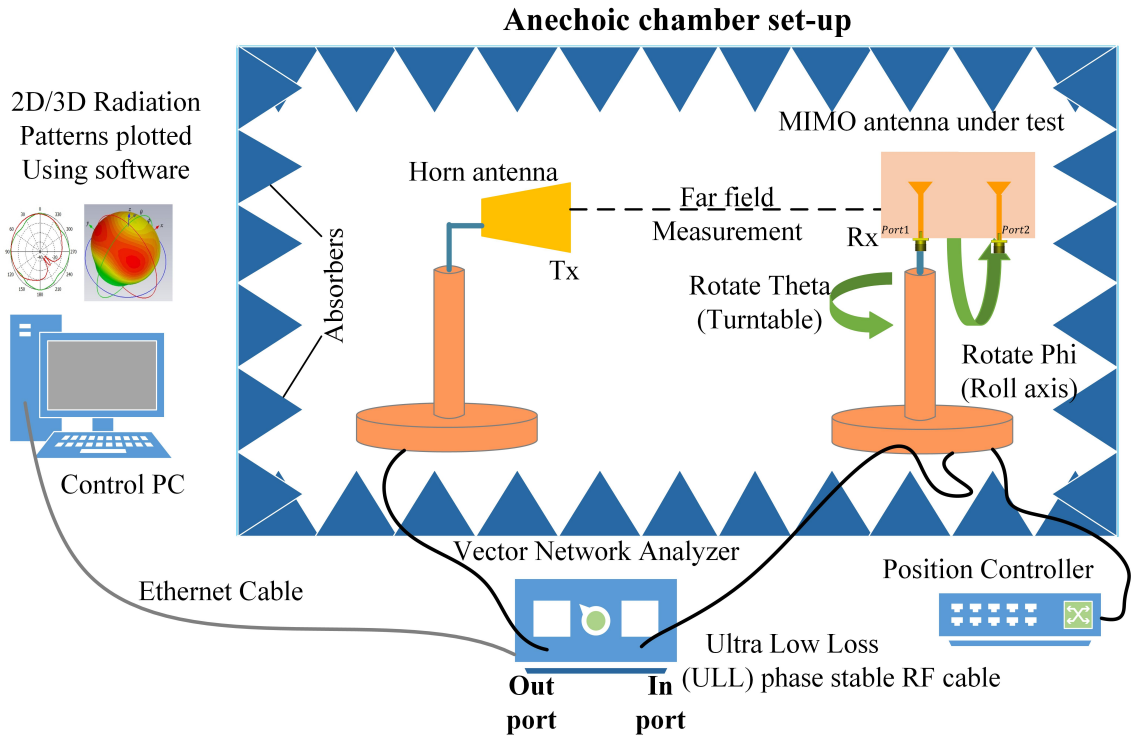

Figure 2.21: Radiation pattern measurement setup (anechoic chamber)

The measured and simulated radiation patterns (E-plane and H-plane) of the reconfigurable MIMO antenna at 3.5, 4.5, and 5.2 GHz for each mode are shown in figure (2.22). During the measurement, port 1 was excited, whereas port 2 was terminated with a 50Ω matched load as shown in figure (2.23). The measurement results show that the proposed antenna has an omnidirectional radiation pattern in the H-plane and bidirectional radiation in the E-plane. Table (2.3) gives the simulated and measured realized gain for the different states of the proposed reconfigurable MIMO antenna at different operating frequencies. A good agreement is observed between simulation and measurement results.

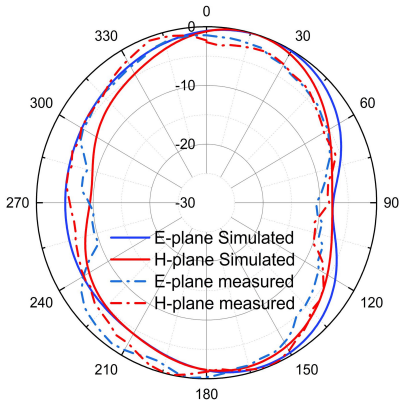

(a) Wideband mode at 5.2 GHz

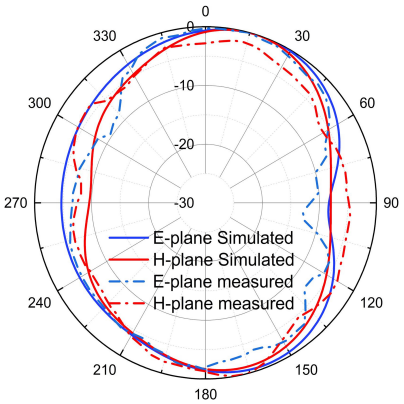

(b) Notched band mode at 5.2 GHz

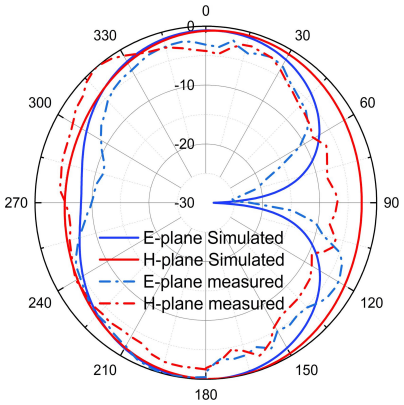

(c) Wideband mode at 3.5 GHz

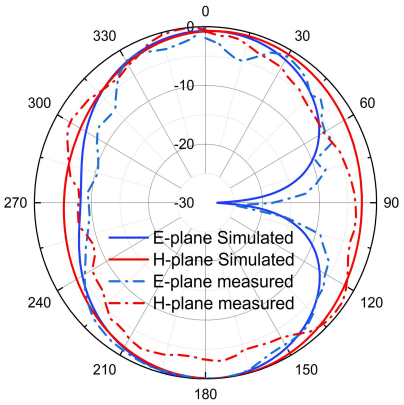

(d) LPF mode at 3.5 GHz

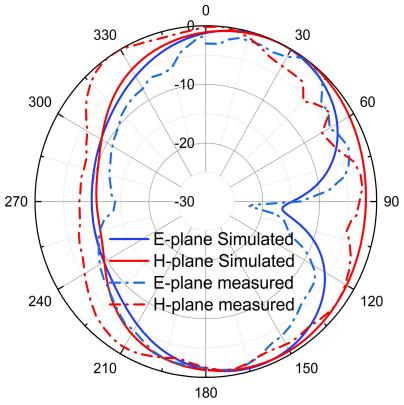

(e) LPF mode at 4.5 GHz

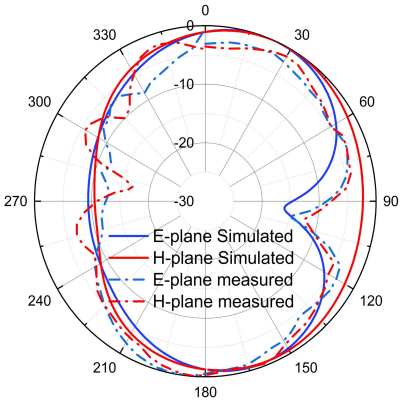

(f) Dual band mode at 4.5 GHz

Figure 2.22: Measured and simulated radiation patterns of the reconfigurable MIMO antenna

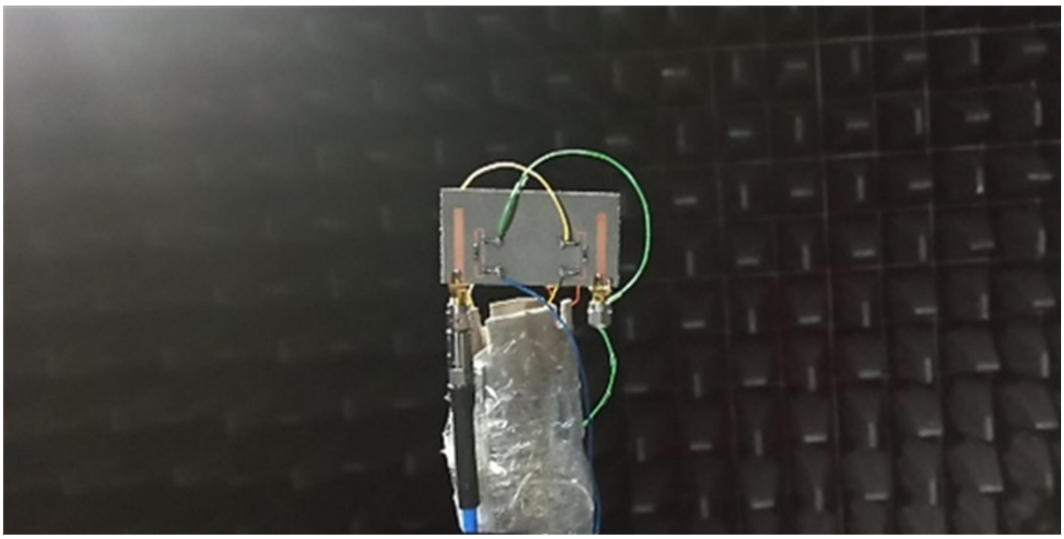

Figure 2.23: Measurement of the proposed antenna's radiation patterns

Table 2.3: Simulated and measured realized gain at different frequencies for all operating modes

Modes	Operating band (GHz)	Frequency (GHz)	Simulated Gain (dBi)	Measured Gain (dBi)
Wideband	2.41 - 6	5.2	5.09	4.64
Notched band	2.41 - 3.2 / 3.66 - 6	5.2	5.09	4.43
LPF	2.4 - 4.7	4.5	4.72	4.45
Dual band	2.41 - 3.16 / 3.64 - 4.7	3 / 4.5	2.88 / 4.78	2.51 / 4.53

c) Diversity performance

To evaluate the diversity performance of the proposed reconfigurable MIMO antenna, parameters were calculated and analysed from the simulated and measured S-parameters. The various numerical equations and the limit values for each parameter (ECC, DG, CCL, TARC, and MEG) can be found in the previous chapter, where we discussed and detailed them.

• Envelope Correlation Coefficient (ECC) and diversity gain (DG)

The simulated and measured ECC using S-parameters of the proposed antenna is illustrated in figure (2.24). A good agreement between simulations and measurements is

obtained. It is less than 0.008 in the whole operating band for the various modes which means a very low correlation between the two antenna elements. The ECC value increases at filtered frequencies (WiMAX / WLAN) while maintaining a good value as shown in figures (2.24b), (2.24c), and (2.24d). This indicates a good decoupling between the two ports even inside the filtered bands. Figure (2.24) also presents simulated and measured diversity gain for the four operating modes. It can be observed that the DG of the MIMO antenna is greater than 9.99 across all operational modes. This value changes only in the filtering bands related to the WiMAX and WLAN bands as shown in figures (2.24b), (2.24c), and (2.24d). These results validate the good diversity performances of the MIMO structure.

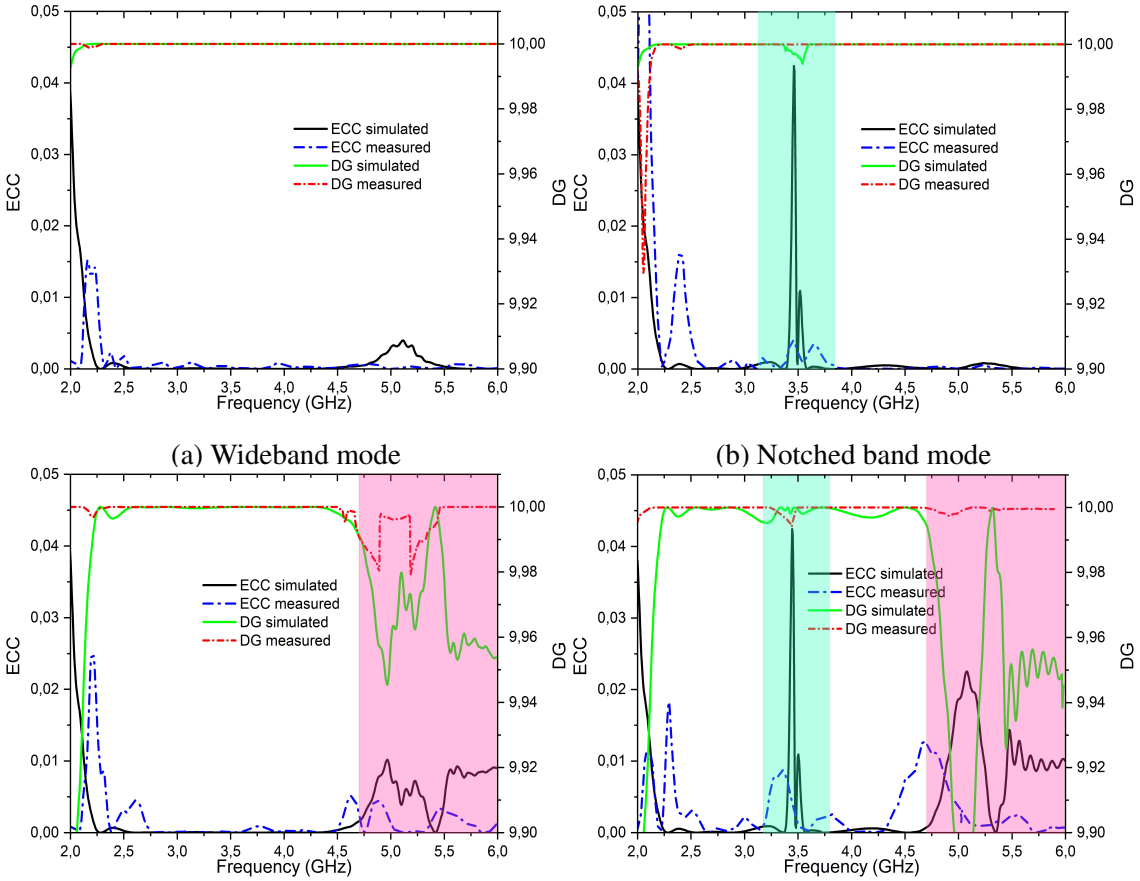

(a) Wideband mode

(b) Notched band mode

(c) LPF mode

(d) Dual band mode

Figure 2.24: Simulated and measured ECC and DG results of the proposed reconfigurable MIMO antenna

• Mean Effective Gain (MEG)

The variation of MEG for the two ports (1 and 2) with frequency (simulated and measured) is depicted in figure (2.25). From the four graphs, it is observed that the MEG performance is approximately -3 dB over the four operating modes. It can also see a low value of -13 dB and -8 dB in the case of rejecting and filtering bands respectively, as shown in figures (2.25b), (2.25c), and (2.25d) which indicates a good performance of the two mechanisms of reconfiguration.

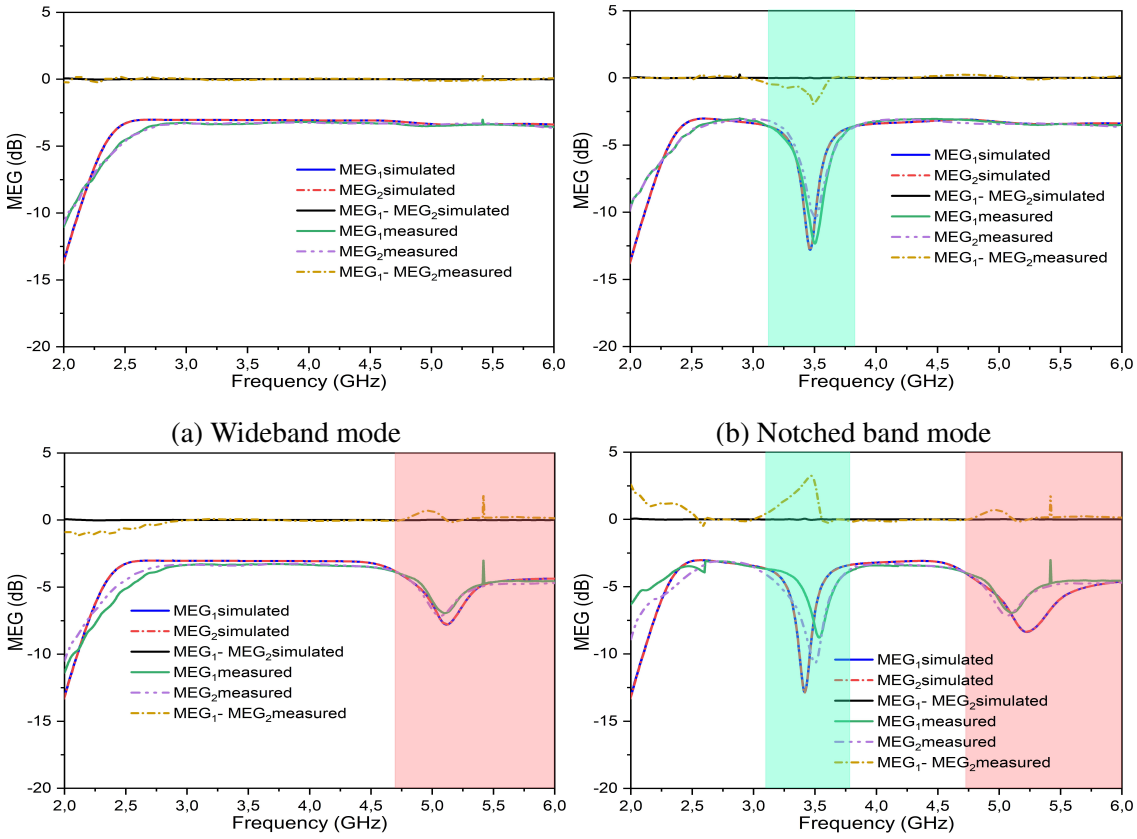

(a) Wideband mode

(b) Notched band mode

(c) LPF mode

(d) Dual band mode

Figure 2.25: Simulated and Measured MEG results of the proposed MIMO antenna

• Channel Capacity Loss (CCL) and Total Active Reflection Coefficient (TARC)

In figure (2.26), it is evident that the CCL remains below 0.4 bits/s/Hz across the diverse operating bands of the proposed antenna. However, this value escalates notably within the notching/filtering bands (figures (2.26b), (2.26c), and (2.26d)). Concurrently,

figure (2.26) also presents the TARC values for all states of the proposed reconfigurable antenna with $\theta = 0$. It is apparent that the TARC consistently registers below -20 dB throughout the entire operating bands across various modes.

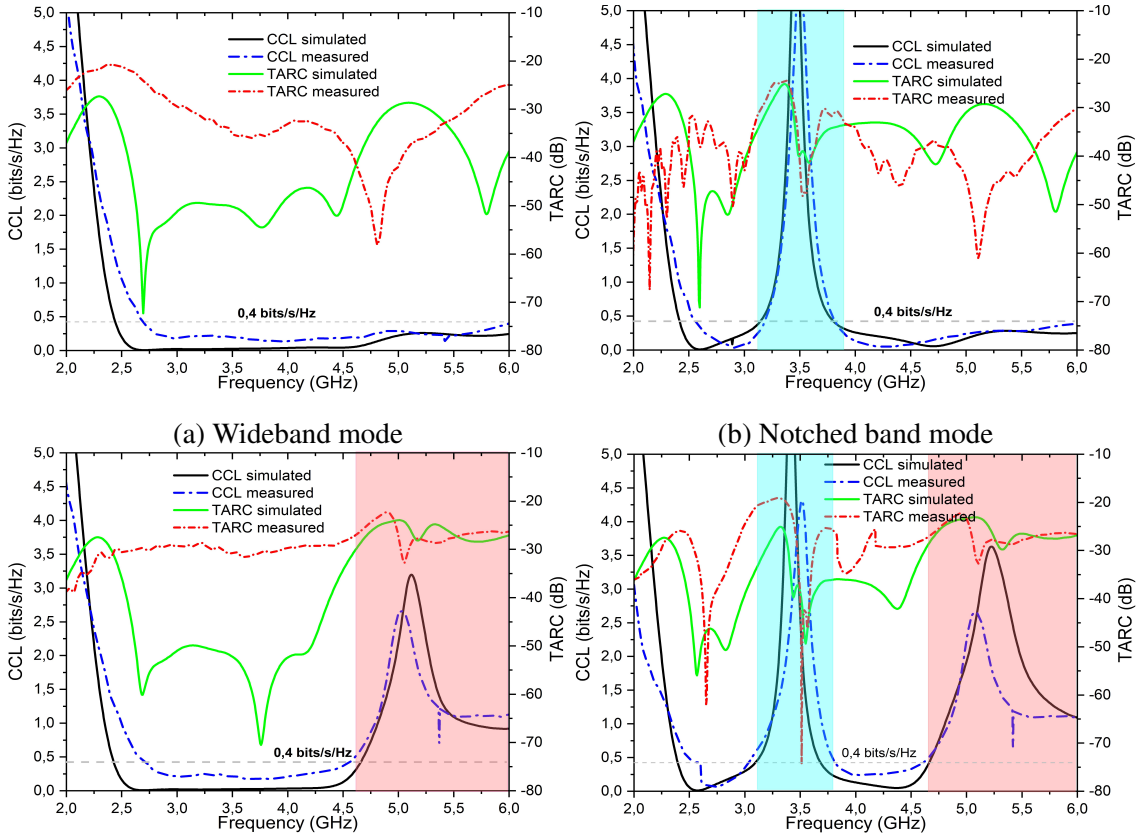

(a) Wideband mode

(b) Notched band mode

(c) LPF mode

(d) Dual band mode

Figure 2.26: Simulated and Measured CCL and TARC results of the proposed MIMO antenna

Table (2.4) provides details on the simulated and measured ECC, DG, CCL and TARC for the antenna's various operating modes.

Table 2.4: Simulated and measured values of ECC, DG, CCL and TARC for the various operating modes

	ECC		**DG**		**CCL(bits/s/Hz)**		**TARC (dB)**	
Mode	**Simu**	**Measu**	**Simu**	**Measu**	**Simu**	**Measu**	**Simu**	**Measu**
Wideband	0.005	0.003	9.99	9.99	0.24	0.28	-26	-20

Notched band	0.003	0.005	9.99	9.99	0.03	0.27	-30	-32.5
LPF	0.001	0.005	9.99	9.99	0.05	0.2	-40	-30
Dual band	0.001	0.008	9.99	9.99	0.15	0.29	-34	-29

2.5 Conclusion

In this chapter, we introduce a prototype of a frequency-reconfigurable two-element MIMO antenna. These designed structures are capable of operating in four different modes contingent upon the presence or absence of interference from the WiMAX or WLAN bands. The reconfigurability feature is ensured through the incorporation of two filtering mechanisms into an initial wideband antenna, achieved by utilizing PIN diodes to enable or disable each filter. Isolation greater than 18 dB is achieved across all four operating modes. Additionally, the diversity performances are evaluated, with envelope correlation coefficient (ECC) less than 0.008, channel capacity loss (CCL) below 0.29 bits/s/Hz, and high diversity gain (DG) exceeding 9.99 for all modes. The simulated and measured performance metrics, including mean effective gain (MEG) and total active reflection coefficient (TARC), exhibit close agreement, validating the proposed approach. All experimental results align well with those obtained via simulation, affirming the efficacy of the proposed antenna design and configuration. The findings of the structural study suggest that the MIMO antenna is well suited for 5G New Radio Sub-6 GHz (n46, n47, n77, n78, n79) applications. Additionally, these antennas are deemed suitable for cognitive radio (CR) applications, wherein they are required to perform sensing operations across a broad frequency spectrum to identify the most suitable frequency range for communication. During the sensing mode, the radio would leverage the wideband capabilities of the antenna to access the entire spectrum of interest. Subsequently, upon identifying the optimal operating mode, the radio can utilize the antenna to communicate within that specific frequency range, thereby ensuring optimal communication conditions.

CHAPTER 3

RECONFIGURABLE MULTI-BAND MIMO ANTENNA

3.1 Introduction

In this chapter, we introduce two frequency-reconfigurable multi-band antennas, which possess the flexibility to operate in any of the three most commonly used wireless standards: WiFi, WiMAX, and WLAN, and in any combination thereof. We aim to comprehensively explain the entire process, the role of each antenna element, and to provide a complete development cycle, from initial investigative simulations to the prototype fabrication using ideal and real switches. Moreover, to provide a holistic understanding of the performance of these reconfigurable multi-band MIMO antennas, extensive measurements and simulations have been conducted, covering various parameters including impedance bandwidth, gain, efficiency, and diversity performance.

3.2 Reconfigurable dual-band two-element MIMO antenna

3.2.1 Dual-band half-bowie antenna

The proposed dual-band single-element antenna is designed on a single-sided FR4 substrate with a thickness of 1.6 mm, a dielectric constant of 4.4, and a loss tangent of 0.02. The antenna is composed of half-bowtie antennas feeding by a CPW line and operates at 5.5 GHz (WLAN band), as depicted in figure (3.1). The dual-band operation behavior is achieved by integrating an inverted L-shaped slot into the original half-bowtie structure, as depicted in figure (3.2).

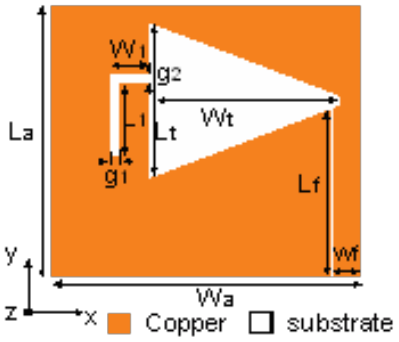

Figure 3.1: Dual-band half-bowie antenna geometry

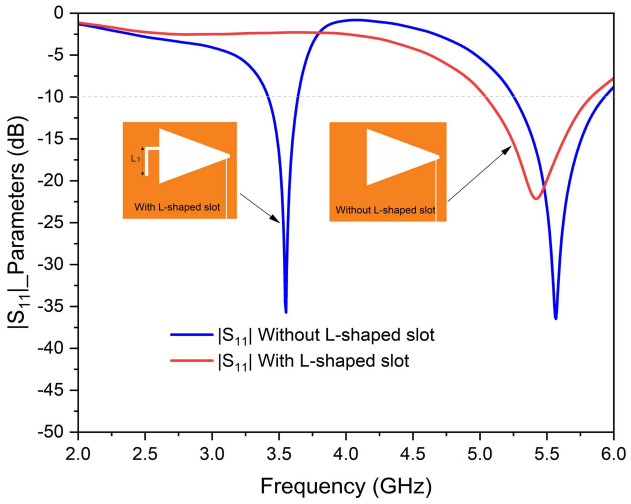

Figure 3.2: $|S_{11}|$ of the dual-band half-bowie antenna with/without inverted L-shaped slot

The length of the inverted L-shaped slot (L1+W1) etched into the side of the basic

antenna element is adjusted to resonate at 3.5 GHz (WiMAX band), as shown in figure (3.3). The dimensions of the proposed structure are listed in Table (3.1).

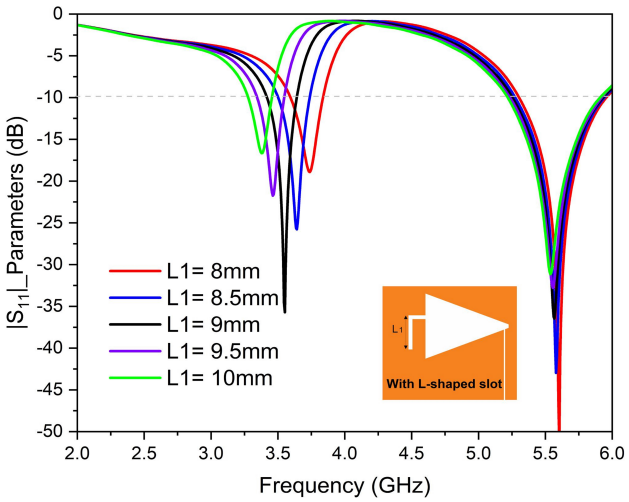

Figure 3.3: parametric study of the WiMAX band by adjusting the electrical length (L_1) of the L-shaped slot

Table 3.1: Dual-band half-bowie antenna dimensions

Parameter	Unit (mm)	Parameter	Unit (mm)
La	30	**Wa**	32
Lf	19	**Wf**	2
Lt	13	**Wt**	21
L1	6.8	**W1**	4.2
g1	1	**g2**	0.4

3.2.2 Dual-band two-element MIMO half-bowtie antenna

The dual-band two-element MIMO antenna proposed here consists of two single antenna elements symmetrically arranged without any additional spacing. Defected ground structures are integrated into the middle of the MIMO structure to reduce mutual coupling between the two elements, particularly in the second band created in low frequencies (3.5 GHz) as shown in figure (3.4).

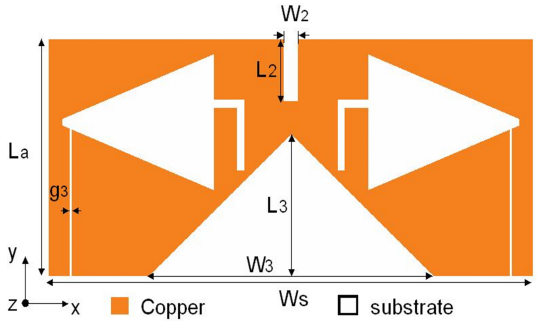

Figure 3.4: Layout of the proposed dual-band two-element MIMO half bowtie antenna, [Ws = 64, W2 = 2, L2 = 6.5, W3 = 34, L3 = 20.2, g3 = 0.4]

The simulated and measured S-parameters of the dual-band MIMO antenna are illustrated in figure (3.5). As can be seen from simulated results, the antenna provides an IBW ($|S_{11}| < -10$ dB) of ($3.35 - 3.62$ GHz) for the first band, and ($5.24 - 5.9$ GHz) for the second band at the mid frequencies of 3.5, 5.6 GHz with minimum isolation of 22 , and 32 dB for the two consecutive frequency bands. However, the measured S-parameters show that the realized prototype covered two operating bands of $3.36 - 3.6$ GHz (WiMAX), and $5.06 - 5.84$ GHz (WLAN). In addition, the minimum measured isolation values across the two operating frequency bands are below than -25 and -27 dB for WiMAX and WLAN, respectively, which indicate a high isolation between the two ports.

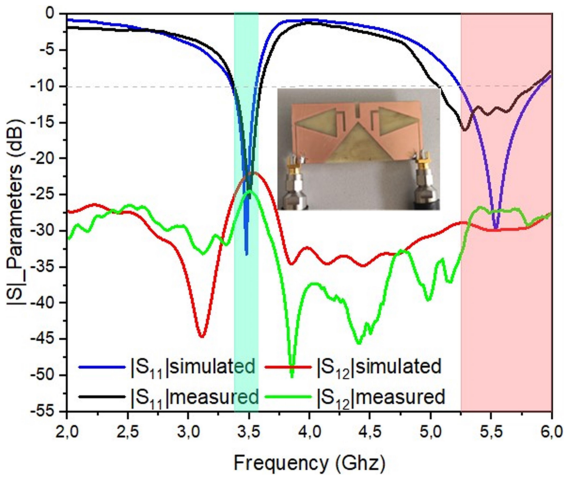

Figure 3.5: Measured and simulated S-parameters of the dual-band two-element MIMO half-bowtie antenna

3.2.3 Frequency reconfigurable dual-band two-element MIMO half Bowtie antenna

For reconfiguration behavior, two pin diodes BAR50-02v from the manufacturer Infineon are used to switch between single and dual-band modes. They are placed at the beginning of the two L-shaped slot extensions, as shown in figure (3.6). For the diodes biasing, a separating slot in the middle is used in addition to three decoupling capacitors of 100 pF. The proposed reconfigurable MIMO structure can operate in two distinct modes, as shown in figure (3.7). The first mode is the dual-band mode, which operates in the WiMAX band from 3.38 GHz to 3.61 GHz, and the WLAN band from 5.25 GHz to 6 GHz, used also for 5G new radio sub-6GHz. It is obtained when all diodes are in the OFF state. The second mode is the single-band mode, which covers the WLAN frequencies $(4.85 - 5.6\ \text{GHz})$ activated when all diodes are in the ON state.

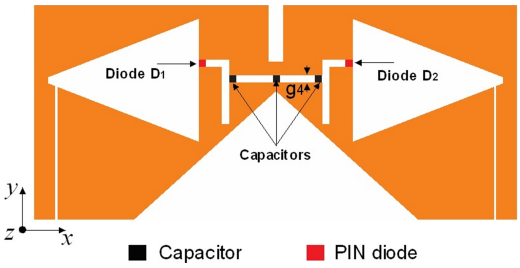

Figure 3.6: Layout of the frequency reconfigurable dual-band two-element MIMO half Bowtie antenna, $[g4 = 0.3]$

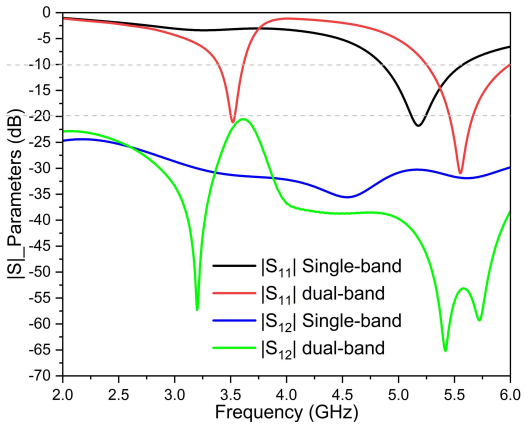

Figure 3.7: |S|-parameters of the frequency reconfigurable dual-band two-element MIMO half Bowtie antenna

a) Isolation Mechanism

Figure (3.8) presents the different configurations studied to improve isolation between the two ports. In the first operating mode (dual-band), the initial structure without modifications (antenna 1), has a low isolation of about 11 dB for the first frequency band $(3.38 - 3.61\ \text{GHz})$ and an isolation of about 20 dB in the second operating band ($5.25 - 6\ \text{GHz}$), as presented in figure (3.9a). Then, by inserting a straight slot of dimension $L_2 \times W_2$ (antenna 2), the isolation increases to 14 dB and 23 dB for WiMAX and WLAN, respectively. Using only a triangularshaped slot (antenna 3), an isolation of 18 dB and 25 dB is obtained for WiMAX and WLAN, respectively. Finally, when both shapes (rectangular and triangular) are used at the same time (antenna 4), the isolation in the WiMAX and WLAN bands reaches the values of 20 dB and 55 dB, respectively. For the second mode of operation (single-band), the antenna has already good isolation without isolation mechanism (antenna 1), with a minimum isolation of 17.5 dB, as shown in (3.9b). After introducing the modifications, the isolation increases by 12.5 dB to reach 30 dB (antenna 4).

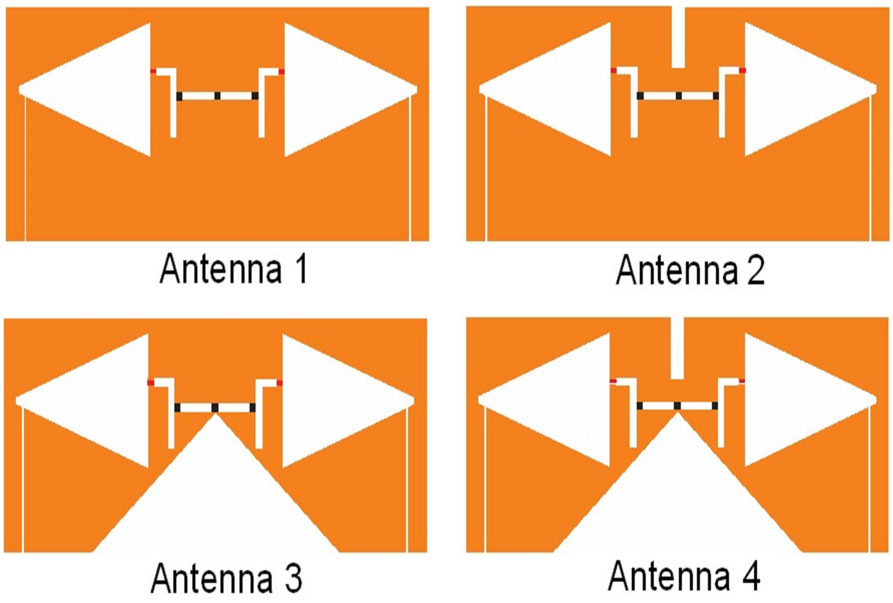

Figure 3.8: Evolution of isolation mechanism for the proposed frequency reconfigurable dual-band two-element MIMO half Bowtie antenna

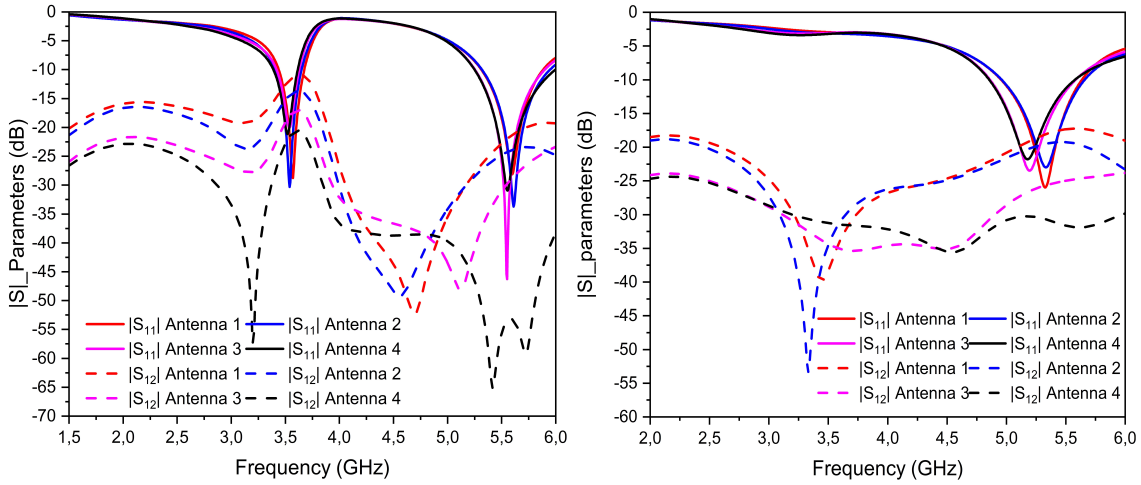

(a) Dual-band mode (b) Single-band mode

Figure 3.9: S-Parameters for the proposed frequency reconfigurable dual-band two-element MIMO half Bowtie antenna

Figure (3.10) shows the current distribution on the antenna surface with and without isolation mechanism for both operating frequencies. We can see the effect of the isolation mechanism introduced on the antenna performance and the improvement of the isolation between the two ports.

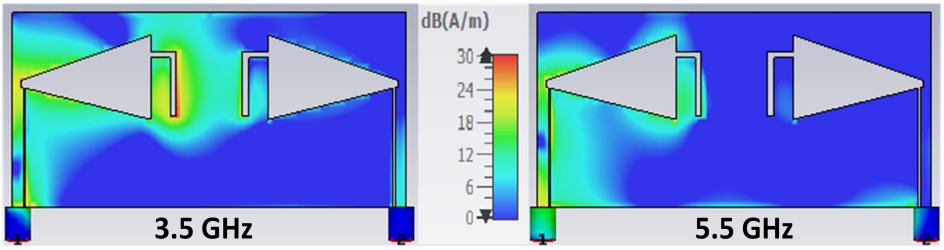

(a) Without isolation

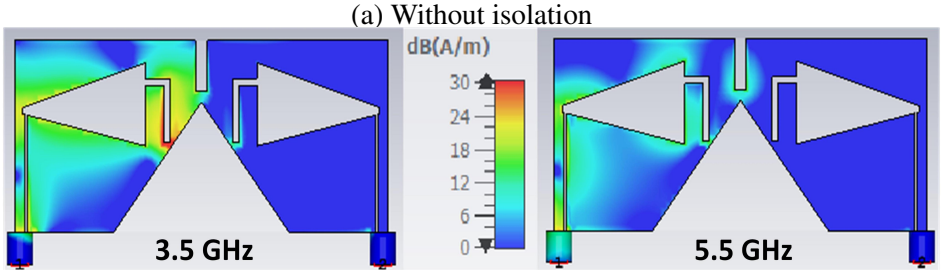

(b) With isolation

Figure 3.10: Surface current distribution for the proposed frequency reconfigurable dual-band two-element MIMO half Bowtie antenna

b) S-parameters

To evaluate the performance of the proposed antenna with the frequency reconfiguration circuit, a prototype was constructed using an FR4 substrate with a permittivity of 4.4 and a thickness of 1.6 mm. Figure (3.11) shows the photograph of the prototype with the Pin diodes and the bias circuit. In order to bias the diodes with DC voltages around 5V, wires and a stabilized power supply incorporating an adjustable current limiter were used, as shown in figure (3.12).

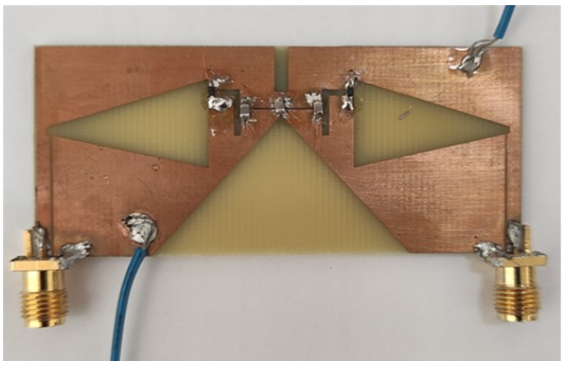

Figure 3.11: Photograph of the realized frequency reconfigurable dual-band two-element MIMO half Bowtie prototype

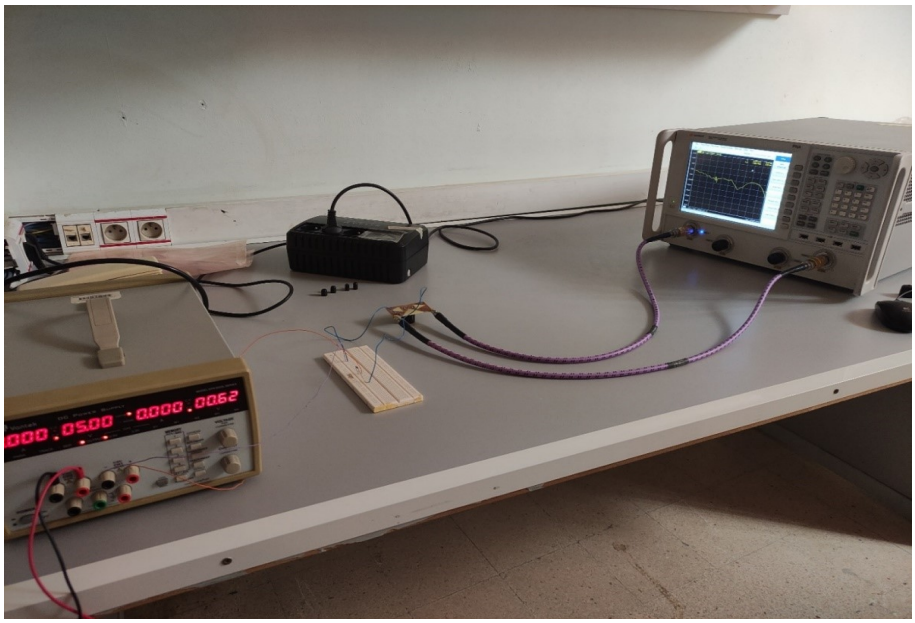

Figure 3.12: Setup for polarizing PIN diodes using a stabilized power source

The simulated and measured S-parameters of the dual-band frequency reconfigurable MIMO antenna for both the two operating modes (single and dual-band) are shown in figures (3.13) and (3.14).

In the case of dual-band mode: the results of the simulation show that the antenna has two bands of operation. The first covers the WiMAX band (3.38-3.61 GHz), and the second covers the WLAN band $(5.25-6\ \text{GHz})$ with a minimum isolation of 20 dB and 55 dB for each band, respectively. For the experimental results, the antenna covers the first band from 3.32 GHz to 3.52 GHz and the second one from 5.06 GHz to 5.94 GHz with a minimum isolation of 20 dB and 30 dB for the two frequency bands, respectively, as depicted in figure (3.13). However, it is noteworthy that the experimental measurements, reflected by S_{11} values of -13 dB and -12 dB for WiMAX and WLAN bands, respectively, are less congruent with the simulated values, which exhibit S_{11} values of -21 dB and -30 dB for WiMAX and WLAN bands, respectively. This discrepancy could be attributed to factors such as the effects of component soldering (PIN diodes with bias circuits), and fabrication quality.

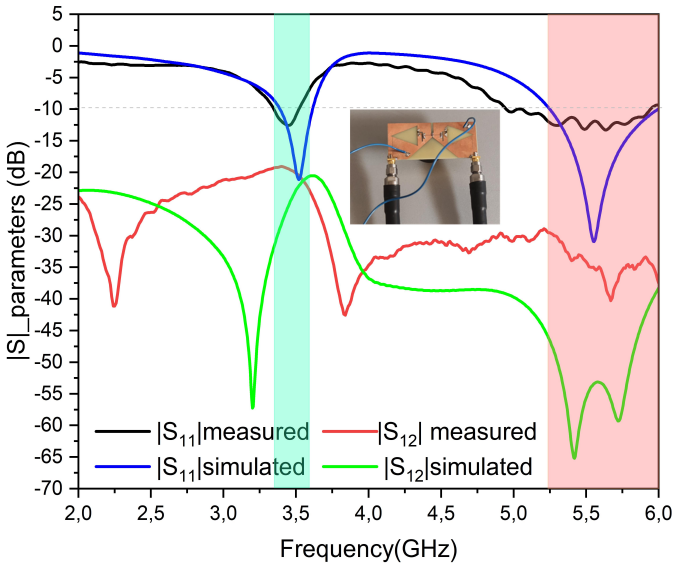

Figure 3.13: Measured and simulated S-parameters of the frequency reconfigurable dual-band two-element MIMO half Bowtie antenna in the case of dual-band mode

In the case of single-band mode: the simulated results show that the operating band is from 4.85 GHz to 5.6 GHz with a minimum isolation of 30 dB. It is also observed that

the measured bandwidth of the fabricated prototype is from 4.7 GHz to 5.62 GHz, with a minimum isolation of 35 dB, as shown in figure (3.14).

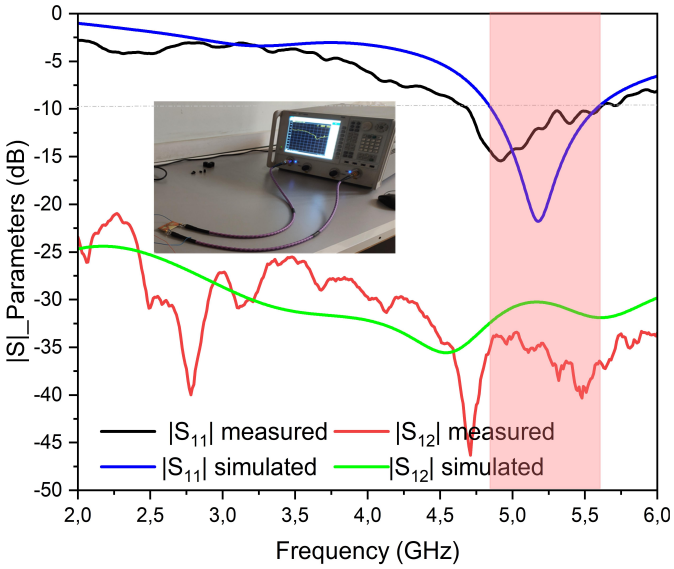

Figure 3.14: Measured and simulated S-parameters of the frequency reconfigurable dual-band two-element MIMO half Bowtie antenna in the case of single-band mode

A good similarity is observed between the results obtained by simulation and measurement, which validates the performance of the proposed structure.

c) Radiation patterns

The normalized radiation pattern measurement is performed inside an anechoic chamber. During the measurement, the port 1 is excited and the second one is terminated by 50Ω load. The radiation patterns of the frequency reconfigurable dual-band two-element MIMO half Bowtie antenna for 3.5GHz and 5.5GHz, are illustrated in figure (3.15a) and figure (3.15b), respectively. A quasi-omnidirectional radiation is observed in the H plane for the two operating bands. In the E-plane, the radiation pattern becomes more directive with the appearance of side lobes.

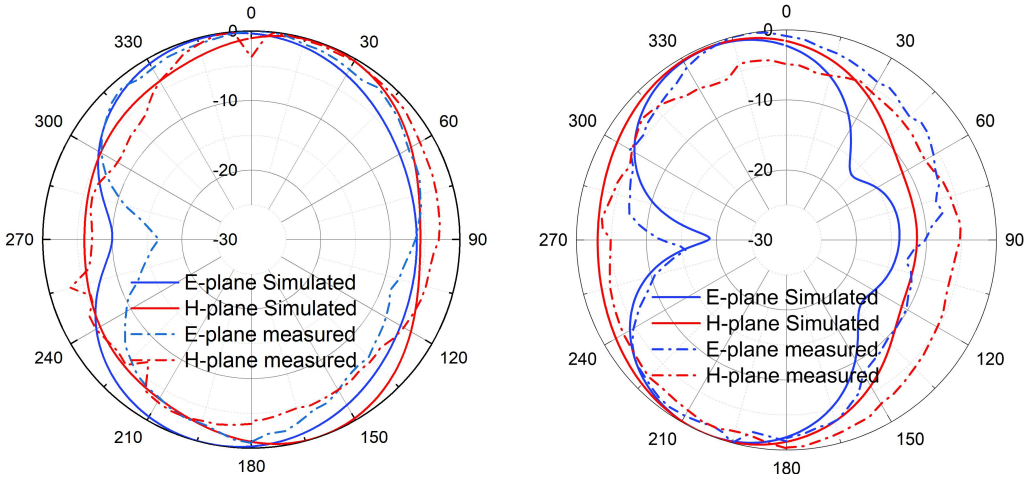

(a) WiMAX band (3.5GHz) (b) WLAN band (5.5GHz)

Figure 3.15: Simulated and measured radiation patterns

Figure (3.16) shows the realized gain as a function of frequency. It can be seen that the designed antenna has a simulated maximum gain of 3.14 dBi and 4.66 dBi, and a measured gain of 3.72 dBi and 5.12 dBi for the two bands of operation, respectively.

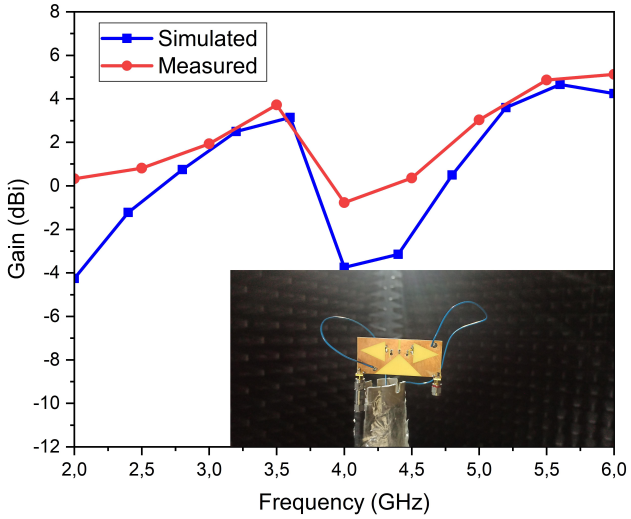

Figure 3.16: Realized gain of the frequency reconfigurable dual-band two-element MIMO half Bowtie antenna (dual band case)

d) Diversity performance

The evaluation of MIMO diversity performance involves the assessment of various parameters, detailed mathematically in the first chapter, including ECC, DG, CCL, TARC,

and MEG. These parameters are analyzed across the two operating modes of the reconfigurable MIMO antenna, as depicted in figure (3.17). Initially, The ECC demonstrates values below 0.002 in both dual-band and single-band modes, indicating robust decoupling between ports. Subsequently, DG values hover around 10 across operating modes, as shown in figure (3.17a). CCL measurements, illustrated in figure (3.17b), consistently remain below 0.4 bits/s/Hz, with values below 0.24 and 0.16 bits/s/Hz for the WiMAX and WLAN bands, respectively, in dual-band mode, and below 0.22bits/s/Hz for single-band mode within the WLAN band. Meanwhile, MEG values maintain proximity to -3 dB across operating bands, with differences between MEG 1 and MEG 2 within ± 3 dB, as outlined in figure (3.17c). Furthermore, TARC measurements, depicted in figures (3.17d), consistently fall below -10 dB for dual-band mode and below -20 dB for single-band mode, underscoring stable performance due to minimal mutual coupling between ports. Table (3.2) depicts the simulated and measured results of ECC, DG, CCL, and MEG of the proposed frequency reconfigurable dual-band twoelement MIMO half Bowtie antenna.

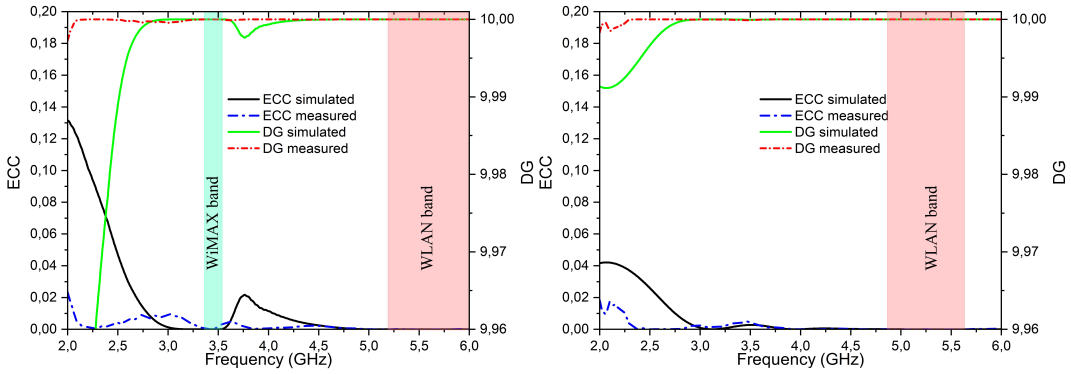

(a) ECC and DG

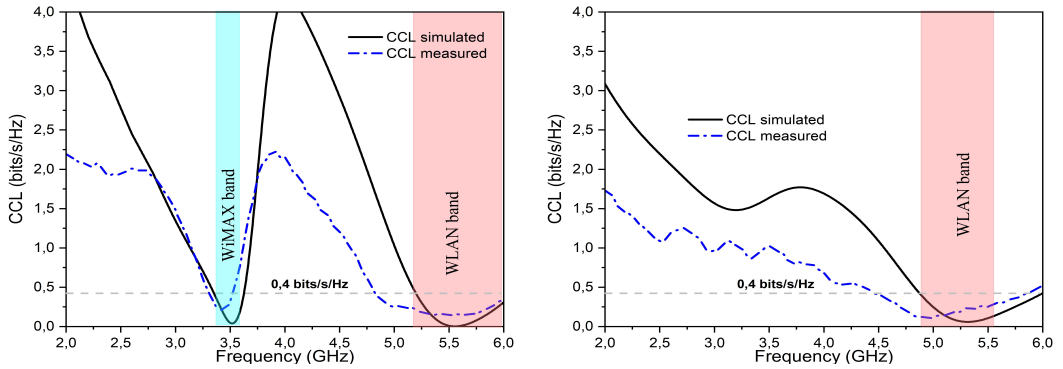

(b) CCL

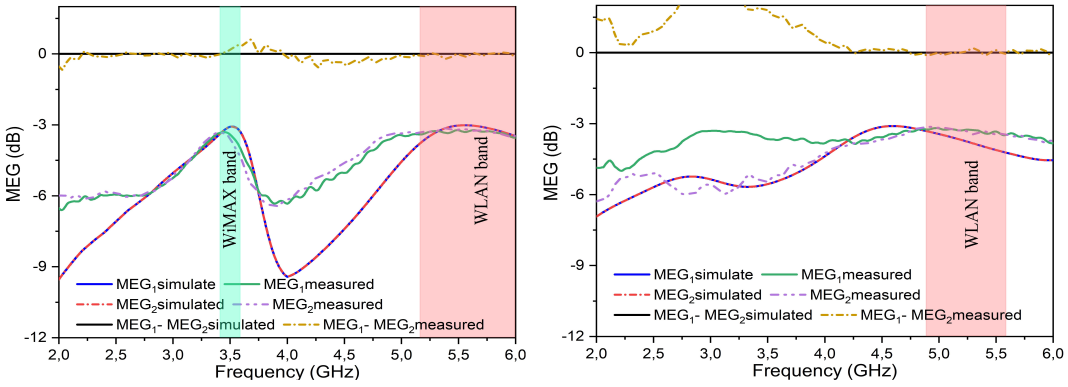

(c) MEG

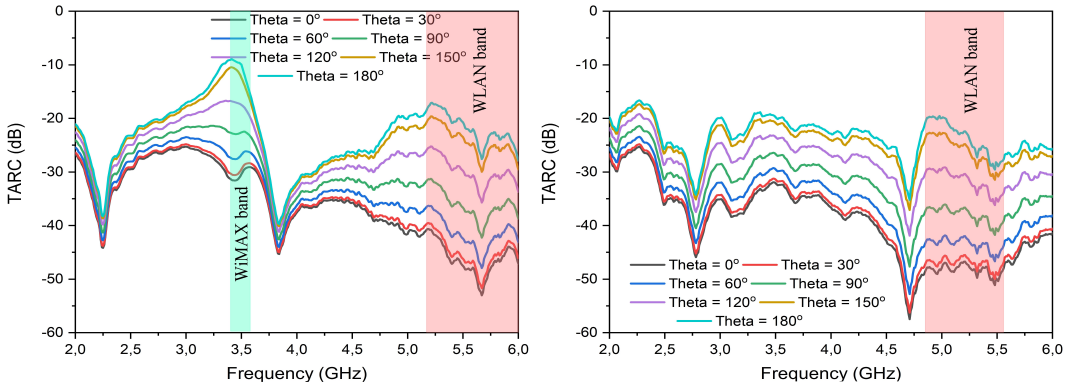

(d) TARC

Figure 3.17: Simulated and measured diversity performance of the proposed frequency reconfigurable two-element MIMO half Bowtie antenna both the two operating mode

Table 3.2: ECC, DG, CCL, and MEG values both the two operating mode of the proposed reconfigurable MIMO antenna

Operating modes	**Operating band (GHz)**	**ECC**		**DG**		**CCL (bits/s/Hz)**		**MEG1- MEG2 (dB)**
		Meas	**Simu**	**Meas**	**Simu**	**Meas**	**Simu**	
Dual-band mode	WiMAX	0.002	0.00001	9.999	10	0.24	0.15	0.16
	WLAN	0.00006	0.000001	10	10	0.16	0.1	-0.025
Single-band mode	WLAN	0.00004	0.000023	10	10	0.22	0.12	0.083

The simulation and measured results for all diversity performance metrics, including

ECC, DG, CCL, TARC, and MEG, demonstrate remarkable coherence. This alignment between experimental and simulation results provides robust validation for the proposed frequency reconfigurable MIMO antenna approach.

3.3 Reconfigurable triple-band two-element MIMO slot antenna

3.3.1 Triple-band slot antenna

The proposed triple-band single element antenna consists of 50Ω stepped microstrip feed line etched on the top layer, as shown in figure (3.18a). In the bottom layer, three open quarter-wave slots of different lengths with the same width 'g' are inserted in the ground plane, as shown in figure (3.18b), for obtaining triple-band antenna operation. The upper and long meandered shaped slot provides the first resonance at 2.51 GHz, and the short meandered shaped slot allows obtaining the second resonance at 3.51 GHz.The straight line slots of dimension $l_{11} \times g$ create the third resonant frequency at 5.75 GHz as depicted in figure (3.19). The dimensions of the proposed structure are listed in table (3.3).

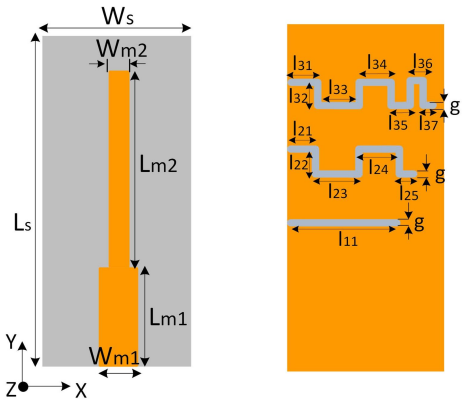

(a) Top view (b) Back view

Figure 3.18: Layout of the proposed single-element triple-band slot antenna

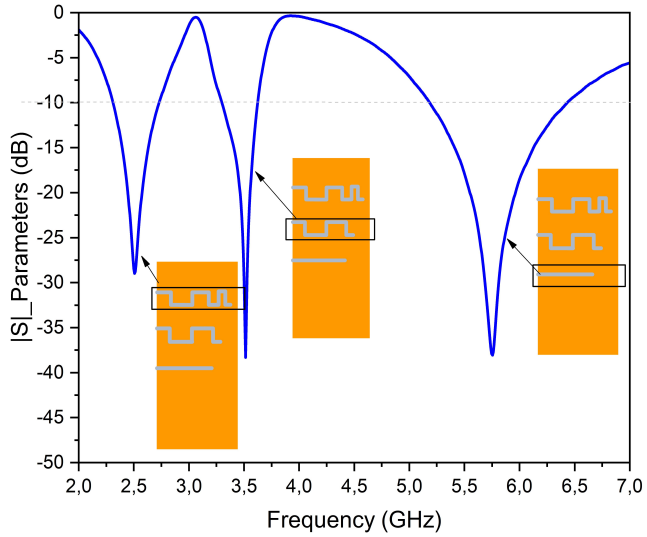

Figure 3.19: Simulated reflection coefficient $|S_{11}|$ of the proposed single-element triple-band slot antenna

Table 3.3: Single-element triple-band slot antenna dimension

Parameter	**Unit (mm)**	**Parameter**	**Unit (mm)**	**Parameter**	**Unit (mm)**
Ls	34	**Ws**	16	**l24**	3.6
Lm1	9.5	**Wm1**	4	**l25**	1.6
Lm2	20.5	**Wm2**	2	**l31**	3
l11	11.5	**l32**	1.8	**l36**	1.8
l21	1.8	**l33**	3	**l37**	1
l22	2.4	**l34**	4	**g**	0.6
l23	5	**l35**	3		

To investigate the effect of the slots dimensions on the performance of the single-element antenna, a parametric study is done, as depicted in figure (3.20). It shows the influence of l_{32} variation on the $|S_{11}|$ when it is varied from 1.8 to 3 mm. It is observed that only the first resonance $f_1 = 2.5$ GHz changes. When l_{22} is varied from 1.6 to 2.4 mm, it is observed that the middle frequency $f_2 = 3.5$ GHz shift toward higher frequencies when l_{22} decreases, which leads that the short meandered shaped slot controls mainly the middle frequency. Finally, varying l_{11} parameter affect mainly the higher resonance $f_3 = 5.75$ GHz. It is concluded that it can control independently the three operation bands.

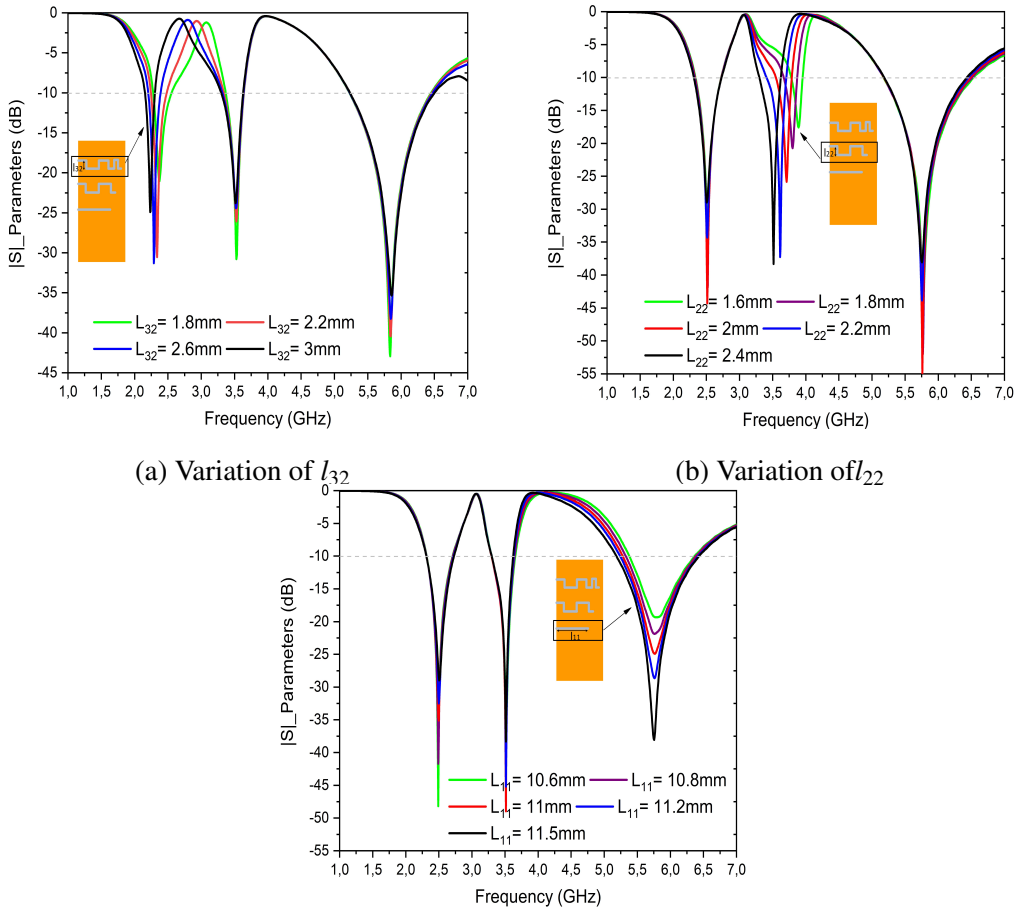

(a) Variation of l_{32}

(b) Variation ofl_{22}

(c) Variation ofl_{11}

Figure 3.20: Parametric studies of the single-element triple-band slot antenna

To analyze the generation of triple-band antenna response, the surface current distributions at 2.47, 3.50, and 5.75 GHz are plotted in figure (3.21). In figure (3.21a), the current distributions mostly reside near the long meander line slot at 2.47 GHz. Also, in figure (3.21b), the currents are concentrated on the short meander line slot at 3.56 GHz. Figure (3.21c) represents the current distribution at 5.43 GHz showing more density of currents in the rectangular slot. Hence, from the surface current distribution, it concluded that the single radiator antenna could generate independent resonance along with the three frequency bands.

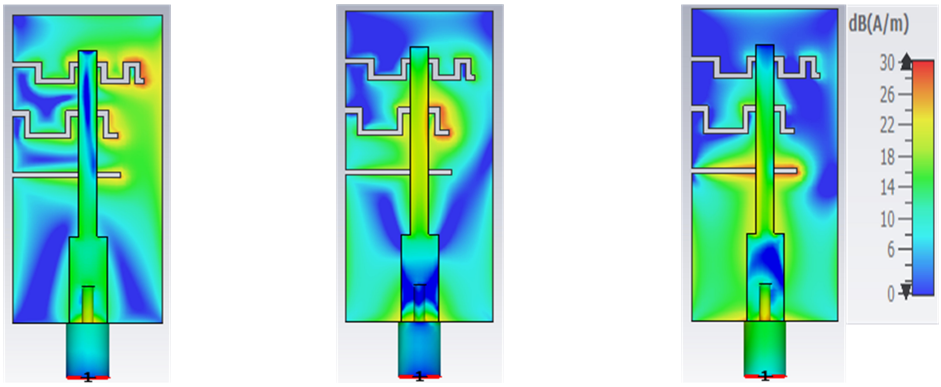

(a) 2.47 GHz (b) 3.50 GHz (c) 5.75GHz

Figure 3.21: Parametric studies of the single-element triple-band slot antenna

The designed antenna is fabricated on Rogers RT5880 substrate with dielectric constant of $\varepsilon_r = 2.2$, thickness of h = 1.57 mm, and loss tangent of $\tan\delta = 0.0009$. The overall dimension of the realized structure, shown in figure (3.22), is 34 mm $\times$ 16 mm $\times$ 1.57 mm.

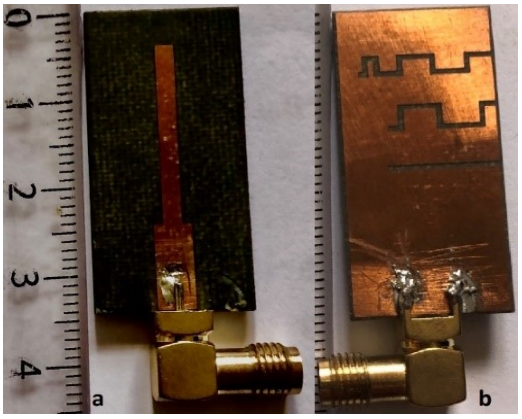

Figure 3.22: Manufactured single-element antenna (a) Top view, (b) Back view

The simulated and measured $|S_{11}|$ are shown in figure (3.23). Simulated results supports three bands of operation: $2.23-2.50$ GHz, $3.53-3.71$ GHz, and $5.46-5.84$ GHz. Experimental results show that the three operating bands $(|S_{11}| \leq -10$ dB$)$ are $2.48-2.81$ GHz, $3.41-3.625$ GHz, and $4.8-6.42$ GHz. The measured results are in good agreement with the simulated ones. A small shift in the frequency bands is observed which is mainly due to the manufacturing quality.

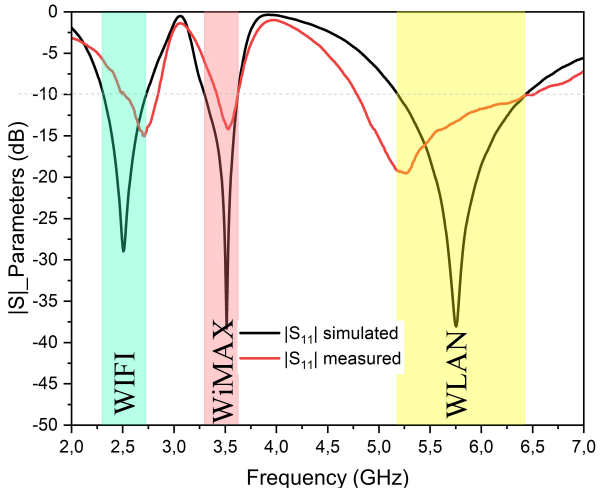

Figure 3.23: Simulated and measured reflection coefficient $|S_{11}|$ of the proposed single-element triple-band slot antenna

3.3.2 Triple-band two-element MIMO slot antenna

The proposed two-element MIMO antenna consists of two unit elements arranged in parallel and shares a common ground plane of 34 mm $\times$ 32.5 mm, with an edge-to-edge distance of 0.5 mm$(0.004\lambda$ at the lowest resonance frequency 2.4GHz$)$, as shown in Figure (3.24). The twoelement MIMO antenna are printed on Rogers RT5880 substrate and fed by two 50-ohm SMA connectors. To obtain better isolation between elements, while keeping a compact structure, an open-ended slot of dimension $L_f \times g_1$ is inserted between the two ports, extended from the center section of the ground plane, as shown in figure (3.24). Photographs of the realized structure are shown in figure (3.25).

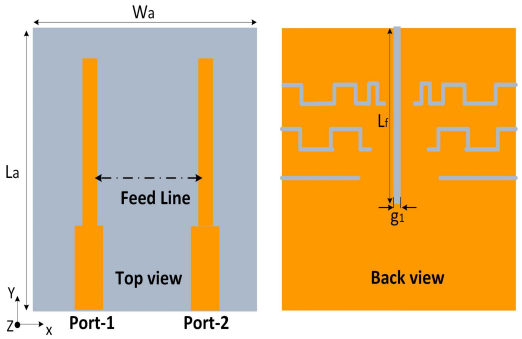

Figure 3.24: Configuration of the triple-band two-element MIMO slot antenna [$L_a = 34$, $W_a = 32.5$, $L_f = 20.2$, $g_1 = 0.5$. (all are in (mm)]

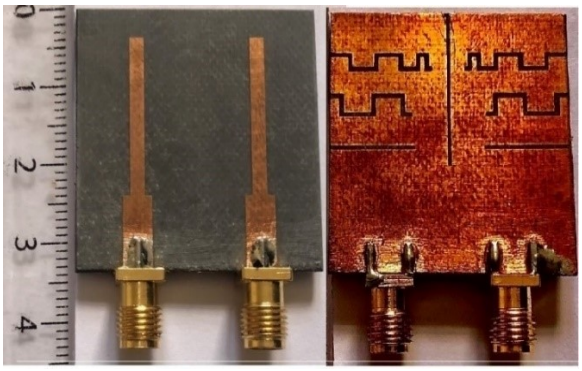

Figure 3.25: The fabricated triple-band two-element MIMO slot antenna (Top and Back view)

a) Isolation technique

The comparison of simulated |S|-parameters of the proposed antenna with and without isolation structure is presented in figure (3.26). It shows that due to the introduction of an open-ended slot, the isolation in the first operating band is improved from 9 dB to 22 dB and the resonant frequency shifts from 2.95 GHz to 2.4 GHz.

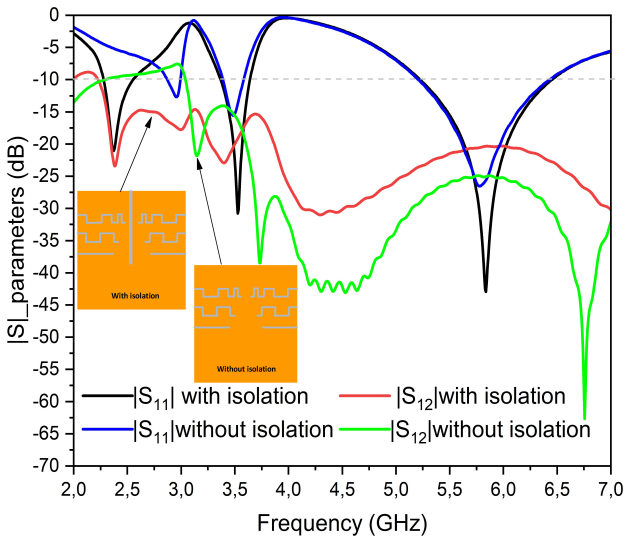

Figure 3.26: Simulated S-parameters for the proposed triple-band two-element MIMO slot antenna with and without isolation structure

To obtain better insight of the isolation mechanism, especially for the WiFi band (2.45GHz), the surface current distribution of the antenna with and without isolation mechanism at

the lower resonant frequency (WiFi), is illustrated in figure (3.27). When there is no slot between the two antenna elements, a large amount of electromagnetic energy is being coupled from port 1 to port 2 at 2.5 GHz, which leads to poor isolation of 9 dB. However, after the introduction of a narrow vertical slot, the mutual coupling is significantly reduced at 2.5 GHz of 22 dB. Moreover, a large amount of surface current is being trapped in around the narrow vertical slots.

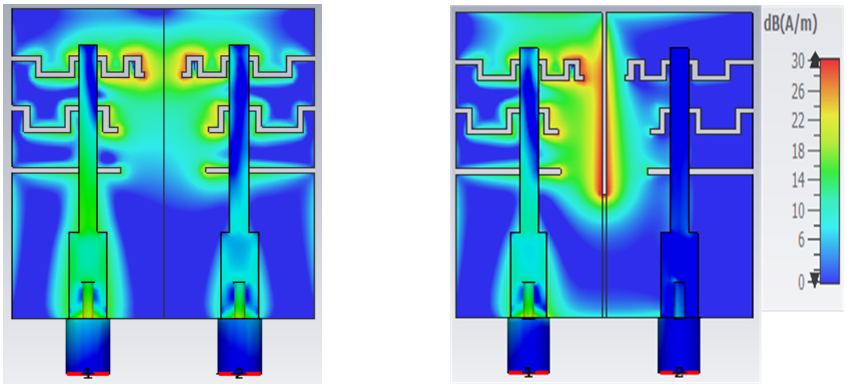

(a) Without isolation (b) With isolation

Figure 3.27: Surface current distribution of the proposed triple-band two-element MIMO slot antenna at WIFI band

b) S-parameters

The simulated and measured |S|-parameters are plotted and presented in figure (3.28). Firstly, the simulated results show that the reflection coefficient is less than -10 dB in the three frequency bands: $2.27-2.55$ GHz (relative bandwidth of 11.8%), $3.36-3.64$ GHz (relative bandwidth of 7.9%) and $5.23-6.42$ GHz (relative bandwidth of 20.51%). It is also observed, that the measured isolation is better than 23 dB, 17 dB, and 20 dB for the three frequency bands; respectively. Secondly, the measured results for the manufactured prototype show that the antenna supports three bands: $2.23-2.50$ GHz (relative bandwidth of 11.42%), $3.53-3.71$ GHz (relative bandwidth of 4.97%), and 5.46-5.84 GHz (relative bandwidth of 6.7%). The isolation obtained is higher than 16 dB, 15 dB, and 30 dB for the three frequency bands, respectively. We can note a good agreement between simulation and measurements. We only notice a small shift in the bands, which is essentially due to the quality of manufacture.

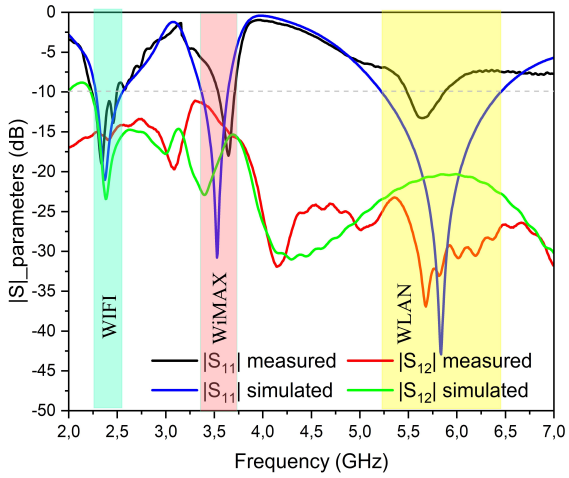

Figure 3.28: Measured and simulated S-parameters for the proposed triple-band two-element MIMO slot antenna

c) Radiation pattern

The Simulated and measured normalized E-plane and H-plane 2D radiation patterns of the proposed triple-band two-element MIMO antenna at port-1 (keeping port-2 connected with a matched load of 50Ω impedance) are depicted in figures (3.29). The radiation patterns at 2.35 and 3.53 GHz show omnidirectional forms of radiation in both the E-plane and H-plane as shown in figure (3.29a) and (3.29b). Moreover, nearly circular radiation behavior at 5.8 GHz is depicted in figure (3.29c). In addition, it is noted that the simulated gains are 2.57, 1.61, and 5.04 dBi at 2.35 GHz (WiFi), 3.53 GHz (WiMAX), and 5.8 GHz (WLAN), respectively, as shown in figure (3.30).

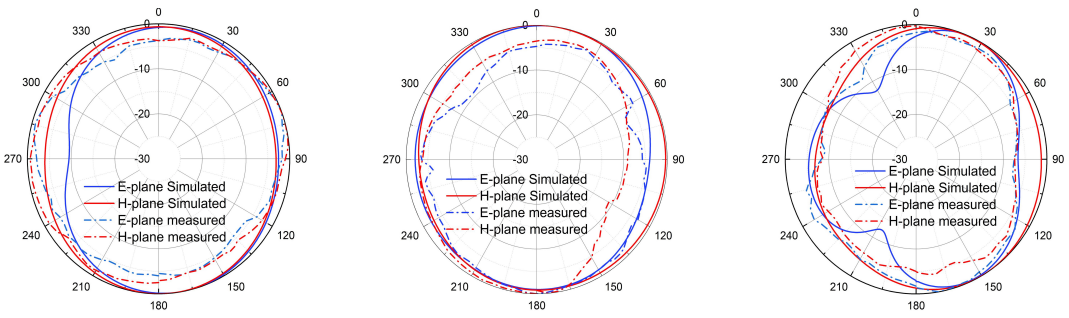

(a) 2.35GHz (b) 3.5GHz (c) 5.8GHz

Figure 3.29: Radiation patterns for the proposed triple-band two-element MIMO slot antenna

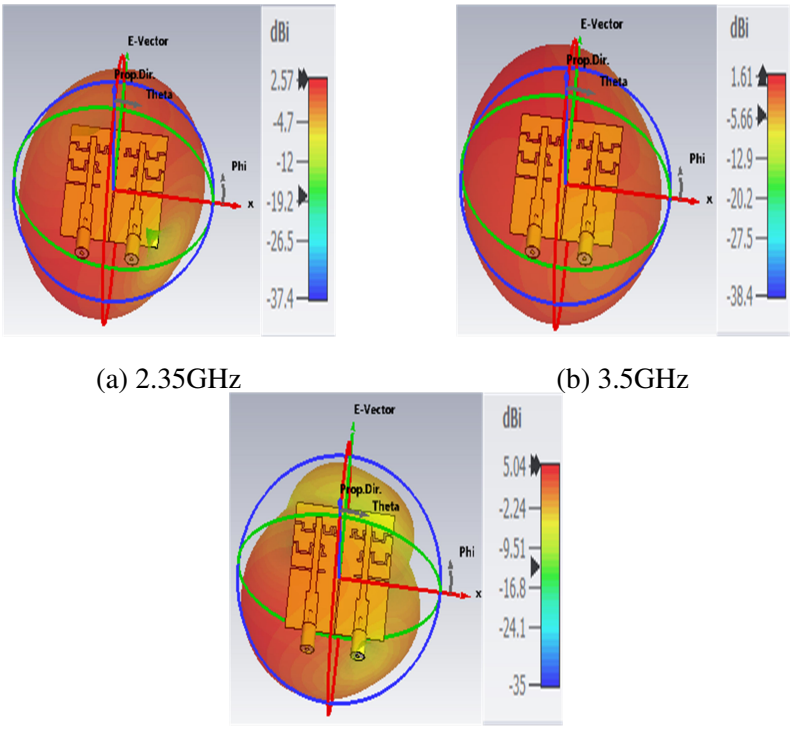

(a) 2.35GHz (b) 3.5GHz

(c) 5.8GHz

Figure 3.30: 3D radiation pattern of the designed triple-band two-element MIMO slot antenna

d) Diversity performance

The performance characteristics of the proposed triple-band two-element MIMO slot antenna, depicted in figure (3.31), reveal consistent ECC values below 0.013, 0.011, and 0.001 across consecutive frequency bands (figure (3.31a)). Both simulated and measured results demonstrate a DG of approximately 10 across all three operating bands. Notably low CCL values of $0.2, 0.29$, and 0.18 bit/s/Hz at frequencies $2.35, 3.6$, and 5.65 GHz, respectively, are observed in figure (3.31b), alongside TARC values showing minima of -31.94 dB, -31.42 dB, and -50.06 dB at the same frequencies. Furthermore, figure (3.31c) reveals that the MEG performance remains below -3 dB across the entire frequency range. These findings collectively highlight the exceptional diversity performance of the proposed design, rendering it highly suitable for MIMO applications. Detailed simulated and measured results for ECC, DG, CCL, and TARC are presented in table (3.4).

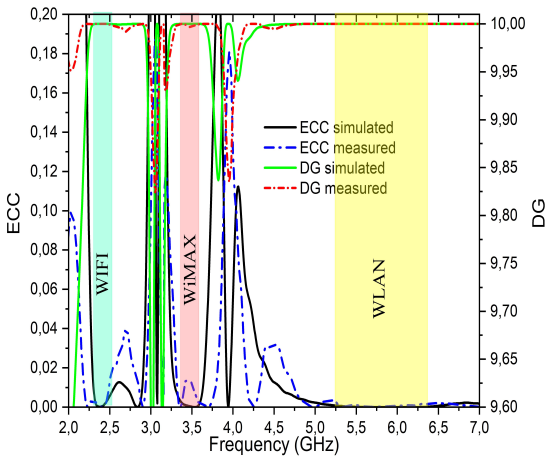

(a) ECC and DG

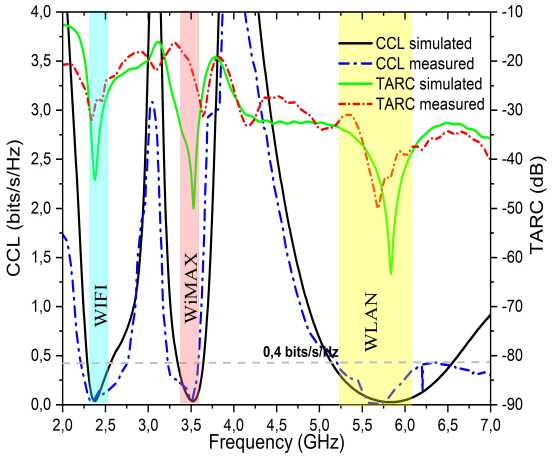

(b) CCL and TARC

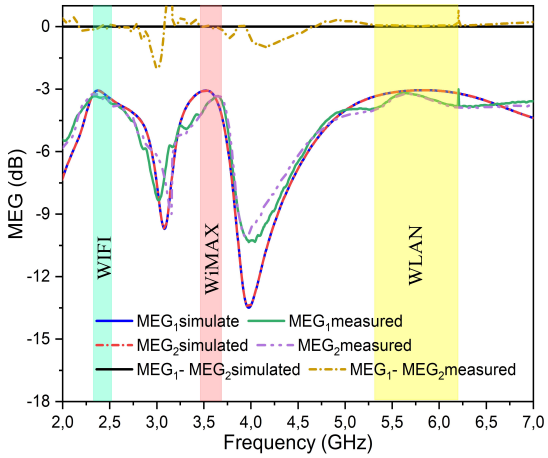

(c) MEG

Figure 3.31: Simulated and Measured diversity performance results of the proposed triple-band two-element MIMO slot antenna

Table 3.4: Simulated and measured ECC, DG, CCL, and TARC for the proposed triple-band two-element MIMO slot antenna

	ECC		**DG**		**CCL (bits/s/Hz)**		**TARC (dB)**	
Frequency	Simu	Meas	Simu	Meas	Simu	Meas	Simu	Meas
2.35GHz	0.001	0.013	10	9.999	0.06	0.2	-43.39	-31.94
3.6GHz	0.015	0.011	10	9.98	0.16	0.29	-49.23	-31.42
5.65GHz	0.00002	0.001	10	9.999	0.08	0.18	-61.81	-50.06

3.3.3 Frequency reconfigurable triple band two-element MIMO slot antenna

proposed triple-band MIMO antenna is capable to work in any combination of bands involving the three most commonly used wireless standards that are: WiFi, WiMAX, and WLAN. For the frequency reconfiguration, 10 switches are integrated on the three open-end quarter-wave slots to switch from one mode of operation to another: 4 switches are used for the long meandered shaped slot, 4 others switches are used for the short meandered shaped slot and 2 others switches are used for the rectangular slot, as shown in figure (3.32).

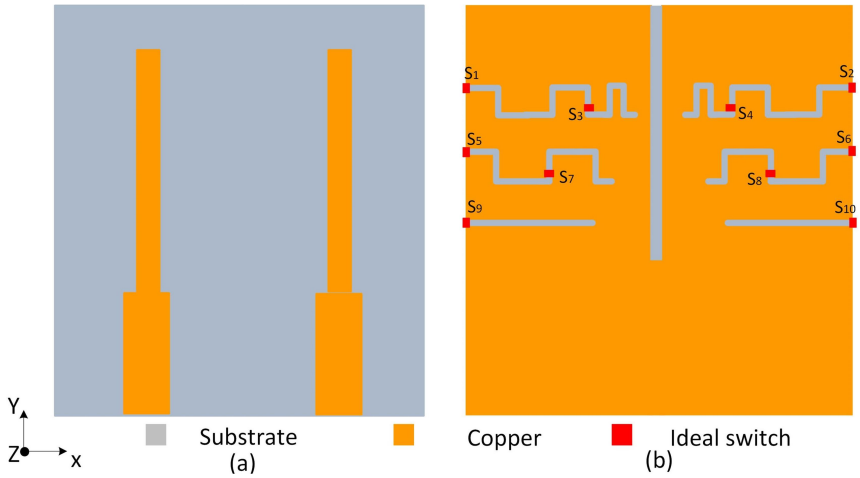

Figure 3.32: Design of the proposed frequency reconfigurable triple band two-element MIMO slot antenna (a) Top view, (b) Back view

In order to validate the reconfiguration mechanism, the two operating states of the switch “on/off” were modeled by the presence/absence of a perfect conductor strip of the same size as that of a real switch. By strategically placing these switches (the switch locations have been optimized to cancel the operation bands when the latter is closed), the antenna can switch between 7 different operating modes (3 single-band modes, 3 dual-band modes, and one triple-band mode), as illustrated in figure (3.33). The different configurations of switches are summarized in table (3.5).

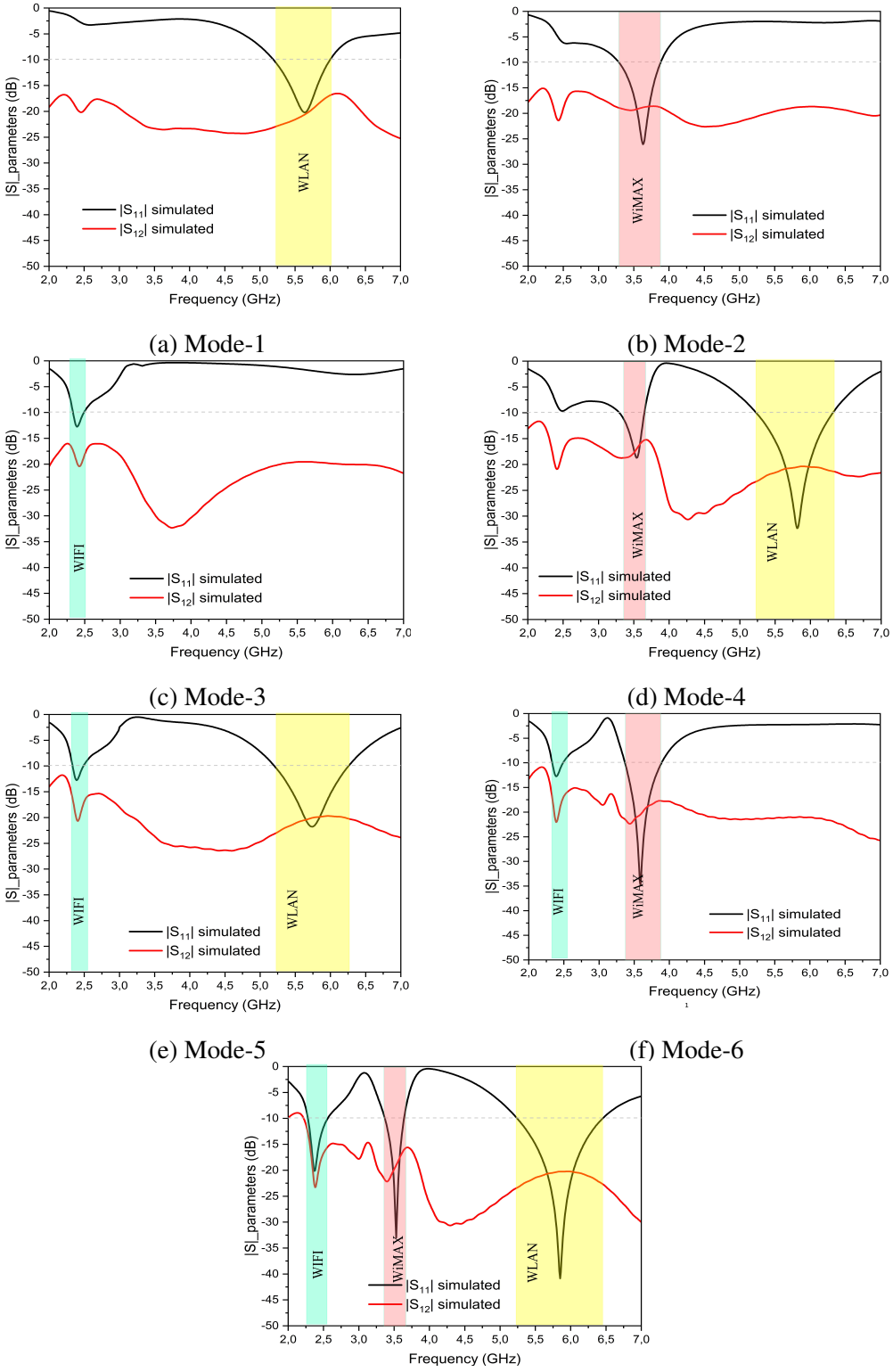

(a) Mode-1

(b) Mode-2

(c) Mode-3

(d) Mode-4

(e) Mode-5

(f) Mode-6

(g) Mode-7

Figure 3.33: Simulated S-parameters of the proposed frequency reconfigurable triple band two-element MIMO slot antenna for different operating modes

Table 3.5: Configuration of switches for different operating modes

Modes	State of the switch			Operating band
	S1-S4	S5-S8	S9, S10	
Mode-1	ON	ON	OFF	WLAN
Mode-2	ON	OFF	ON	WiMAX
Mode-3	OFF	ON	ON	WIFI
Mode-4	ON	OFF	OFF	WLAN, WiMAX
Mode-5	OFF	ON	OFF	WIFI, WLAN
Mode-6	OFF	OFF	ON	WIFI, WiMAX
Mode-7	OFF	OFF	OFF	WiFi, WLAN, WiMAX

3.4 Conclusion

In this chapter, two frequency-reconfigurable MIMO antennas were introduced, demonstrating high-frequency agility. The first antenna structure features a unique design, serving as the fundamental element with a half-bowtie shape optimized for operation within the WLAN band (5.5 GHz). Dual-band functionality is achieved by integrating a pair of inverted L-shaped slots on each side of the two antenna elements, with slot dimensions tailored for WiMAX band operation (3.5 GHz). Reconfigurability is facilitated by including two Infineon PIN diodes, enabling seamless switching between single-band and dual-band operation. Additionally, defected ground structures (DGS) introduced in the middle of the antenna are utilized to reduce mutual coupling between the two ports to less than 20 dB. This frequency-reconfigurable antenna demonstrates excellent MIMO diversity performance, with an envelope correlation coefficient (ECC) below 0.002 and a channel capacity loss (CCL) below 0.24 bps/Hz. Based on these results, it can be inferred that the proposed antenna is suitable for use in MIMO and cognitive radio systems, and can even be applied in Sub-6 GHz 5G applications. The second structure consists of reconfigurable multi-antenna triple-band systems. Here, three open quarter-wave slots of varying lengths are incorporated into the ground plane of each antenna element to enable triple-band operation. The operating principle has been demonstrated by utilizing ten ideal switches to control the operation of these slots. The designed two-port multi-antenna

system can seamlessly switch between seven different operating modes, including single-band, dual-band, and triple-band configurations, while maintaining robust performance characteristics, particularly in terms of isolation.

CHAPTER 4

RECONFIGURABLE UWB MIMO ANTENNA WITH REJECTED BANDS

4.1 Introduction

THIS chapter aims to design MIMO antenna systems operating within the millimeter-wave band. The first proposed structure is a two-element SWB MIMO antenna operating from 3.2 to 50 GHz. However, due to practical limitations, only simulated results will be presented. The second proposed structure features a reconfigurable UWB antenna, operating from 3.27 to 23 GHz, with capabilities for filtering and controlling two interference bands. Diversity performances are conducted using simulation and measurement data. These proposed antennas represent innovative approaches to enhancing the performance of wireless communication systems across diverse applications, ranging from MMW 5G networks to UWB systems.

4.2 Super wideband band MIMO antenna

4.2.1 Single element SWB antenna

The single-element antenna geometry for SWB application is depicted in figure (4.1). Utilizing an FR4 substrate measuring 22 mm × 15 mm × 1.6 mm, characterized by a thickness of 1.6 mm, a loss tangent of 0.025 , and a dielectric constant of 4.3 , forms the basis of the antenna design. Simulation of the proposed structure was conducted using CST Microwave Studio. The top layer of the single planar monopole incorporates a tapered microstrip feedline, denoted by dimensions $L_f \times W_f$. The primary radiating element (patch) is constructed in a trapezoidal shape supplemented by a semicircular extension. The additional circular component, featuring a radius R and an angle 2θ (where $\theta = 80^\circ$), facilitates SWB operation. The bottom layer comprises a partial ground plane measuring 6.6 mm × 15 mm, illustrated in figure (4.1). The antenna demonstrates comprehensive impedance matching across a frequency range spanning from 4 GHz to beyond 50 GHz, as illustrated in figure (4.2).

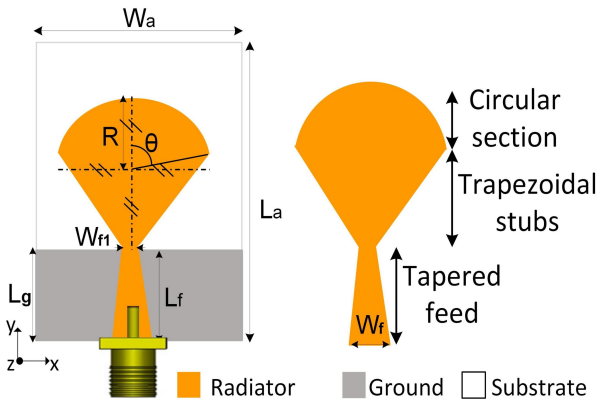

Figure 4.1: Single-element SWB antenna geometry [$L_a = 22$, $W_a = 15$, $L_f = 7$, $L_g = 6.6$, $W_f = 3$, $W_{f1} = 0.7$, $R = 5.5$ (all are in mm)]

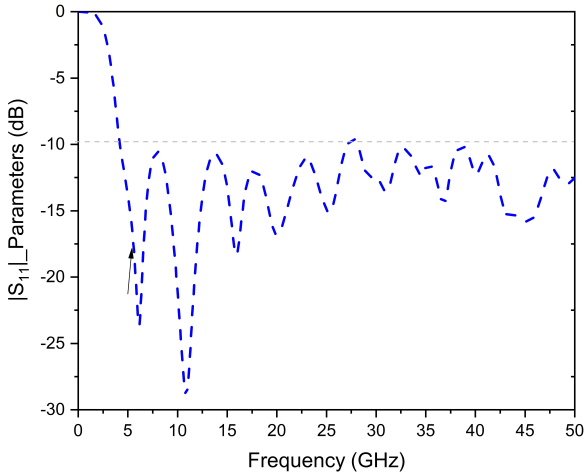

Figure 4.2: Simulated $|S_{11}|$ of the single-element SWB antenna

To understand the impact of dimensional variations in the circular segment (radius R and angle 2θ) on antenna performance, a detailed parametric study was conducted. Figure (4.3a) illustrates the influence of R variation on the reflection coefficient $|S_{11}|$. It is evident that the operational bandwidth exhibits improved suitability for lower frequencies as R ranges from 2.5 mm to 5.5 mm, with $|S_{11}| \leq -10$ dB. Subsequently, figure (4.3b) depicts the effect of altering the angle θ on $|S_{11}|$. Notably, a discernible alteration in the operational bandwidth occurs as θ diminishes from 160° to 80°, particularly within the frequency spectrum below 10 GHz.

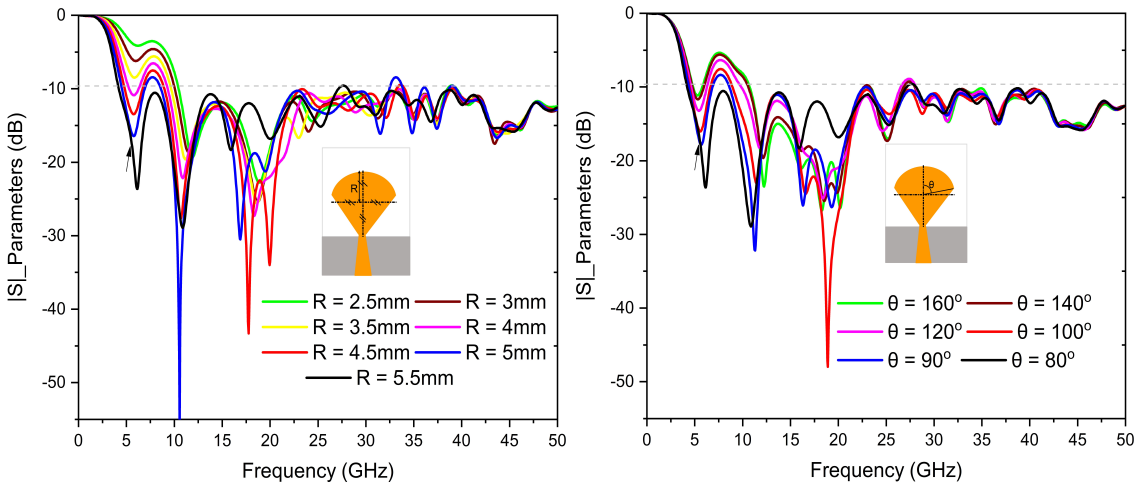

(a) Variation of Radius 'R' (b) Variation of angle 'θ'

Figure 4.3: Parametric study for the single-element SWB antenna

4.2.2 Two element SWB MIMO antenna

The MIMO antenna described in this study features dimensions of 34 mm × 22 mm × 1.6 mm and possesses a straightforward design. Consisting of two symmetrical elements arranged in parallel and sharing a common ground plane, the antenna elements are spaced 4 mm apart from edge to edge. The feeding of the two elements is facilitated by two 50Ω SMA connectors. To enhance isolation between the two elements without compromising on compactness, an inverted L-shaped ground stub with a wide rectangular slot etched into the partial ground plane is strategically incorporated between them, as depicted in figure (4.4).

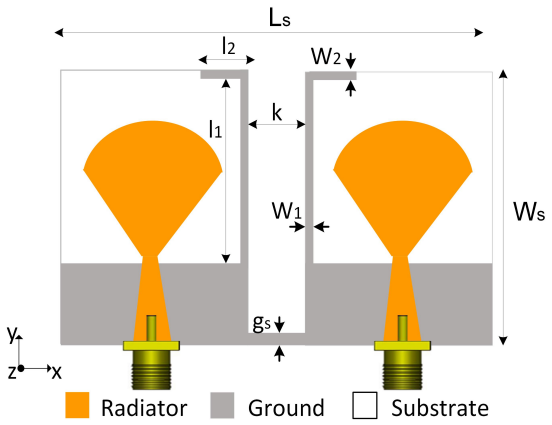

Figure 4.4: Proposed two-element SWB MIMO antenna, [$L_s = 34$, $W_s = 22$, $l_1 = 26.9$, $l_2 = 4$, $W_1 = 0.5$, $W_2 = 0.5$, $g_s = 1$, $k = 4$ (all are in mm)]

The design process of the MIMO antenna is elucidated through various stages, outlined in figure (4.5). The progression of the simulated S-parameter curve concerning the structure's geometry evolution is demonstrated in figure (4.6). Initially, two simple elements are positioned with a 4 mm separation (Antenna 1), juxtaposed with a basic rectangular partial ground plane measuring 6.6 mm × 34 mm. In this configuration, the simulated $|S_{11}|$ curve, displayed in figure (4.6a), indicates antenna operation spanning from 3.6GHz to 50 GHz, exhibiting an impedance bandwidth (IBW) of 46.4 GHz (relative bandwidth of 173.8%). Notably, the simulated transmission coefficient suggests exceptionally low isolation, particularly at lower frequencies, as depicted in figure (4.6b). Subsequently, the partial ground plane undergoes modification with the introduction of a rectangular-shaped slot measuring 5.6 mm × 4 mm (Antenna 2). This alteration reduces mutual coupling

($|S_{21}|$) to below -13 dB across the operational band, while the bandwidth remains unchanged, as evidenced in figure (4.6a). Further enhancement in bandwidth is achieved by incorporating two vertical stubs with dimensions of 15.4 mm $\times$ 0.5 mm into the ground plane (Antenna 3). In this configuration, the operational range extends from 3.2 GHz to 50 GHz, exhibiting an impedance bandwidth of 46.8 GHz (relative bandwidth of 176%). However, isolation in the case of Antenna 3 remains low within the frequency range below 4 GHz. Ultimately, the implementation of an inverted Lshaped stub (Antenna 4) yields high isolation exceeding 19 dB, as presented in figure (4.6b), rendering it suitable for SWB MIMO systems performance.

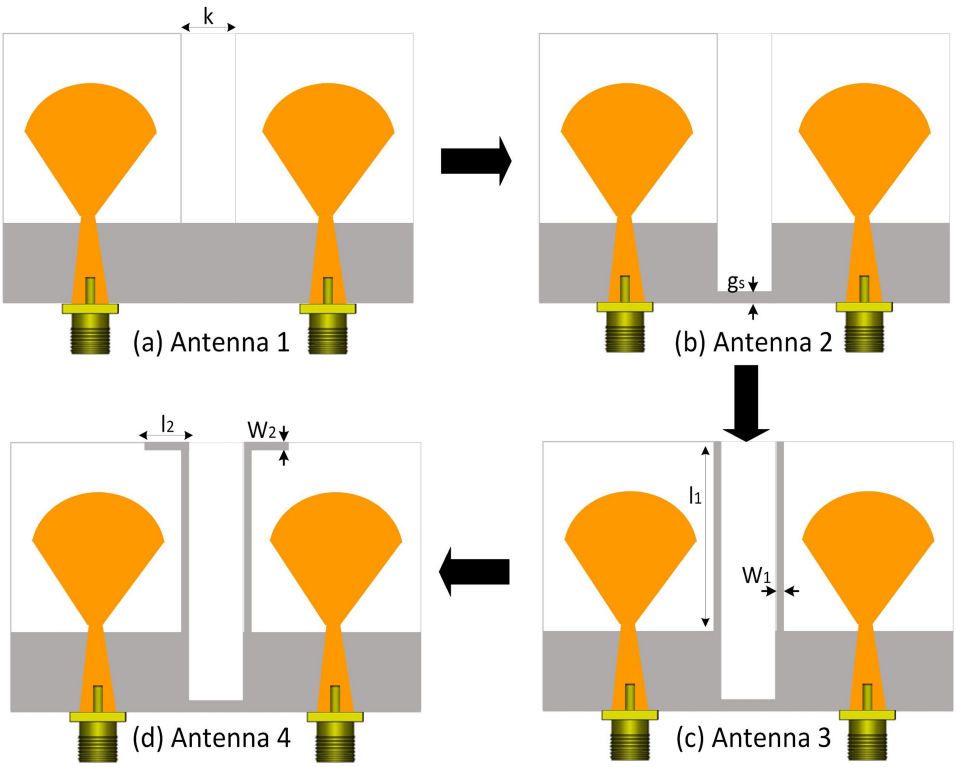

Figure 4.5: Geometry evolution of the proposed two-element SWB MIMO antenna

It is noteworthy that the measurement validation has been constrained by the available instrument measurement at the laboratory (Vector Network Analyzer, diodes, and cables), which operate to frequencies up to 23 GHz. Consequently, the next sections will focus on UWB MIMO antenna design operating within a frequency range spanning from 3.2 GHz to 23 GHz.

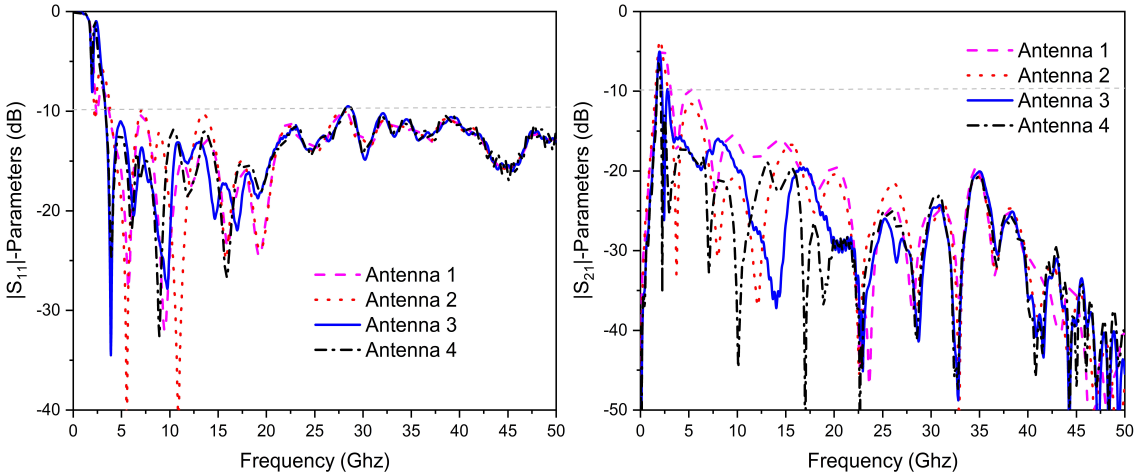

(a) $|S_{11}|$-parameters (b) $|S_{21}|$-parameters

Figure 4.6: Simulated and superimposed S-parameters for each configuration

4.3 Ultra wideband MIMO antenna

4.3.1 Two element UWB MIMO antenna

A prototype of the proposed two-element UWB MIMO antenna with the same dimensions given in figure (4.4) is fabricated as depicted in figure (4.7) and measured.

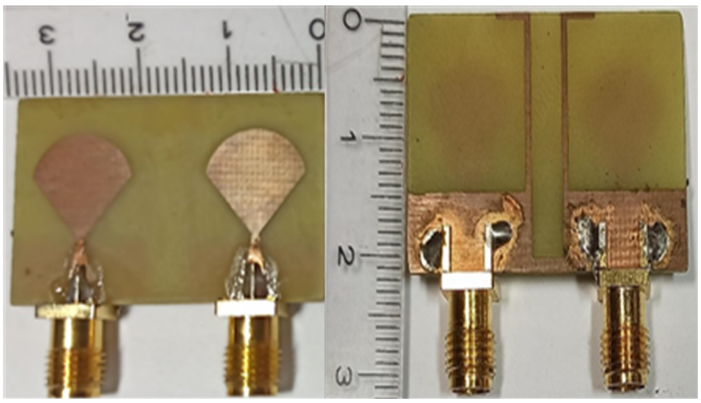

Figure 4.7: Photographs of the realized two-element UWB MIMO antenna

a) S-parameters

The simulated and measured |S|-parameters are plotted in figure (4.8). The simulated results demonstrate that the antenna boasts a broad operating band at -10 dB, spanning from

3.27 GHz to 23 GHz, with a remarkable bandwidth of 150.2%. Moreover, the simulated isolation consistently exceeds 19 dB across the entire operating band. Upon evaluating the measured results of the fabricated prototype, it is evident that the antenna effectively operates within a frequency range from 3.2 GHz to 23 GHz, showcasing a bandwidth of 151.1%. Similar to the simulated results, the measured isolation remains above 19 dB throughout the working band. The comparative analysis between the simulation and measurement results validates the proposed concept, with only a minor disparity observed in the frequency bands. This deviation can probably attributed to manufacturing errors.

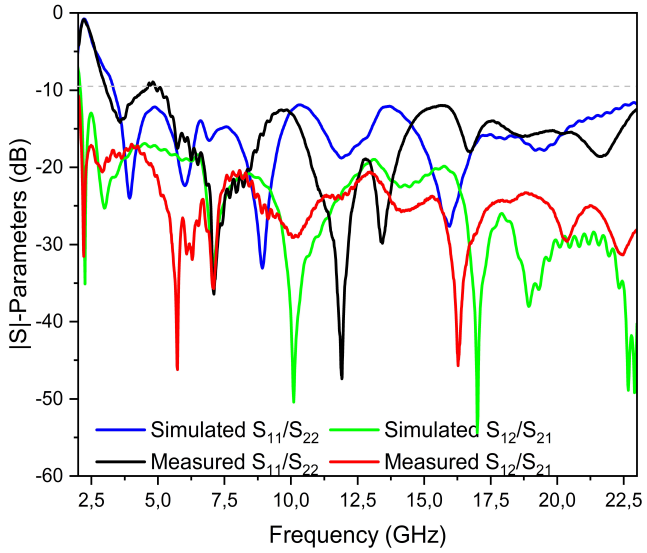

Figure 4.8: Simulated and measured S-parameters of the proposed two-element UWB MIMO antenna

b) Radiation patterns

The simulated and measured normalized E-plane and H-plane 2D radiation patterns at 6 GHz, 7 GHz, 8 GHz, 11 GHz, 15 GHz, and 17 GHz of the proposed UWB two-element MIMO antenna, with port-1 fed and port-2 loaded of 50Ω impedance are depicted in figure (4.9). Notably, at lower frequencies as shown in figures ((4.9a), (4.9b), (4.9c)), the radiation pattern exhibits a near-omnidirectional distribution. This signifies the antenna's capability to cover a wide azimuthal area, rendering it suitable for applications necessitating expansive coverage. Conversely, at higher frequencies (figures (4.9d), (4.9e), and (4.9f)), the radiation is influenced by higher-order modes, leading to the splitting of the

radiation lobe.

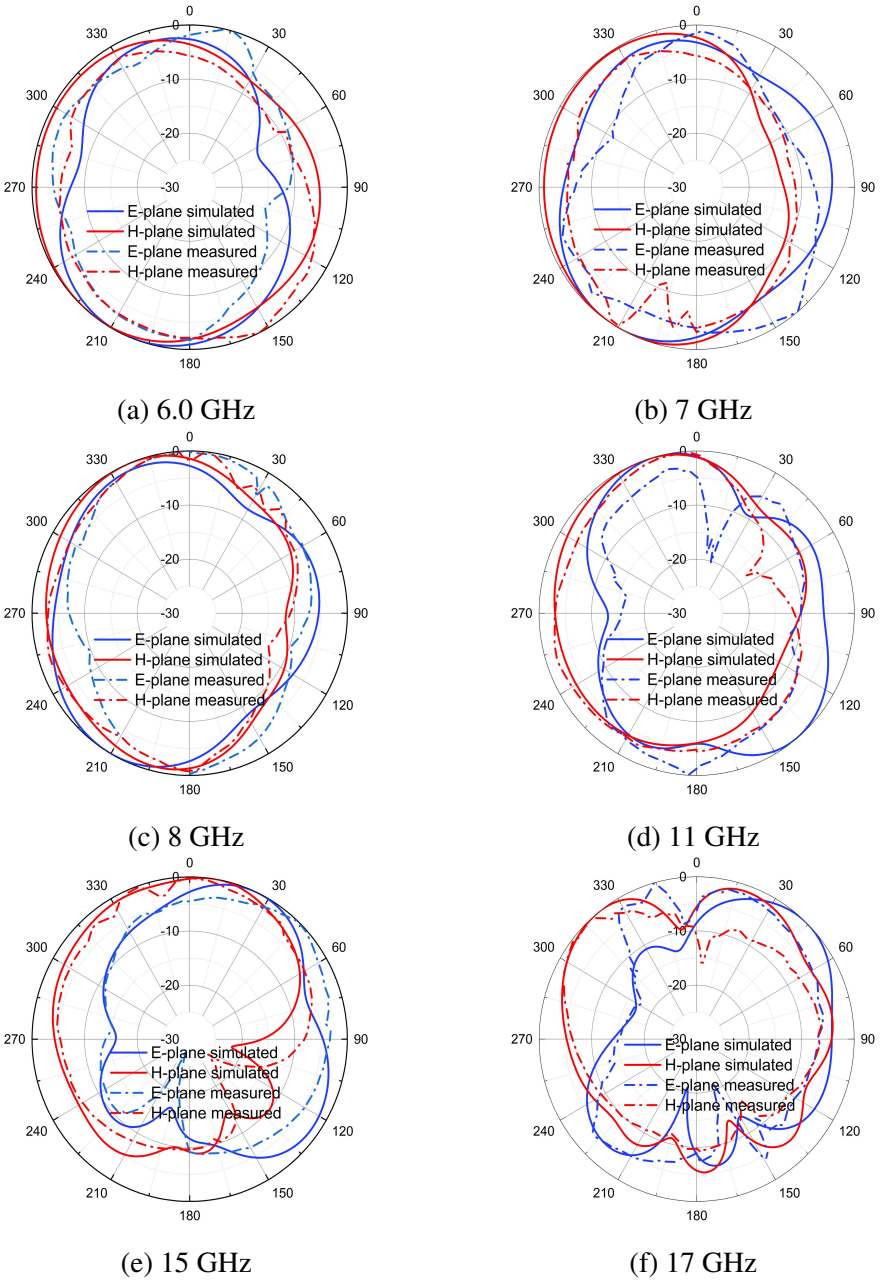

(a) 6.0 GHz (b) 7 GHz

(c) 8 GHz (d) 11 GHz

(e) 15 GHz (f) 17 GHz

Figure 4.9: Radiation patterns for the proposed two-element UWB MIMO antenna

Figure (4.10) shows the realized gain versus frequency for the proposed UWB two-port MIMO antenna. The measured and simulated realized gain is varying from -1.14 to 5.54 dB and 0.78 to 6.36 dB, respectively. We noticed some differences between the simulated and measured results. Specifically, there is a significant gap of 1.6 GHz between 5 and

6.25 GHz, and within the high operating frequency band of 17 GHz to 23 GHz, where differences exceeding 1 dB between simulated and measured values are observed. These substantial variations could be ascribed to several factors, including connector losses and fabrication tolerances.

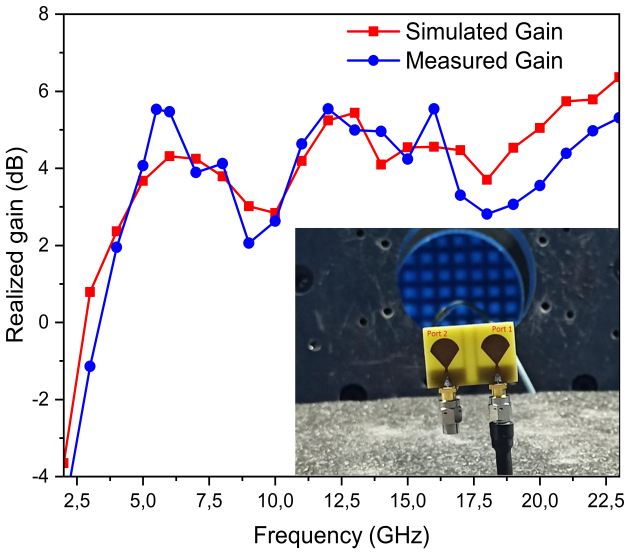

Figure 4.10: Realized gain of the proposed two-element UWB MIMO antenna versus frequency

c) Diversity performance

The acceptable performance of a MIMO antenna system can be evaluated based on several key parameters. Among these parameters, the envelope correlation coefficient (ECC), diversity gain (DG), channel capacity loss (CCL), and mean effective gain (MEG) play crucial roles in determining the effectiveness and reliability of the system. Initially, the ECC and DG metrics of the proposed UWB two-port MIMO antenna are depicted in figure (4.11a). Over the entire UWB spectrum, the antenna demonstrates an ECC below 0.002 and achieves a diversity gain of approximately 10. Subsequently, figure (4.11b) illustrates both the simulated and measured channel capacity loss (CCL). It is noteworthy that the CCL consistently maintains a low value of 0.29 bits/s/Hz across the entire operational frequency range. This value comfortably falls below the accepted threshold of 0.4 bits/s/Hz, signifying the robust performance of the system. Finally, the variation of Mean Effective Gain (MEG) for both simulated and measured data across the fre-

quency spectrum is presented in figure (4.11c). Analysis of the graph reveals that the MEG consistently remains below -3 dB throughout the operating band, indicating the steady performance of the system across frequencies.

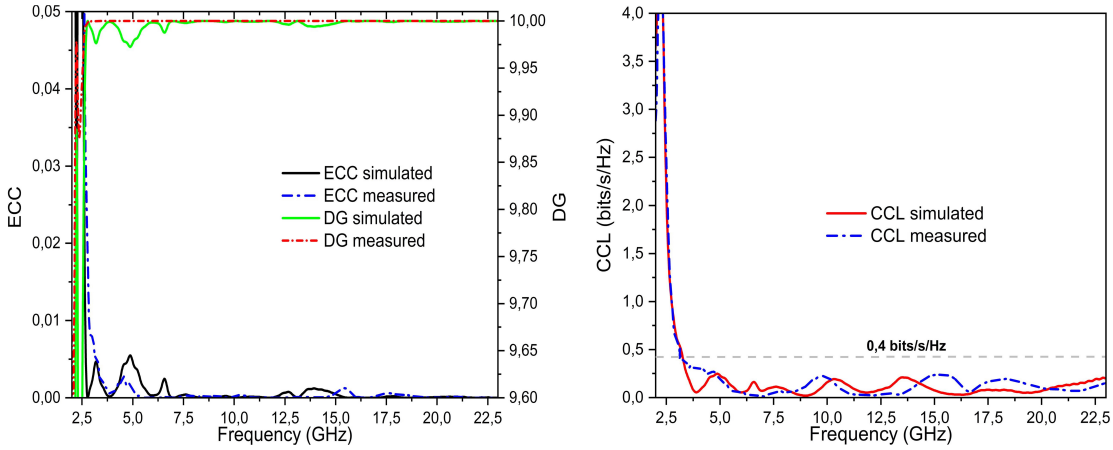

(a) ECC and DG

(b) CCL

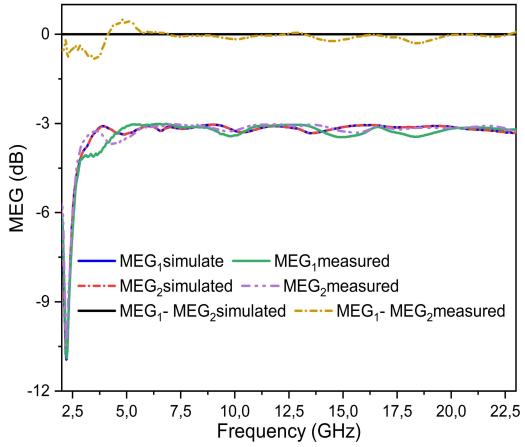

(c) MEG

Figure 4.11: Simulated and Measured diversity performance results of the proposed two-element UWB MIMO antenna

4.3.2 UWB MIMO antenna with dual rejected bands

The proposed two-element MIMO antenna with dual-band notched characteristics is illustrated in figure (4.12). Each radiating element of the initial UWB two-element MIMO antenna incorporates two filtering mechanisms. The first filtering mechanism comprises a quarter-wavelength L-shaped slot designed to establish the first notched band at 5.3 GHz (WLAN-band), while the second filter comprises a half-wavelength C-shaped slot, pro-

viding the second notched band at 6.6 GHz (INSAT C-band). The antenna is constructed on an FR4 substrate with a dielectric constant of $\varepsilon_r = 4.4$, thickness of h = 1.6 mm, and loss tangent of $\tan\delta = 0.025$.

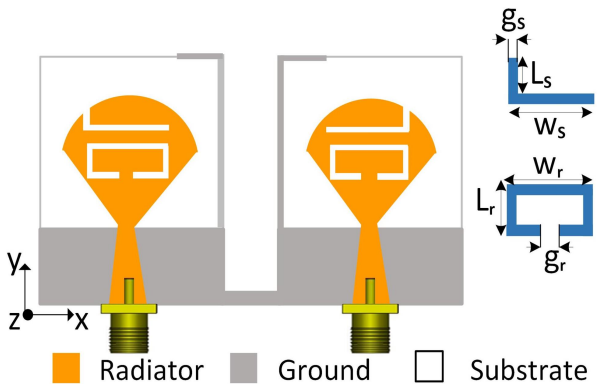

Figure 4.12: Layout of the proposed dual-band notch UWB MIMO antenna, [$g_s = 0.5$, $L_s = 1.4$, $W_s = 6.6$, $L_r = 1.4$, $W_r = 6.2$, $g_r = 0.7$]

The proposed UWB two-element MIMO antenna, featuring dual band-notched characteristics, undergoes two distinct stages of geometric evolution, which are depicted in figure (4.13). Initially, a quarter-wavelength L-shaped slot is strategically inserted into the two symmetrical radiating elements to effectively filter the Wireless Local Area Network (WLAN) band, as illustrated in figure (4.13) (Antenna 1). Analysis of the reflection coefficient, presented in figure (4.14), reveals that the simulated notched band spans from 4.6 GHz to 5.8 GHz for WLAN band with S_{11} of -4.4 dB. Subsequently, to mitigate interference stemming from the C-band, a half-wavelength C-shaped slot is meticulously etched beneath the initial slot in the primary radiating patch, as showcased in figure (4.13) (Antenna 2). Examination of the simulated reflection coefficient for this configuration highlights the antenna's operational band extending from 3.2 GHz to 23 GHz, characterized by dual-notch band features spanning from 4.4 GHz to 5.7 GHz for WLAN band with maximum $|S_{11}|$ of -3.2 dB at 5.25 GHz and from 6.3 GHz to 7.4 GHz for IEEE INSAT/Super-Extended C-band with maximum $|S_{11}|$ of -4.6 dB at 6.5 GHz, as illustrated in (4.14) (Antenna 2). It is noteworthy that, according to prevalent literature, an $|S_{11}|$ bandwidth greater than -10 dB is deemed acceptable for effective notch band rejection [83], [41], [84], [85], [86].

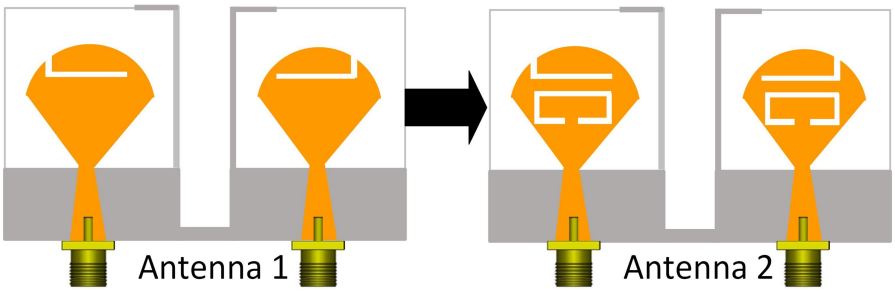

Figure 4.13: Evolution of the proposed dual-band notch UWB MIMO antenna geometry

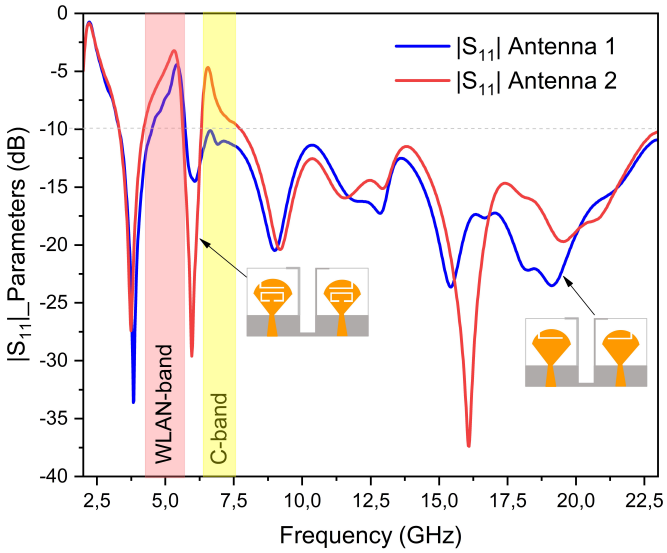

Figure 4.14: Simulated reflection coefficient S_{11} of the different geometry of the proposed dual-band notch UWB MIMO antenna

Figure (4.15) shows the antenna surface current distributions when port 1 is excited, and port 2 is terminated with a load-matched impedance of 50Ω, at frequencies of 5.3 GHz, 6.6 GHz, 14 GHz, and 22 GHz. In figure (4.15a) and (4.15b), it can be seen that a strong current density exists around the edges of the L-shaped and C-shaped slots, at 5.3 GHz and 6.6 GHz respectively, which demonstrates the operation of filtering in the WLAN band, and super-extended/INSAT C-band, respectively. For other frequencies at 14 GHz and 22 GHz, there is a concentration of current over the feedline, radiator, and common ground plane, which indicates that the antenna operates at these frequencies and confirms the UWB performance across the whole band, as shown in figure IV.16 (4.15c) and (4.15d). We also notice a very low surface current density on the second antenna

(port 2) which proves the good isolation between the proposed MIMO antenna and the efficiency of the decoupling mechanism used in the ground plane.

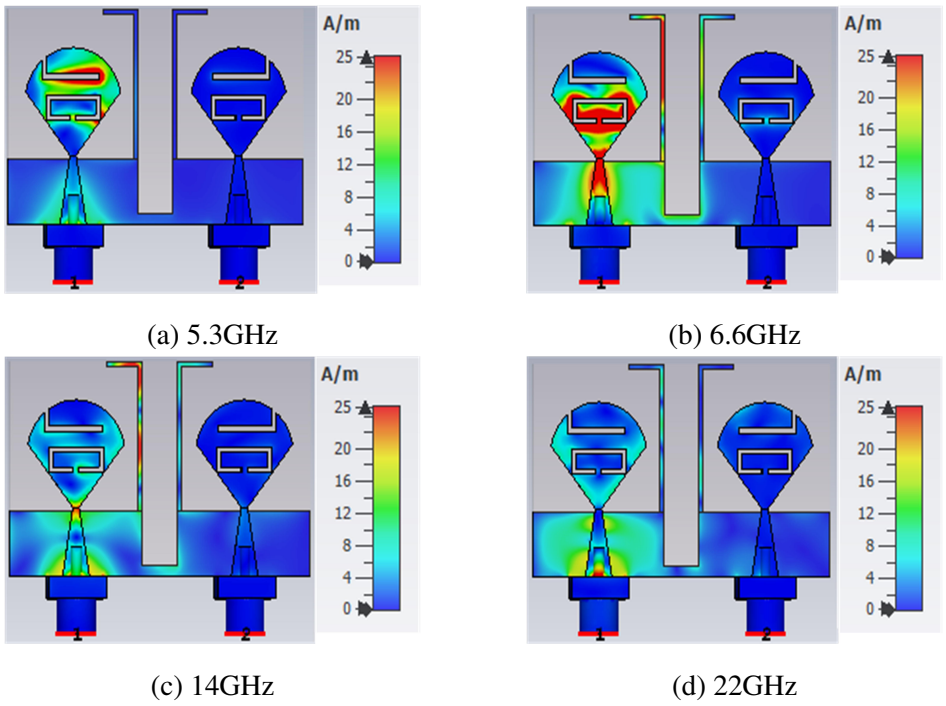

(a) 5.3GHz (b) 6.6GHz

(c) 14GHz (d) 22GHz

Figure 4.15: Surface current distributions for the proposed dual-band notch UWB MIMO antenna

a) Parametric study

To investigate the impact of the slots length variations on the notched band, a parametric study was conducted. Figure (4.16a) illustrates the effect of the parameter W_s (variation of the length of the L-shaped slot) on the reflection coefficient of the antenna. The W_s parameter ranges from 6.2 to 7.8 mm. It is evident that as the parameter W_s increases, the first notched band shifts from 5.6 GHz to 4.67 GHz, confirming that the length of the L-shaped slot controls the position of the first rejected band (WLAN). The optimal value to achieve the desired notched band is determined to be 6.6 mm. The overall length L_{m1} of the L-shaped slot can be computed using equation (IV.1):

$$L_{m1} = L_s + W_s + 2 \times g_s \tag{IV.1}$$

This slot works as a quarter-wavelength resonator, the resonance is calculated using the equation (IV.2) and (IV.3):

$$f_{\text{notches}} = \frac{c}{4L_{m1}\sqrt{\varepsilon_{\text{eff}}}} \tag{IV.2}$$

$$\varepsilon_{\text{eff}} = \frac{\varepsilon_r + 1}{2} \tag{IV.3}$$

With c the speed of light, and ε_r the relative dielectric constant.

Table (4.1) presents a comparison between the rejected frequency values calculated from Equation (IV.2) for various values of W_s and those obtained from simulations. The considered rejected frequencies are taken for a maximum $|S_{11}|$ of -3.2 dB. It is evident that the two sets of values closely align, with only a slight discrepancy of 230 MHz observed between the computed and simulated values at the specified rejected frequency (W_s= 6.6 mm). Furthermore, a maximum difference of 290 MHz is observed for W_s= 6.2 mm, while a minimum difference of 200 MHz is obtained for W_s= 7.8 mm. This small disparity can be attributed to the inherent limitation of the equation in accurately accounting for electromagnetic interactions with the adjacent slot (C-shaped slot).

Table 4.1: Frequency values rejected as a function of W_s compared with the simulation (L_s= 1.4 mm, g_s= 0.5 mm)

Ws (mm)	**Lm1 (mm)**	**Rejected frequency (GHz)**	
		Design equation	**simulated**
6.2	8.6	5.31	5.6
6.6	9	5.07	5.3
7	9.4	4.85	5.12
7.4	9.8	4.65	4.86
7.8	10.2	4.47	4.67

Figure (4.16b) shows the influence of the C-shaped slot parameter W_r on the reflection coefficient of the proposed antenna. The W_r parameter value is varied from 4.6 to 6.2 mm. It can be seen that the second notched band shifts from 8.3 GHz to 6.6 GHz when the parameter W_r is increased, confirming that the C-shaped slot controls the second rejected band (IEEE super-extended/ INSAT C-band). The value $W_r = 6.2$ mm is chosen as the

optimal value to get the desired notch frequency. The overall length L_{m2} of the C-shaped slot can be calculated using equation (IV.4):

$$L_{m2} = 2 \times (W_r + L_r) - (g_r) \tag{IV.4}$$

The resonance of the notched band is calculated using equation (IV.5):

$$f_{\text{notches}} = \frac{c}{2L_{m2}\sqrt{\varepsilon_{\text{eff}}}} \tag{IV.5}$$

Table (4.2) shows a comparison between the rejected frequency values calculated from equation (IV.5) for different values of W_r with the simulation results. A minimum difference of 240 MHz between the computed and simulated values is observed for Wr = 6.2 mm, while the maximum difference of 300 MHz is noted for $W_r = 5.4$ mm. However, a discrepancy of 260 MHz is observed at the specified rejected frequency of 6.3 GHz. This disparity can be attributed to the inherent limitation of the equation in accounting for electromagnetic interactions with the adjacent slot (L-shaped slot). Furthermore, the simulated results are captured at the peak S_{11} value, reaching -4.6 dB.

Table 4.2: Frequency values rejected as a function of Wr compared with the simulation (Lr= 1.4 mm, gr= 0.5 mm)

Wr (mm)	**Lm2 (mm)**	**Rejected frequency (GHz)**	
		Design equation	**simulated**
4.6	11.3	8.07	8.3
5	12.1	7.54	7.83
5.4	12.9	7.1	7.4
5.8	13.7	6.66	6.9
6.2	14.5	6.3	6.56

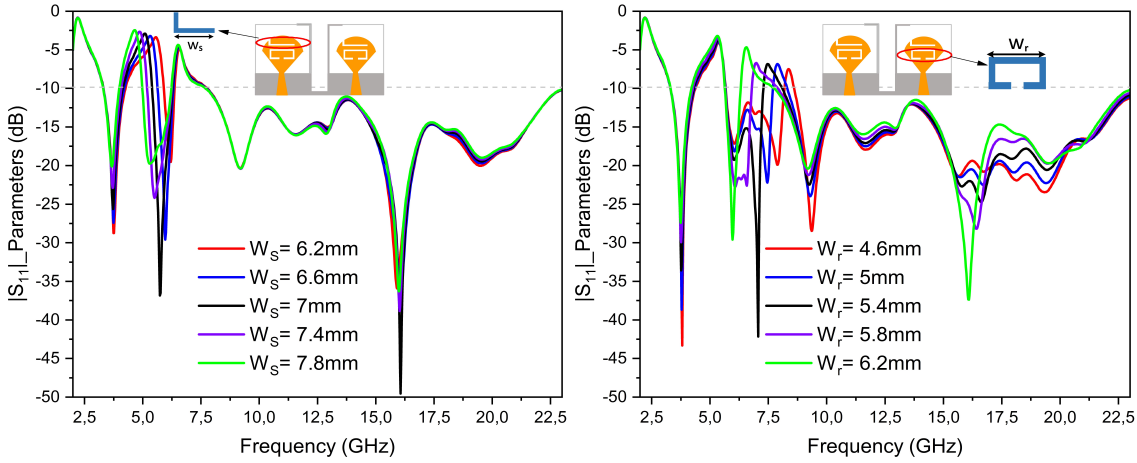

(a) Variation of $|W_s|$ (b) Variation of $|W_r|$

Figure 4.16: Parametric study for the proposed dual-band notch UWB MIMO antenna

b) S-parameters

Photographs of the realized prototype are depicted in figure (4.17). The simulated and measured S-parameters are shown in figure (4.18). According to the simulations, the antenna exhibits an operational bandwidth extending from 3.2 GHz to 23 GHz ($S_{11} < -10$ dB), corresponding to a relative bandwidth of 151.1%. Notably, dual band-notched characteristics are observed from 4.3 to 5.7 GHz (WLAN) with a peak of about -3.2 dB at 5.25 GHz and from 6.3 GHz to 7.4GHz (C band) with a peak of about -4.6 dB at 6.5GHz. Additionally, the simulated isolation exceeds 19 dB across the operating band. For the measured results, the antenna demonstrates an operational bandwidth spanning from 3.1 GHz to 23 GHz, equivalent to a relative bandwidth of 152.4%. Dual-band notched characteristics are observed, the first band extends from 4.7 GHz to 6 GHz with a peak of about -2.1 dB at 5.3 GHz. A slight deviation of 300 MHz between the measured and simulated results is observed in this rejected band (WLAN), attributable to manufacturing quality. The second band extends from 6.3 GHz to 7.3 GHz with a peak of about -4.5 dB at 6.5 GHz. Furthermore, the measured isolation demonstrates better performance, with a minimum value of 22 dB across the operating band.

The close agreement between the measured and simulated results validates the performance of the proposed MIMO antenna. It successfully achieves UWB characteristics with dual band-notched features, while demonstrating robust isolation throughout the op-

erational band.

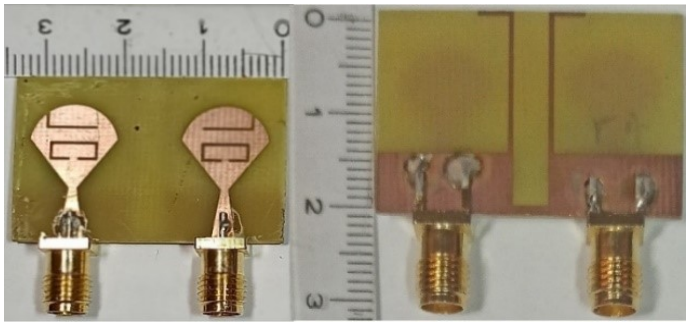

Figure 4.17: The fabricated prototype (Front and back view)

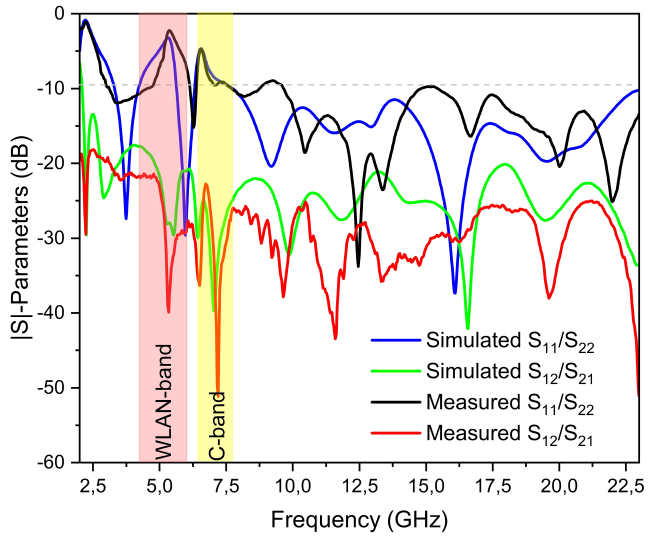

Figure 4.18: Measured and simulated S-parameters of the dual-band notch UWB MIMO antenna

c) Radiation patterns

The simulated and measured normalized radiation patterns (E-plane and H-plane) of the dual band notch MIMO antenna at 4.0 GHz, 5.3 GHz, 6.6 GHz, 9 GHz, 13 GHz, and 18 GHz are shown in figure (4.19). During the measurement, port 1 was excited while port 2 was terminated with a 50Ω matching load. The proposed antenna has a nearly omnidirectional radiation pattern over the desired operating band as shown in figures (4.19a, 4.19b, 4.19c, and 4.19d). Furthermore, figure (4.19e), and (4.19f) shows that the

radiation patterns deteriorate at the higher frequencies due to the splitting of the radiation lobes.

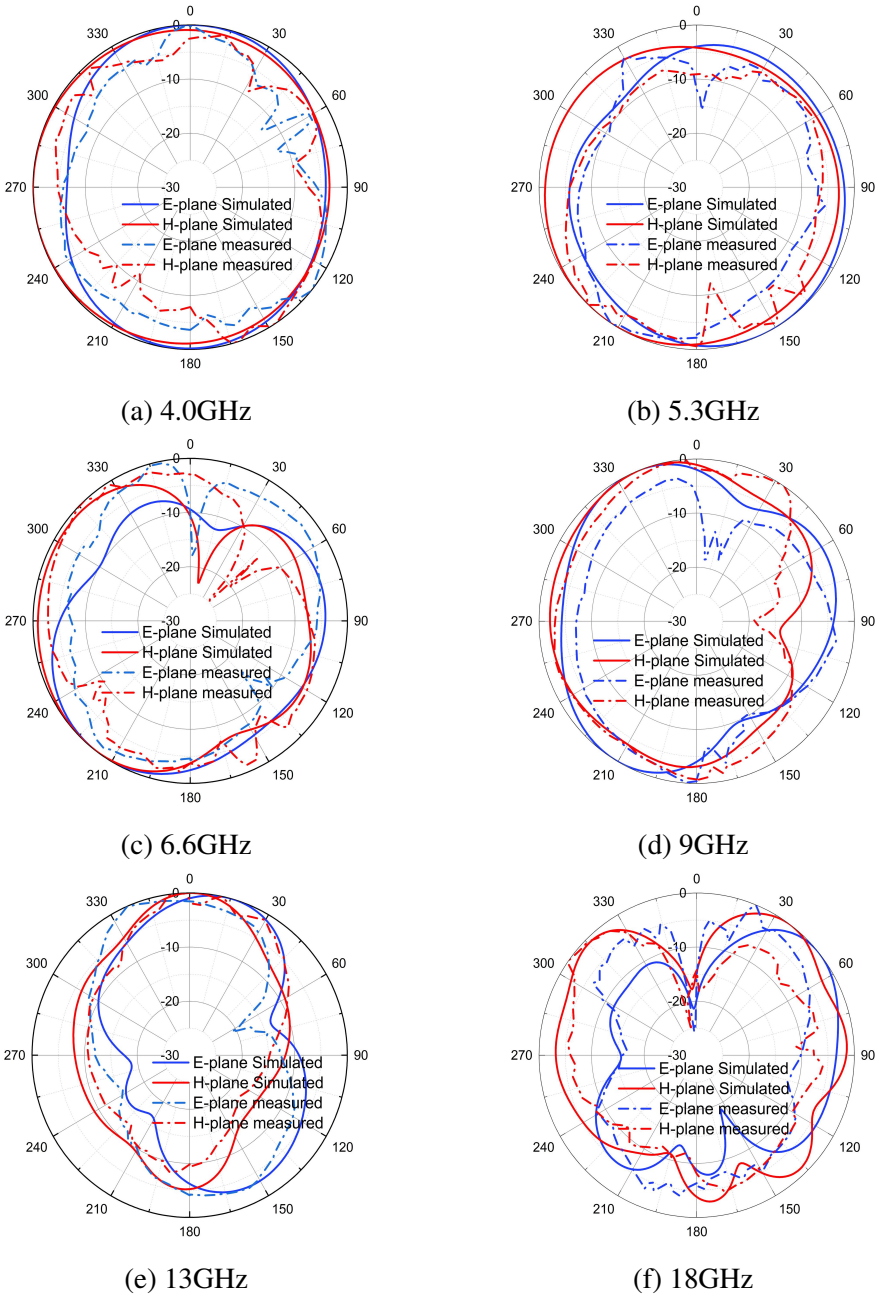

(a) 4.0GHz (b) 5.3GHz

(c) 6.6GHz (d) 9GHz

(e) 13GHz (f) 18GHz

Figure 4.19: Radiation patterns for the proposed dual-band notch UWB MIMO antenna

In figure (4.20), the simulated and measured realized gain as a function of frequency is shown. It can be seen that the realized gain gradually increases with increasing frequency over the operating band, with a maximum gain of 6.2 dB and 6.34 dB for simulation and

measurement, respectively. We can also see that for the rejected bands, the simulated realized gain decreases significantly to -3.05 dB at 5.3 GHz and -0.83 dB at 6.6 GHz, while the measured realized gain is -2.43 dB at 5.3 GHz and -0.74 dB at 6.6 GHz. A good agreement is observed between the measurement and simulation results, with small differences noted, particularly at 6 GHz and 11.25 GHz with a difference of 2 dB. These differences are probably due measurement setup.

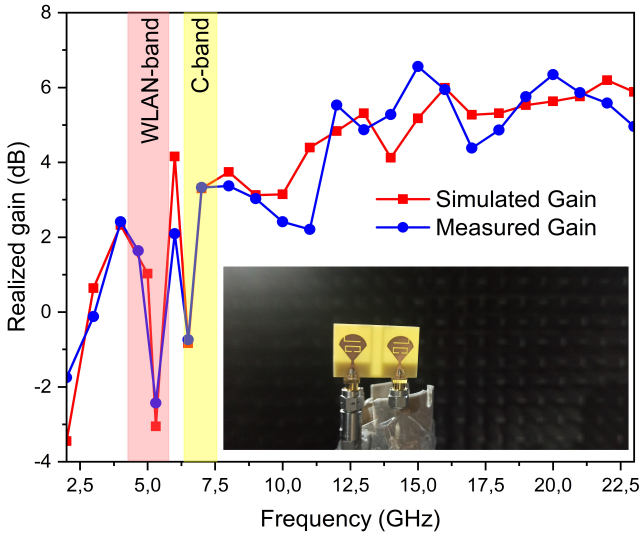

Figure 4.20: Realized gain for the proposed dual-band notch UWB MIMO antenna

Figure (4.21) shows the simulated total efficiency for port 1 and the multiplexing efficiency, which is calculated using equation (IV.6).

$$\eta_{mux} = \sqrt{\eta_1 \eta_2 \left(1 - |r|^2\right)} \tag{IV.6}$$

Where η_1 and η_2 represent the total efficiencies of port 1 and port 2 respectively, and r is the complex correlation coefficient between the two ports of the proposed antenna (ECC $\approx |r|^2$). It is observed that the total efficiency for single port 1 and the multiplexing efficiency are almost the same due to the low correlation between the two ports. In addition, the multiplexing efficiency is higher than 68.5% in the entire operating band except in the filtered bands, where the efficiency decreases drastically to 20.38% and 21.98% at 5.3 GHz and 6.6 GHz, respectively.

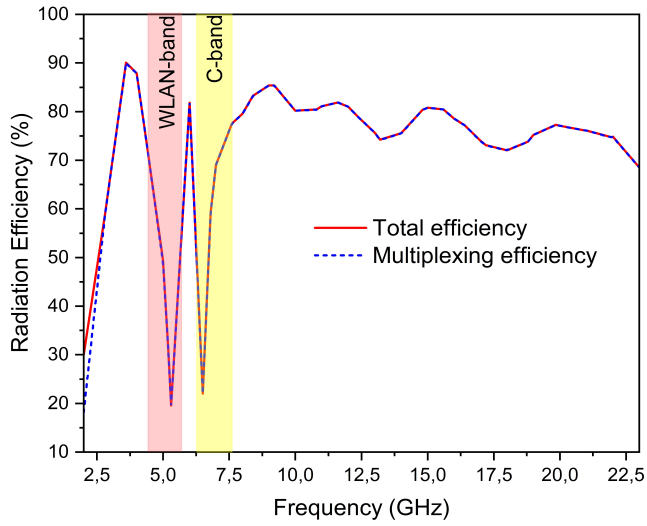

Figure 4.21: Efficiency for the proposed dual-band notch UWB MIMO antenna

d) Diversity performance

To comprehensively evaluate the diversity performance of the proposed UWB MIMO antenna featuring dual-band notched characteristics, we conducted calculations for the ECC, DG, CCL, MEG, and TARC using data obtained from both measurement and simulation. The simulated and measured Envelope Correlation Coefficient (ECC) and Diversity Gain (DG) using S parameters of the MIMO proposed dual-band notch UWB MIMO antenna are presented in figure (4.22a), revealing a strong agreement between measured and simulated outcomes. Notably, the ECC consistently remains below 0.001 across the entire operating band, indicating minimal correlation between the two antenna elements. Furthermore, within the rejected bands (WLAN and C bands), the ECC values increase to 0.02 and 0.05, respectively, maintaining favorable levels and affirming effective decoupling between the two ports even within filtered frequency ranges. Conversely, the DG of the antenna remains nearly constant at approximately 10 throughout the operating band, with variations observed only within the two notched bands where the DG drops to 9.9 (WLAN band) and 9.95 (C band), respectively, underscoring the robust diversity performance of the MIMO structure. However, the analysis of simulated and measured Channel Capacity Loss (CCL) and Total Active Reflection Coefficient (TARC) values using S-parameters is depicted in figure (4.22b). The data indicate that the CCL remains below 0.29 bits/s/Hz across the operational frequency bands of the antenna. Furthermore,

the TARC for the proposed dual-band notch Ultra-Wideband (UWB) antenna, with an input feeding phase of $\theta = 0^{\circ}$, exhibits values less than -35 dB throughout the entirety of the UWB band, as observed in both the simulated and measured results (figure (4.22b)). Finally, the variation of simulated and measured Mean Effective Gain (MEG) for the two ports as a function of frequency is shown in figure (4.22c). It is observed that the value of the MEG is below -3 dB over the operating band, indicating good diversity performance of the proposed dual-band notch UWB MIMO antenna. Additionally, low values of -6.8 dB and -4.7 dB are noticed in the rejected bands (WLAN and IEEE super-extended/INSAT C bands), respectively. Table (4.3) provides a comprehensive overview of the simulated and measured values, including ECC, DG, CCL, and MEG, delineating between the rejected bands (WLAN and IEEE super-extended/INSAT C) and the antenna's operational bands.

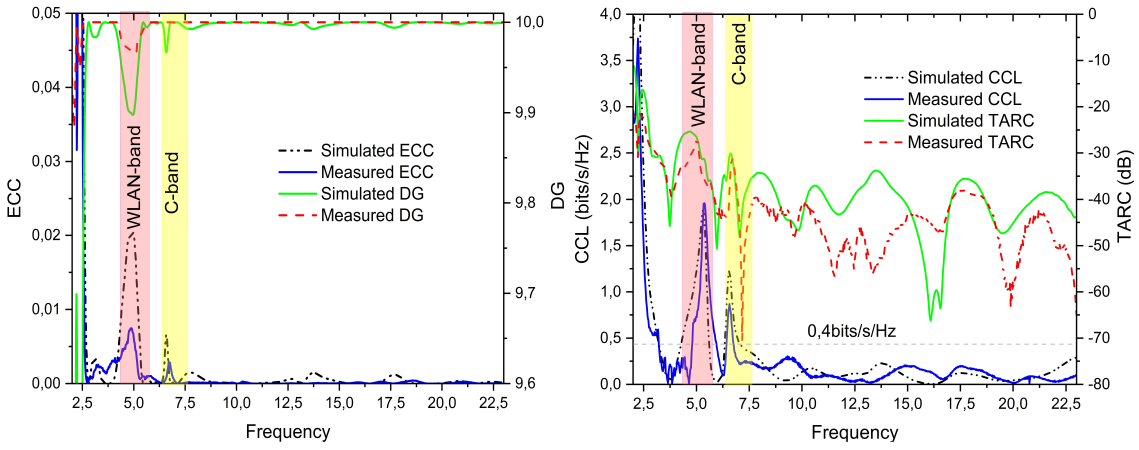

(a) ECC and DG

(b) CCL and TARC

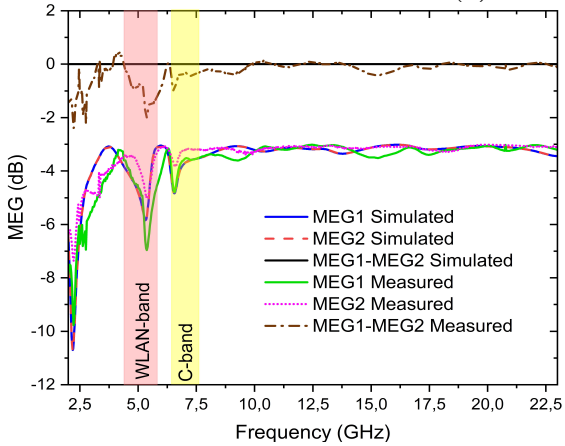

(c) MEG

Figure 4.22: Simulated and Measured diversity performance for the proposed dual-band notch UWB MIMO antenna

Table 4.3: Simulated and measured values of ECC, DG, CCL and MEG

	WLAN		C-band		Operating band	
Parameters (Min Value)	**Sim**	**Meas**	**Sim**	**Meas**	**Sim**	**Meas**
ECC	0.02	0.0074	0.0065	0.002	0.0014	0.001
DG	9.9	9.98	9.96	9.99	9.99	9.99
CCL (bits/s/Hz)	1.88	1.95	1.22	0.81	0.3	0.29
MEG1 (dB)	-4.9	-6.8	-4.84	-4.7	3.2	3.3

4.3.3 Reconfigurable UWB MIMO antenna with dual rejected bands

In order to introduce frequency agility, a straightforward reconfiguration mechanism employs a single diode for each filter (two diodes for each antenna element), as depicted in figure (4.23). With this reconfiguration structure, the antenna can operate across the entire UWB band. However, in the presence of interference from the WLAN or INSAT C-band bands, the antenna effectively rejects the respective interfering bands.

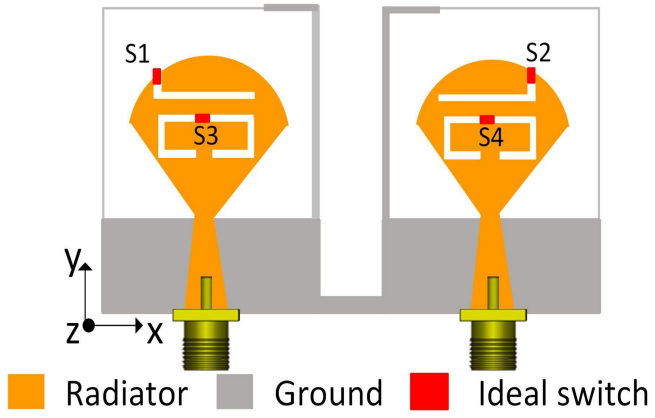

Figure 4.23: Design of the proposed reconfigurable dual-band notch UWB MIMO antenna

In this section, we utilized an ideal switch where the two operating states of the switch "on/off" are modeled by the presence/absence of a perfect conductor strip of the same size as that of a real switch to validate the reconfiguration mechanism. The simulation of the reconfigurable UWB MIMO antenna encompasses four distinct operating modes, as outlined in Table (4.4). Figure (4.24) depicts the simulation results, focusing on reflection

coefficients and isolations. In mode 1 (all switches OFF), the two-port exhibits a UWB operating bandwidth spanning from 3.2 GHz to 23 GHz (refer to figure (4.24a)), with a minimum isolation of 14dB. Transitioning to mode 2 (all switches ON), the MIMO antenna maintains an operating band from 3.2 GHz to 23 GHz, featuring dual band-notched characteristics from 4.3 GHz to 5.7GHz (WLAN) with a peak of about -3.2 dB at 5.25 GHz and from 6.3 GHz to 7.4GHz (C band) with a peak of about -4.6 dB at 6.5GHz. Simulated isolation surpasses 19 dB across the operating band (figure (4.24b)). In mode 3 (S1 and S2 OFF, S3 and S4 ON), the MIMO antenna exhibits an operating bandwidth extending from 3.2 GHz to beyond 23 GHz, while rejecting approximately 1 GHz bandwidth from 4.5 GHz to 5.7 GHz (WLAN band) with S_{11} of -4.4 dB. Isolation levels remain above 19 dB for this mode as shown in figure (4.24c). Finally, in mode 4 (S1 and S2 ON, S3 and S4 OFF), the designed antenna maintains its ultra-wide operating mode, while effectively rejecting the INSAT C-band (5.9 GHz to 7.1 GHz) with S_{11} of -3.2 dB, and isolation exceeding 14 dB across the entire operating band as depicted in figure (4.24d).

Table 4.4: Configuration of switches for operating modes

Modes	**State of the switch**		**Operating band**
	S1, S2	**S3, S4**	
Mode-1	OFF	OFF	UWB
Mode-2	ON	ON	UWB with dual notched band (WLAN and C-band)
Mode-3	OFF	ON	UWB with single-notched WLAN-band
Mode-4	ON	OFF	UWB with single-notched C-band

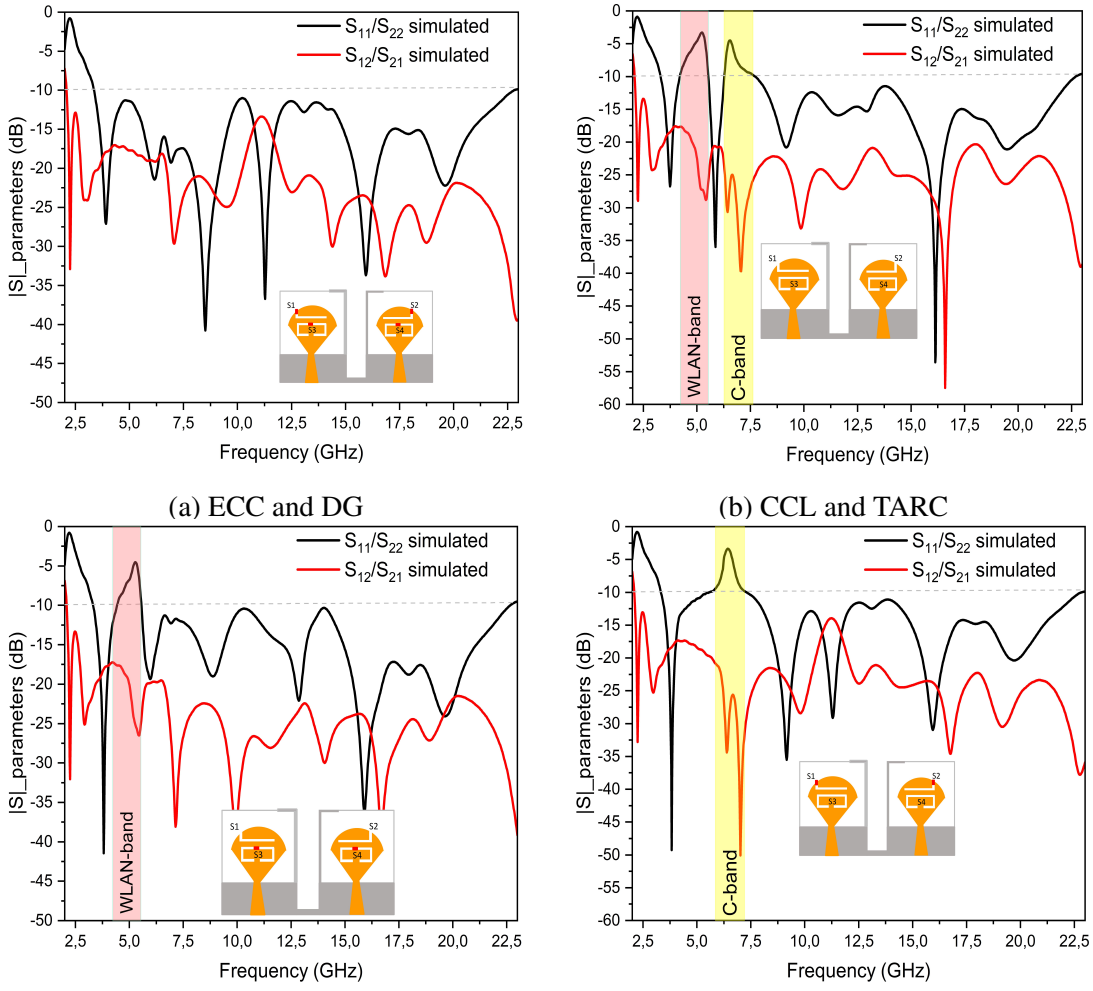

(a) ECC and DG

(b) CCL and TARC

(c) MEG

(d) MEG

Figure 4.24: Simulated S-parameters of the proposed reconfigurable dual-band notch UWB MIMO antenna

4.4 Conclusion

In this chapter, we have explored two essential aspects of designing and optimizing MIMO antennas for advanced wireless communication systems. We began by introducing a SWB MIMO antenna tailored for 5G communication applications in millimeter waves. Characterized by an extensive operating frequency band spanning from 3.2 GHz to 50 GHz. It boasts remarkable radiation efficiency levels ranging from 71.2% to 89%. Additionally, it demonstrates robust port isolation characteristics, achieving 19 dB isolation across the entire operating band. This isolation is achieved through the strategic introduc-

tion of inverted L-shaped stubs with a rectangular cut. These features collectively render the SWB antenna a promising solution poised to address the escalating demands for data rate and network capacity within burgeoning 5G networks. However, the measurement validation has been constrained by the available instrument measurement at laboratory, which operate to frequencies up to 23 GHz.

Subsequently, we investigated the design of a compact MIMO antenna with dual band-notched characteristics for UWB communication systems. Despite its wide range of operating frequencies from 3.1 to 23 GHz, this antenna demonstrates excellent MIMO performance, including high port isolation (greater than 22 dB), low ECC (< 0.001), DG is greater than 9.99, CCL is lower than 0.29bits/s/Hz, and TARC value is lower than -35 dB over the entire operating band. Furthermore, the introduction of a reconfiguration mechanism has introduced the antenna's versatility, allowing it to dynamically adapt to different network environments and minimize interferences.

In conclusion, the MIMO antennas presented in this chapter offer innovative solutions to enhance the performance and efficiency of wireless communication systems across a wide range of applications, from 5G MMW networks to UWB systems. Their innovative design and remarkable performance pave the way for new advancements in the field of wireless communication technologies.

GENERAL CONCLUSION

THE work presented in this thesis aimed to simultaneously consider the elements determining the performance of MIMO communications with the integration constraints related to radio-frequency devices and the advantages of integrating a reconfiguration mechanism into these multi-antenna systems for advanced wireless communications. This approach led us to structure this thesis into four parts. The first chapter, starting with describing a communication chain, introduces the context of the study and provides important elements for understanding multi-antenna techniques. It particularly emphasizes the effects of multi-path propagation, consequences of stationary or non-stationary obstacles encountered by electromagnetic waves, such as reflection, diffraction, and dispersion. The presence of multiple paths between transmitters and receivers requires new approaches to transmitting information. The work presented in this thesis focused on techniques based on multiple antennas because this solution allows for increased throughput without increasing bandwidth, advantageous in the context of allocated band saturation. More specifically, we demonstrated that diversity-based multi-antenna systems are better suited for communications subject to multi-path propagation. However, their use poses new challenges for integration into compact terminals. To meet these conditions with closely spaced radiating elements, we emphasized the importance of isolating access points, thereby improving overall efficiency. In the last part of the first chapter, we discussed the different types of reconfigurable antennas, especially frequency-reconfigurable antennas, which will be the subject of our subsequent chapters. We highlighted the significant interest of combinations between MIMO systems and reconfigurable antenna tech-

nology in cognitive radios and the new generation of 5G communications, offering essential frequency flexibility for their operation. After highlighting the importance of reconfigurable MIMO antennas, we presented the design method for these types of antennas and the management of switch usage for reconfiguration. Two reconfiguration approaches were proposed: the use of real switches with bias circuits, and the use of ideal switches modeling the two operating states by the presence or absence of a perfectly matched conductive strip.

The first antenna proposed in chapter 2 focuses on the design of a novel frequency-reconfigurable two-port antenna for cognitive radio and 5G new radio sub-6 GHz applications. In this antenna, two filtering mechanisms are incorporated into an initial wideband antenna. The first mechanism consists of a rectangular slotted-band filter (RSR rectangular [RSRR]) integrated next to the feeding line, and the second mechanism consists of a low-pass filter (LPF) (a straight slot engraved in the ground plane). The optimization process of essential parameters for the antenna, including the dimensions of antenna elements and MIMO configuration, as well as the evolution of the decoupling structure among the antenna elements, is explained in detail. This optimization ensures that the antenna design meets the desired performance criteria. An important aspect addressed in this chapter is the utilization of both ideal and real switch approaches for reconfiguration among the antenna elements. Finally, it presents the measurement results of the 2-port reconfigurable wideband MIMO antenna for the four operating modes. The measurements encompass various aspects, such as impedance bandwidth, gain, efficiency, and MIMO diversity parameters (both ideal and real switches). These measurements provide comprehensive insights into the reconfigurable MIMO antenna's performance.

Chapter 3 is dedicated to the design and development of two frequency-reconfigurable multiband MIMO antennas suitable for various wireless standards such as WiFi, WiMAX, WLAN, cognitive radio (CR), and 5G Sub-6 GHz applications. The first antenna structure features a unique design, serving as the fundamental element with a half-bowtie shape optimized for operation within the WLAN band. Dual-band functionality is achieved through the integration of a pair of inverted L-shaped slots on each side of the two antenna elements, with slot dimensions tailored for WiMAX band operation. Reconfigurability is facilitated by the inclusion of two Infineon PIN diodes, enabling seamless switching be-

tween single-band and dual-band operation. In the subsequent section of this chapter, our investigation extends to multi-antenna triple-band systems. Here, three open quarter-wave slots of varying lengths are incorporated into the ground plane of each antenna element to enable triple-band operation. Utilizing ten ideal switches to control the operation of these slots, the designed two-port multi-antenna system can seamlessly switch between seven different operating modes, including single-band, dual-band, and triple-band configurations, while maintaining robust performance characteristics, particularly in terms of isolation. Simulated and measurement data are provided to facilitate comparison and validation of the proposed antenna prototypes, allowing for a comprehensive assessment of their performance and effectiveness.

In the final chapter, we delved into two critical aspects of MIMO antenna design for advanced wireless communication systems. Firstly, we introduced a super-wideband (SWB) MIMO antenna tailored for 5G millimeter wave communication, demonstrating exceptional radiation efficiency and robust port isolation across a wide frequency range. Secondly, we explored a compact MIMO antenna with dual band-notch characteristics for ultra-wideband (UWB) systems, boasting excellent MIMO performance and enhanced adaptability through reconfiguration. Overall, these antennas provide innovative solutions to enhance wireless communication system performance across various applications, from 5G MMW networks to UWB systems, heralding new possibilities in wireless communication technology.

In perspective, some of the points addressed in the previous chapters could benefit from improving the obtained results :

- The tri-band two-port MIMO antenna system introduced in Chapter 3 should be implemented with real switches such as PIN diodes to validate the approach of frequency reconfiguration of this system, thereby enhancing the advantages of this antenna for advanced wireless communications.

- The UWB two-element MIMO antenna with dual-band notched introduced in chapter 4 can also be implemented with PIN diodes to validate the simulated introduced reconfiguration approach using ideal switch .

- Furthermore, the work presented in this thesis could be extended to study different

aspects. In terms of design, one could work on combining the various reconfiguration approaches proposed in this thesis to offer antennas with maximum functionality. On the technological level, attention could be focused on switches that would be most suitable for such MIMO antenna systems, taking into consideration parameters such as transient regime, energy efficiency, non-linearities, etc.

SCIENTIFIC PRODUCTION

International publication

1. Benghanem Y, Mansoul A, and Mouffok L. Frequency reconfigurable two-element MIMO antenna for cognitive radio and 5G new radio sub-6 GHz applications. *International Journal of Microwave and Wireless Technologies*, 2023,
DOI: 10.1017/S1759078723001289

2. Benghanem Y, Mansoul A, and Mouffok L. A Compact Two-element MIMO Antenna with High Isolation and Dual Band-Notched Characteristics for UWB Communication Systems. *Wireless Personal Communications*, 2024,
DOI: 10.1007/s11277-024-11319-5

3. Benghanem Y, Mansoul A, and Mouffok L. Reconfigurable CPW-fed slotted half-bowtie MIMO antenna for cognitive radio and 5G Sub 6 GHz applications. (Submitted)

International Conference

1. Benghanem Y, Mansoul A, and Mouffok L. Compact Tri-Band Two-Element MIMO Slot Antenna for 5G Sub-6 GHz Frequency Bands. *2nd International Conference on Advanced Electrical Engineering (ICAEE). IEEE, 2022*.
DOI: 10.1109/ICAEE53772.2022.9962087

2. Benghanem Y, Mansoul A, and Mouffok L. Compact Super Wideband Two-element MIMO Antenna for 5G Millimeter-Wave Applications.*International Conference on Advances in Electronics, Control and Communication Systems (ICAECCS). IEEE, 2023*.
DOI: 10.1109/ICAECCS56710.2023.10105086

APPENDIX A

FUNDAMENTAL MIMO ANTENNA SYSTEM PARAMETERS

1) S-Parameters

Considering an array of n antenna elements as a network with n ports, we assume that the incident waves at the n ports are labeled as $a_1, a_2 ... a_n$, while the corresponding outgoing waves are denoted as $b_1, b_2 ... b_n$. The relationship between the outgoing and incoming waves can be expressed by equation (A.1) [87]:

$$\begin{cases} b_1 = S_{11}a_1 + S_{12}a_2 + \cdots + S_{1n}a_n \\ b_2 = S_{21}a_1 + S_{22}a_2 + \cdots + S_{2n}a_n \\ \cdots \\ b_n = S_{n1}a_1 + S_{n2}a_2 + \cdots + S_{nn}a_n \end{cases} \tag{A.1}$$

Equation (A.1) is expressed in matrix form as follows:

$$b = S.a \tag{A.2}$$

Of which:

$$\begin{aligned} a &= [a_1, a_2, \ldots, a_n]^T \\ b &= [b_1, b_2, \ldots, b_n]^T \end{aligned} \tag{A.3}$$

$$S = \begin{bmatrix} S_{11} & S_{12} & \dots & S_{1n} \\ S_{21} & S_{22} & \dots & S_{2n} \\ \dots & \dots & \dots & \dots \\ S_{n1} & S_{n2} & \dots & S_{nn} \end{bmatrix} \tag{A.4}$$

Among them, S_{ii} is called the 'reflection coefficient', indicating the voltage reflection at port ' i ' when other ports are connected to the matching load. As is commonly known, the operational bandwidth of a MIMO system is determined by its impedance matching situation. The addition of any decoupled structures will alter the radiation impedance of the proposed antenna arrays. Therefore, S_{ii} must be considered when contemplating decoupling design as it indirectly represents impedance matching. Adjusting S_{ii} allows for the attainment of the desired operational bandwidth. S_{ij} is termed the 'transmission coefficient', representing the voltage transmission from port ' j ' to port ' i ' when the ' i ' element is connected to the matching load. The mutual coupling degree of two ports is measured by S_{ij}. Additionally, modifying S_{ij} achieves the preferred isolation. The unit of these parameters is usually expressed in ' dB '. To ensure that the RF element is in a normal working state, it is generally required that S_{ii} be less than -10 dB, and Sij be less than -15 dB [63].

Taking the two-port network as an example, assume that 1 is the feed port and 2 is the coupling port. The S-parameters of the two-port network are given in equation (A.5):

$$S = \begin{bmatrix} S_{11} & S_{12} \\ S_{21} & S_{22} \end{bmatrix} \tag{A.5}$$

In this context, S_{11} represents the input reflection coefficient, also referred to as input return loss; S_{22} corresponds to the output reflection coefficient or output return loss; S_{12} denotes the reverse transmission coefficient or isolation; and S_{21} signifies the forward transmission coefficient [63].

If we denote the power of port 1 as P_1 and the power of port 2 as P_2, the isolation between the ports can be expressed using equation (A.6) [63]:

$$S_{12}(dB) = 20\log|S_{21}| = 10\log\frac{P_2}{P_1} \tag{A.6}$$

The degree of mutual coupling of the antenna element is inversely related to the absolute value of the transmission coefficient. Therefore, the larger the absolute value of the

transmission coefficient, the smaller the degree of mutual coupling of the antenna.

2) Resonant frequency and bandwidth

The definition of the resonant frequency (f_{res}) is the frequency at which the real part of the input impedance is maximum and its imaginary part is zero. The bandwidth Δf is considered the frequency range in which the reflection coefficient of the antenna is less than -10 dB. This band is situated between a minimum value minimum value f_1 and a maximum value f_2 around a central frequency f_c (the antenna resonance frequency) [15].

$$\Delta f = f_2 - f_1 \tag{A.7}$$

It can also be expressed as a relative bandwidth Br (percentage value expressed as the ratio of the band to the center frequency f_c):

$$Br = \frac{\Delta f}{f_c} \times 100 \tag{A.8}$$

Antennas traditionally operate in a narrow frequency band. However, with recent advancements in radio systems, an increasing number of antennas exhibit wide to ultrawide frequency bands. Some antennas can also operate in multiple distinct frequency bands, making them multi-band antennas. Bandwidth can be classified according to its width, as shown in table (A.1):

Table A.1: Classification of bandwidth by width

Narrow-band	$B_r < 1\%$
Wide-band	$1\% < B_r < 20\%$
Ultra-wideband	$B_r > 20\%$

3) Gain

Another important parameter for describing antenna performance is the gain 'G', which is defined as "the ratio of the power density radiated by the antenna in a given direction, to the power density radiated by a reference isotropic antenna (an antenna that radiates uniformly in all directions)". The isotropic radiated power corresponds to the radiation

intensity is equal to the power accepted (input) by the antenna divided by 4π. This can be expressed as follows (equation (A.9)) [15]:

$$\text{Gain } = 4\pi \times \frac{\text{radiated power density}}{\text{total input (accepted) power}} = 4\pi \times \frac{U(\theta,\varphi)}{P_{\text{in}}} \tag{A.9}$$

Where $U(\theta,\varphi)$ is antenna radiated power density, and P_{in} is the power injected into the antenna. Gain is expressed in decibels relative to the isotropic antenna (dBi). A positive gain value indicates that the antenna is more effective in the specified direction compared to an isotropic radiator, while a negative gain value suggests less effectiveness.

4) Directivity

The directivity ' D ' of an antenna is a measure of its ability to direct or accentuate radiated fields in a specific angular direction. It is defined as the ratio of the radiation intensity in a given direction of the antenna to the radiation intensity of an isotropic source (an isotropic source radiates the same power in all directions, and its radiation intensity is equal to the total power radiated by the antenna divided by 4π). It can be written as in equation (A.10) [15]:

$$D(\theta,\varphi) = \frac{U(\theta,\varphi)}{P_{\text{ray}}/4\pi} \tag{A.10}$$

Where $U(\theta,\varphi)$ is antenna radiation intensity, and P_{ray} is the total radiated power. If the direction is not specified, it means the direction of maximum radiation intensity (maximum directivity).

5) Radiation efficiency and total efficiency

The total efficiency of an antenna is the ratio between the power radiated by the antenna and the incident power on its feed port. This value takes into account reflection losses caused by the mismatch between the antenna and the electronic circuit, as well as ohmic and dielectric losses in the materials making up the antenna. It is calculated by integrating the radiation pattern as expressed in equation (A.11) [15] [56]:

$$\eta_{tot} = \frac{\int_0^{2\pi}\int_0^{\pi}\left(G_\theta(\theta,\varphi)+G_\varphi(\theta,\varphi)\right)\mathrm{d}\Omega}{4\pi} \tag{A.11}$$

Where $G_\theta(\theta,\varphi)$ and $G_\varphi(\theta,\varphi)$ are the antenna gains in the θ and φ directions. To simplify the calculation, we can also use the radiated efficiency η_{ray} of the antenna (does not take into account the various losses) and the mismatch efficiency η_d, the total efficiency is directly related to the parameters S as shown in equation (A.15):

$$\eta_{tot} = \eta_{\text{ray}} \cdot \eta_d \tag{A.12}$$

$$\eta_d = 1 - |S_{11}|^2 \tag{A.13}$$

$$\eta_{\text{ray}} = \frac{P_{\text{ray}}}{P_{\text{acc}}} \tag{A.14}$$

$$\eta_{tot} = \eta_{\text{ray}} \cdot \left(1 - |S_{11}|^2\right) \tag{A.15}$$

In summary, radiation efficiency is specifically about the efficiency of converting power into radiation, while total efficiency provides a more comprehensive measure by taking into account all losses in the antenna system. These parameters are crucial for the design and evaluation of antennas for various applications, including communication systems. In addition, the antenna gain can be calculated from its radiation efficiency and directivity by the following equation (A.16):

$$G(\theta,\varphi) = \eta_{\text{ray.}} .D(\theta,\varphi) \tag{A.16}$$

6) Multiplexing Efficiency

Although the data rate improvement of MIMO systems is usually indicated using the channel capacity of the system, this measure is less intuitive for antenna designers and a power based or related one measure is more appreciable, so a new metric that combines the effect of antenna efficiency as well as the correlation between the antenna-ports was named multiplexing efficiency [88].

Multiplexing efficiency is a metric for describing the performance of a MIMO antenna system in spatial multiplex mode (high SNR mode), taking efficiency and correlation of the MIMO antenna elements into account. This measurement can be evaluated for a MIMO antenna system using equation (A.17) [88]:

$$\eta_{mux} = \left(\prod_{m=1}^{N} \eta_m\right)^{\frac{1}{N}} \det(\bar{R})^{\frac{1}{N}} \tag{A.17}$$

In this context, η_m represents the efficiency of each individual antenna element, and $\bar{R}$ is the normalized correlation matrix. The diagonal elements of $\bar{R}$ are 1 , while the other elements consist of the complex correlation coefficients between the 3D radiation patterns of the corresponding antenna elements in that position. For a simplified approximation in a 2×2 MIMO case, the multiplexing efficiency is expressed by equation (A.18):

$$\eta_{\text{mux}} = \sqrt{\eta_1 \eta_2 \left(1 - |\rho|^2\right)} \tag{A.18}$$

BIBLIOGRAPHY

[1] Foschini GJ. Layered space-time architecture for wireless communication in a fading environment when using multi-element antennas. *Bell labs technical journal*, vol. 1, no 2, pp. 41–59, 1996.

[2] Foschini GJ, and Gans MJ. On limits of wireless communications in a fading environment when using multiple antennas. *Wireless personal communications*, vol. 6, no 3, pp. 311–335, 1998.

[3] Ojaroudi Parchin N, Jahanbakhsh Basherlou H, Al-Yasir YI, M. Abdulkhaleq A, and A. Abd-Alhameed R. Reconfigurable antennas: Switching techniques—A survey. *Electronics*, vol. 9, no. 2, pp. 336, 2020.

[4] Zhao X, and Riaz S. A dual-band frequency reconfigurable MIMO patch-slot antenna based on reconfigurable microstrip feedline. *IEEE Access*, vol. 6, pp. 41450–41457, 2019.

[5] Hassan MM, and Zahid Z, Khan AA, Rashid I, Rauf A, Maqsood M, and Bhatti FA. Two element MIMO antenna with frequency reconfigurable characteristics utilizing RF MEMS for 5G applications. *Journal of Electromagnetic Waves and Applications*, vol. 34, no. 9, pp. 1210–1224, 2020.

[6] AMathur R, and Dwari S. Compact planar reconfigurable UWB-MIMO antenna with on-demand worldwide interoperability for microwave access/wireless local

area network rejection. *Microwave and Optical Technology Letters*, vol. 13, no. 10, pp. 1684–1689, 2019.

[7] Du Ke-Lin, and Swamy Madisetti NS. Wireless communication systems: from RF subsystems to 4G enabling technologies. *Cambridge University Press*, 2010.

[8] Tounou Charles. Contribution à l'étude de systèmes à diversité d'antennes sur terminaux compacts: mesures de performances en environnement réel. *Doctoral dissertation, University of Limoges*, 2008.

[9] Zhong C. Capacity and performance analysis of advanced multiple antenna communication systems. *University College London*, 2010.

[10] Molisch Andreas F. *Wireless communications*. Vol. 34, John Wiley & Sons, 2010.

[11] Commsbrief. Mobile Data Speed with 2G, 3G, 4G and 5G Cellular Networks. 2023. *https://commsbrief.com/mobile-data-speed-with-2g-3g-4g-and-5g-cellular-networks/*

[12] 5G Americas. Understanding Millimeter Wave Spectrum for 5G Networks. 2023. *https://www.5gamericas.org/understanding-millimeter-wave-spectrum-for-5g-networks*

[13] 5G Spectrum Public Policy. *https://www-file.huawei.com/-/media/CORPORATE/PDF/public-policy/public_policy_position_5g_spectrum.pdf*

[14] Jankiraman M. Space-time codes and MIMO systems. *Artech House*, 2004.

[15] Balanis C A. Antenna theory: analysis and design. *John wiley & sons*, 2016.

[16] Saunders S.R. Antennas and propagation for wireless communication systems. *John Wiley & Sons*, 1999.

[17] Poularikas Alexander D. MIMO system technology for wireless communications. *CRC press*, 2018.

[18] Biglieri E, Calderbank R, Constantinides A, Goldsmith A, Paulraj A, and Poor HV. MIMO wireless communications. *Cambridge university press*, 2007.

[19] Jagannath M, Patnaik A and Kartikeyan M.V. Compact antennas for high data rate communication. *Springer*, 2018.

[20] Saunders SR, and Aragón-Zavala A. Antennas and propagation for wireless communication systems. *John Wiley & Sons*, 2007.

[21] Janaswamy R. Radiowave propagation and smart antennas for wireless communications. *Springer Science & Business Media*, 2001.

[22] Brown TW. Antenna Diversity for Mobile Terminals. *Phd Thesis, University of Surrey, Guildford, centre for Communication Systems Research, School of Electronics and Physical Sciences*, 2002.

[23] Vaughan RG. Switched Parasitic Elements for Antenna Diversity. *IEEE Transactions on Antennas and Propagation*, vol. 47, no. 2, pp. 399–405, 1999.

[24] Dong L, Ling H, and Heath RJ. Multiple-Input Multiple-Output Wireless Communication Systems Using Antenna Pattern Diversity. *Global Telecommunications Conference, IEEE*, vol. 1, pp. 997–1001, 2002.

[25] Choumane A. Synthèse d'un canal de propagation par système multi-antennes pour la caractérisation de terminaux mobiles à diversité. *Doctoral dissertation, University of Limoges*, 2011.

[26] Gao Y. Characterisation of Multiple Antennas and Channel for Small Mobile Terminals. *PhD Thesis, University of London Queen Mary*, 2007.

[27] Lee WC, and Yeh Yu. Polarization diversity system for mobile radio. *IEEE Transactions on Communications*, vol. 20, no. 5, pp. 912–923, 2007.

[28] Lempiainen JJ, and Laiho-Steffens JK. The performance of polarization diversity schemes at a base station in small/micro cells at 1800 MHz. *IEEE Transactions on Vehicular Technology*, vol. 47, no. 3, pp. 1087–1092, 1998.

[29] Mori K, Moriyama E, and Arai H. Base station polarization diversity antenna for private mobile communications. *Electronics and Communications in Japan (Part I: Communications)*, vol. 86, no. 4, pp. 10–18, 2003.

[30] Eggers PCF, Toftgard J, and Oprea AM. Antenna systems for base station diversity in urban small and micro cells. *IEEE Journal on selected Areas in Communications*, vol. 11, no. 7, pp. 1046–1057, 1993.

[31] Chouhan S, Panda DK, Gupta M, and Singhal S. Multiport MIMO antennas with mutual coupling reduction techniques for modern wireless transreceive operations: A review. *International Journal of RF and Microwave Computer-Aided Engineering*, vol. 28, no. 2, pp. e21189, 2018.

[32] Malviya L, Panigrahi RK, and Kartikeyan MV. MIMO Antennas for Wireless Communication: Theory and Design. *CRC Press*, 2020.

[33] Nadeem I, and Choi DY. Study on mutual coupling reduction technique for MIMO antennas. *IEEE Access*, vol.7, pp. 563–586, 2018.

[34] Naktong W, and Ruengwaree A. Four-port rectangular monopole antenna for UWB-MIMO applications. *Progress In Electromagnetics Research B*, vol. 78, pp. 19–38, 2020.

[35] Ekrami H, and Jam S. A compact triple-band dual-element MIMO antenna with high port-to-port isolation for wireless applications. *AEU-International Journal of Electronics and Communications*, vol. 96, pp. 219–227, 2018.

[36] Raheja DK, Kumar S, and Kanaujia BK. Compact quasi-elliptical-self-complementary four-port super-wideband MIMO antenna with dual band elimination characteristics. *AEU-International Journal of Electronics and Communications*, vol. 114, pp. 153001, 2020.

[37] Srivastava K, Kumar A, Kanaujia BK, Dwari S, and Kumar S. A CPW-fed UWB MIMO antenna with integrated GSM band and dual band notches. *International Journal of RF and Microwave Computer-Aided Engineering*, vol. 29, no. 1, pp. e21433, 2019.

[38] Iqbal A, Saraereh OA, Ahmad AW, and Shahid B. Mutual coupling reduction using F-shaped stubs in UWB-MIMO antenna. *IEEE access*, vol. 6, pp. 2755–2759, 2017.

[39] Zhao Y, Zhang FS, Cao LX, and Li DH. A compact dual band-notched MIMO diversity antenna for UWB wireless applications. *Progress In Electromagnetics Research C*, vol. 89, pp. 161–169, 2019.

[40] Nandi S, and Mohan A. A compact dual-band MIMO slot antenna for WLAN applications. *IEEE antennas and wireless propagation letters*, vol. 16, pp. 2457–2460, 2017.

[41] Bahmanzadeh F, and Mohajeri F. Simulation and fabrication of a high-isolation very compact MIMO antenna for ultra-wide band applications with dual band-notched characteristics. *AEU-International Journal of Electronics and Communications*, vol. 128, pp. 153505, 2021.

[42] Ren J, Hu W, Yin Y, and Fan R. Compact printed MIMO antenna for UWB applications. *IEEE antennas and wireless propagation letters*, vol. 13, pp. 1517–1520, 2014.

[43] Li Z, Yin C, and Zhu X. Compact UWB MIMO Vivaldi antenna with dual band-notched characteristics. *IEEE Access*, vol. 7, pp. 38696–38701, 2019.

[44] Pannu P, and Sharma DK. A low-profile quad-port UWB MIMO antenna using defected ground structure with dual notch-band behavior. *International Journal of RF and Microwave Computer-Aided Engineering*, vol. 13, no. 9, pp. e22288, 2020.

[45] Jetti CR, and Nandanavanam VR. Trident-shape strip loaded dual band-notched UWB MIMO antenna for portable device applications. *AEU-International Journal of Electronics and Communications*, vol. 83, pp. 11–21, 2018.

[46] Zhang S, and Pedersen GF. Mutual Coupling Reduction for UWB MIMO Antennas with a Wideband Neutralization Line. *IEEE antennas and wireless propagation letters*, vol. 15, pp. 166–169, 2015.

[47] Rakesh NT, Prabhakar S, Binod KK, and Kunal S. Neutralization technique based two and four port high isolation MIMO antennas for UWB communication. *AEU*

- *International Journal of Electronics and Communications*, vol. 15, pp. 152828, 2019.

[48] Liu R, An X, Zheng H, Wang M, Gao Z, and Li E. Neutralization line decoupling tri-band multiple-input multiple-output antenna design. *IEEE Access*, vol. 8, pp. 27018–27026, 2020.

[49] Yang D, Kim D, and Kim C. Design of dual-band MIMO monopole antenna with high isolation using slotted CSRR for WLAN. *Microwave and Optical Technology Letters*, vol. 56, pp. 2252–2257, 2014.

[50] Venkatesan R, and Rengasamy R. SRR Loaded Compact Tri-Band MIMO Antenna for WLAN/WiMAX Applications. *Progress In Electromagnetics Research Letters*, vol. 95, pp. 43–53, 2021.

[51] Jabire AH, Ghaffar A, Li XJ, Abdu A, Saminu S, Alibakhshikenari M, Falcone F, and Limiti E. Metamaterial Based Design of Compact UWB/MIMO Monopoles Antenna with Characteristic Mode Analysis. *Applied Sciences*, vol. 11, no. 4, pp. 1542, 2021.

[52] Xiaoyan Z, Xinxing Z, Bincheng L, and Yiqiang Y. A Dual-Polarized MIMO Antenna with EBG for 5.8GHz WLAN Application. *Progress In Electromagnetics Research Letters*, vol. 51, pp. 15–20, 2015.

[53] Dabas T, Gangwar D, Kanaujia BK, and Gautam AK. Mutual coupling reduction between elements of UWB MIMO antenna using small size uniplanar EBG exhibiting multiple stop bands. *AEU-International Journal of Electronics and Communications*, vol. 93, pp. 32–38, 2018.

[54] Maturi T, and Baranikunta H. Electronic band-gap integrated low mutual coupling dual-band MIMO antenna. *International Journal of Electronics*, vol. 107, no. 7, pp. 1166–1176, 2020.

[55] Mohamadzade B, and Afsahi, M. Mutual coupling reduction and gain enhancement in patch array antenna using a planar compact electromagnetic bandgap structure. *IET Microwaves, Antennas and Propagation*, vol. 11, no. 12, pp. 1719–1725, 2017.

[56] Sharawi Mohammad S. Printed MIMO antenna engineering. *Artech House*, 2014.

[57] Blanch S, Romeu J, and Corbella I. Exact representation of antenna system diversity performance from input parameter description. *Electronics letters*, vol. 39, no. 9, pp. 705–707, 2003.

[58] Malviya L, Panigrahi RK, and Kartikeyan MV. MIMO Antennas for Wireless Communication: Theory and Design. *CRC Press*, 2020.

[59] Sharma P, Tiwari RN and Singh P, Kumar P , and Kanaujia BK. MIMO antennas: Design approaches, techniques and applications. *Sensors*, vol. 22, no. 20, pp. 7813, 2022.

[60] Manteghi M, and Rahmat SY. Multiport characteristics of a wide-band cavity backed annular patch antenna for multipolarization operations. IEEE Transactions on Antennas and Propagation, vol. 53, no. 1, pp. 466–474, 2005.

[61] Kumar A, Ansari AQ, Kanaujia BK, and Kishor J. A novel ITI-shaped isolation structure placed between two-port CPW-fed dual-band MIMO antenna for high isolation. *AEU-International Journal of Electronics and Communications*, vol. 104, pp. 35–43, 2019.

[62] Mathur R, and Dwari S. Compact planar reconfigurable UWB-MIMO antenna with on-demand worldwide interoperability for microwave access/wireless local area network rejection. *AEU-International Journal of Electronics and Communications*, vol. 13, no. 10, pp. 1684–1689, 2019.

[63] Kulkarni Jayshri, Heng TH, Brian G, Yang L, Chow-Yen-Desmond S, and Vigneswaran D. Transparent and Flexible MIMO Antenna Technologies for 5G Applications: Transforming 5G with Transparent & Flexible MIMO Antennas. *Springer Innovations in Communication and Computing*, 2023.

[64] Al khaylani HH, Elwi TA, and Ibrahim AA. Optically remote-controlled miniaturized 3D reconfigurable CRLH-printed MIMO antenna array for 5G applications. *Microwave and Optical Technology Letters*, vol. 65, no. 2, pp. 603–610, 2023.

[65] Cetiner BA, Akay E, Sengul E, and Ayanoglu E. A MIMO system with multifunctional reconfigurable antennas. *IEEE Antennas and Wireless Propagation Letters*, vol. 5, pp. 463–466, 2006.

[66] Xu Z, Sun YT, Zhou QQ, Ban YL, Li YX, and Ang SS. Reconfigurable MIMO antenna for integrated-metal-rimmed smartphone applications. *IEEE Access*, vol. 5, no. 2, pp. 21223–21228, 2017.

[67] Ojaroudi N, and Ojaroudi M. A novel design of reconfigurable small monopole antenna with switchable band notch and multi-resonance functions for UWB applications. *Microwave and Optical Technology Letters*, vol. 55, no. 3, pp. 652–656, 2013.

[68] Ali M. Reconfigurable antenna design and analysis. *Artech House*, 2021.

[69] Han L, Ping Y, Liu Y, Han G, and Zhang W. A low-profile pattern reconfigurable MIMO antenna. *IEEE Access*, vol. 8, pp. 34500–34506, 2020.

[70] Thangarasu D, Palaniswamy SK, and Thipparaju RR. Quad port multipolarized reconfigurable MIMO antenna for sub 6 GHz applications. *International Journal of Antennas and Propagation*, vol. 2023, 2023.

[71] Shereen MK, Khattak MI , and Al-Hasan M. A frequency and radiation pattern combo-reconfigurable novel antenna for 5G applications and beyond. *Electronics*, vol. 9, no. 9, pp. 1372, 2020.

[72] Padmanathan S, Al-Hadi AA, Elshirkasi AM, Al-Bawri SS, Islam MT, Sabapathy T, Jusoh M, Akkaraekthalin P, and Soh PJ. Compact multiband reconfigurable MIMO antenna for sub-6GHz 5G mobile terminal. *IEEE Access*, vol. 10, pp. 60241–60252, 2022.

[73] Tawk Y, Costantine J, and Christodoulou CG. Reconfigurable filtennas and MIMO in cognitive radio applications. *IEEE Transactions on Antennas and Propagation*, vol. 62, no. 3, pp. 1074–1083, 2013.

[74] Hussain R, and Sharawi MS. A cognitive radio reconfigurable MIMO and sensing antenna system. *IEEE Antennas and Wireless Propagation Letters*, vol. 14, pp. 257–260, 2014.

[75] Riaz S, Zhao X, and Geng S. A frequency reconfigurable MIMO antenna with agile feedline for cognitive radio applications. *International Journal of RF and Microwave Computer-Aided Engineering*, vol. 30, no. 3, pp. e22100, 2020.

[76] Hussain R and Sharawi MS. Integrated reconfigurable multiple-input–multiple-output antenna system with an ultra-wideband sensing antenna for cognitive radio platforms. *IET Microwaves, Antennas & Propagation*, vol. 9, no. 9, pp. 940–947, 2015.

[77] Zhao X, Riaz S, and Geng S. A reconfigurable MIMO/UWB MIMO antenna for cognitive radio applications. *IEEE access*, vol. 7, pp. 46739–46747, 2019.

[78] Srikar D, Nella A, Mamidi R, Babu A, Das S, Lavadiya S, Algarni AD, and El-Shafai W. A Novel Integrated UWB Sensing and 8-Element MIMO Communication Cognitive Radio Antenna System. *Electronics*, vol. 12, no. 2, pp. 330, 2023.

[79] Pant A, Singh M, and Parihar MS. A frequency reconfigurable/switchable MIMO antenna for LTE and early 5G applications. *AEU-international Journal of Electronics and Communications*, vol. 131, pp. 153638, 2021.

[80] Singh G, Kumar S, Abrol A, Kanaujia BK, Pandey VK, Marey M, and Mostafa H. Frequency reconfigurable quad-element MIMO antenna with improved isolation for 5G systems. *Electronics*, vol. 12, no. 4, pp. 796, 2023.

[81] Alam T, Thummaluru SR, and Chaudhary RK. Integration of MIMO and cognitive radio for sub-6 GHz 5G applications. *IEEE Antennas and Wireless Propagation Letters*, vol. 18, no. 10, pp. 2021–2025, 2019.

[82] Alam T, Thummaluru SR, and Chaudhary RK. Frequency reconfigurable antenna array for mm-Wave 5G mobile handsets. *Broadband Communications, Networks, and Systems: 9th International EAI Conference*, Proceedings 9, pp. 438–445, 2019.

[83] Chattha HT, Latif F, Tahir FA, Khan MU, and Yang X. Small-sized UWB MIMO antenna with band rejection capability. *IEEE Access*, vol. 7, pp. 121816–121824, 2019.

[84] Gautam AK, Yadav S, and Rambabu K. Design of ultra-compact UWB antenna with band-notched characteristics for MIMO applications. *IET Microwaves, Antennas & Propagation*, vol. 12, no. 12, pp. 1895–1900, 2018.

[85] Banerjee J, Gorai A, and Ghatak R. Design and analysis of a compact UWB MIMO antenna incorporating fractal inspired isolation improvement and band rejection structures. *AEU-International Journal of Electronics and Communications*, vol. 122, pp. 153274, 2020.

[86] Luo S, Wang D, Chen Y, Li E, and Jiang C. A compact dual-port UWB-MIMO antenna with quadruple band-notched characteristics. *AEU-International Journal of Electronics and Communications*, vol. 136, pp. 153770, 2021.

[87] Du k, Wang Y, and Hu Y. Design and analysis on decoupling techniques for mimo wireless systems in 5g applications. *Applied Sciences*, vol. 12, no. 8, pp. 153770, 3816, 2022.

[88] Tian, Ruiyuan, Buon K.L, and Ying Z. Multiplexing efficiency of MIMO antennas. *IEEE antennas and wireless propagation letters*, vol. 10, pp. 183-186, 2011.